Biomimetic Approaches for Bone Tissue Engineering

by

Ming Dang

A dissertation submitted in partial fulfillment
of the requirements for the degree of
Doctor of Philosophy
(Macromolecular Science and Engineering)
in The University of Michigan
2018

Doctoral Committee:

Professor Peter X. Ma, Chair
Professor Renny Franceschi
Professor Laurie K. McCauley
Professor Richard E. Robertson

Ming Dang

dangming@umich,edu

ORCID ID: 0000-0001-7918-791X

DEDICATION

I dedicate my dissertation to my loving family

ACKNOWLEDGEMENTS

I am using this opportunity to express my warm thanks to all the people who made this dissertation possible. Foremost, I express my sincere gratitude to my adviser, Professor Peter X. Ma, for his invaluable support of my PhD study and research, for his guidance, motivation and inspiration. Besides I would like to thank the rest of my thesis committee and other faulty member, Dr. Laurie K. McCauley, Dr. Richard E. Robertson, Dr. Renny Franceschi and Dr. Benjamin Levi, for their encouragement and insightful comments to my scientific training and growth.

My numerous thanks also go to my past and present labmates in both Ma lab and McCauley lab: Dr. Xiaobing Jin, Amy J. Koh, Dr. Wei Wang, Dr. Ganjun Feng, Dr. Zhanpeng Zhang and UROP students who have worked for me, for the stimulating discussions and productive collaborations. I am also grateful to Dr. Xuming Xie and Dr. Yitao Liu in Tsinghua University for enlightening me the first glance of research.

Last but not the least, I thank my family for supporting me spiritually throughout my life.

Thank you,

Ming Dang

Table of Contents

LIST OF FIGURES

ABSTRACT

Bone tissue engineering is an attractive alternative to transplanting harvested tissue for bone defect repair. Various signals are involved in the regulation of stem/progenitor cell behavior, development and healing, which could be beneficially utilized in bone tissue engineering. However, bone tissue engineering research has very limited success in translation into the clinic, which often stems from the inappropriate administration of these signaling molecules due to the lack of optimal delivery systems. Therefore, this project is aimed at the development of new approaches to bone tissue engineering by mimicking advantageous features of the native extracellular matrix and signaling processes involved in development and natural healing.

The author first develops preprogrammed drug delivery systems to achieve long-term pulsatile delivery of parathyroid hormone (PTH). A series of techniques, including polymer synthesis, drug formulation and device fabrication are developed to control the physical and chemical properties of the delivery devices so as to achieve spatiotemporal controlled drug release. Systemic pulsatile PTH release from the delivery device is demonstrated to increase bone volume and mineralized bone density, thereby providing a promising complying-friendly alternative to the standard daily PTH injection treatment for osteoporosis. Then PTH is repurposed successfully for local bone regeneration in a mouse calvarial bone defect regeneration model by using the pulsatile delivery system in combination with a biomimetic nanofibrous PLLA scaffold developed in our lab. Such

system could possibly be utilized to regenerate various bone defects.

Considering that the native bone defect healing process is initiated by macrophages via engulfing dead cells, the author develops a novel bioconjugation strategy to fabricate biodegradable microspheres to mimic apoptotic cells to target macrophages to initiate a biomimetic bone healing process. The biodegradable apoptotic cell-mimicking microspheres (BAM) are decorated with “eat me signal” and are shown to significantly enhance macrophage phagocytosis and enhance bone marrow stromal cell (BMSCs) migration via increased secretion of chemokines. Implanting a 3D space-defining biomimetic nanofiberous (NF) scaffold loaded with BAM results in a drastic increase in endogenous mesenchymal stem/progenitor cell recruitment into the scaffold compared to the same scaffold loaded with control microspheres, leading to critical-sized bone defect repair. This novel biomimetic approach opens a potential new avenue for bone regeneration without the need for exogenous cells.

CHAPTER 1

Bone Tissue Engineering

1.1 Introduction

Bone loss or damage can result from various causes including degenerative disease, surgery, and trauma, and significantly compromises patient quality of life[1, 2]. Generally bone possesses an intrinsic ability to self-repair, but there are many situations where complete bone regeneration cannot occur and needs to be stimulated[3]. Millions of patients suffering from bone defects require bone grafts and substitutes procedure. The bone grafts and substitutes market was valued at over USD 2.3 billion in 2015 and is expected to reach over USD 3.6 billion between 2016 and 2024[4]. Currently, the standard bone-grafting approach widely used in clinical practice is autologous, allogeneic or xenogeneic[5, 6]. Autologous bone grafting is considered the gold standard treatment, in which host bone is removed from another site to fill the defect. However, many limitations remain including multiple required surgeries, potential morbidity and the limited quantity of donor tissues[7-9]. Allogeneic or xenogeneic graft, the transplantation of bone tissue from another human or species donors, is an optional treatment but has inherent limitations including immunogenic responses, infection risks and pathogen transmission[10-13]. For these reasons, an alternative approach, bone tissue engineering, has emerged as a potential new therapy. The tissue engineering approach utilizes biomaterials to provide the

microenvironment for regenerative cells, supporting cell attachment, proliferation, differentiation and tissue synthesis[14, 15]. While osteogenic scaffolds have been developed, they have not yet been sufficient to robustly regenerate high quality bone[16, 17]. The addition of stem and/or progenitor cells has proved to initiate and promote improved and/or faster bone healing[18-22]. Cell-based therapies are very promising to enhance bone regeneration but suffer major limitations such as the source of cells, the *in vitro* manipulation, the rigorous regulatory approval process and associated high costs[23-25]. Acellular biomaterials are emerging to overcome the need for addition of external cells. Such cell-free system require advanced biomimetic approaches, which draw on biological knowledge and engineering tools to mimic and replicate the certain advantageous features of the natural extracellular matrix (ECM). At the same time some artificially engineered features can be incorporated so as to stimulate and accelerate the regeneration process[14, 26, 27].

In many situations (e.g. large defect repair, impaired tissue function), endogenous signal cues are usually not sufficient in type and/or amount, thus the addition of exogenous signal cues is necessary. The biomimetic drug delivery strategy aims to deliver signal cues, mimicking the signaling process of the natural bone healing and to accelerate bone repair and regeneration[24, 28].

1.2 Scientific Challenges and Significance

Growth factors (GFs) are one important group of signal molecules, which have been intensively studied. A multitude of growth factors are involved in regulating the bone regeneration process and some have demonstrated great potential in numerous preclinical

studies. However, the promising outcomes achieved in the animal models have only partially been translated to human, mainly due to their side effects and safety issue including systemic hypotension and edema, heterotopic bone formation and increased cancer risk. Besides growth factors, other types of signal molecules have exhibited attractive potential in bone tissue engineering applications.

One example is Parathyroid Hormone (PTH), an endocrine secretion molecule, which is a key regulator of the bone remolding process[29]. Its efficacy, minor side effects in improving bone micro-architecture, mineral density and reducing fractures has been well established and demonstrated in multiple clinical trials [30]. PTH needs to be delivered at specific time points and follow a certain release pattern in order to exert the desired therapeutic effects[31]. While the majority of drug delivery systems developed thus far can achieve a prolonged and sustained delivery, there has been limited progress in designing controlled release systems to couple the spatiotemporal sensitivity of a patient to PTH to enable or optimize its therapeutic effect[32].

Another important group of signal molecules are the membrane lipid molecules, which are widely involved in cell-cell recognition and interaction, thus regulating the tissue development process[33, 34]. Due to the hydrophobic structure of the lipids, most of lipid molecules are formulated into liposome, and administered systemically[35, 36]. However, systemic liposome treatments have several disadvantages[37, 38] including instability in the blood stream, short half-lives and off-target effects. This route of administration is suitable for localized defect repair, which often requires spatially-controlled and prolonged presentation of the signal cues.

1.3 Aims and Dissertation Overview

The main hypotheses of this thesis are: 1. An implantable delivery device capable of long-term PTH pulsatile delivery can be developed and the engineered PTH release can promote bone growth systemically; 2. PTH can be repurposed for local bone defect repair. The pulsatile release promotes bone regeneration whereas the continuous release inhibits bone regeneration. The local release is advantageous over the standard systemic injection in repairing local defects; 3. Biodegradable apoptotic-cell mimicking (BAM) microspheres can target macrophages and regulate macrophage activities.

The specific aims of this thesis are listed below:

1. Fabricate an implantable drug delivery device capable of long-term pulsatile and continuous drug release, characterize the device materials and structure, achieve a controlled drug release profile *in vitro* and evaluate the biological function of the released molecules both *in vitro* and *in vivo*. Specifically, we focus on developing a PTH pulsatile delivery device, which could achieve daily pulse release for 21 days and a PTH continuous delivery device, which could release drug in a linear manner for 21 days.

2. Repurpose PTH in a local bone defect model and evaluate the local PTH release effects on bone repair. Specifically, we develop a 3D nanofibrous (NF) scaffold and PTH release devices and combine the two components so that the device delivers PTH locally into the scaffold. The biological function of distinct PTH release kinetics in bone regeneration will be examined and evaluated to determine the optimal release pattern in terms of osteogenic outcome. The optimal delivery system will then be compared with the standard PTH injection.

3. Develop BAM microspheres to target macrophages and manipulate macrophage function. Specifically, we develop a novel bioconjugation strategy to conjugate "eat me signal" lipid molecules onto the microspheres surface. The biological function of the BAM microsphere and the interaction between the BAM microspheres and the macrophages will be evaluated both *in vitro* and *in vivo*.

The chapter arrangements of this thesis are listed below:

Chapter 2 provides a general literature review of the current biomimetic drug delivery in bone tissue regeneration from two aspects: (1) general considerations in delivery systems and (2) specific delivery strategies for various types of bioactive signal molecules.

Chapter 3 begins the research part of this thesis with the fabrication of a long-term PTH delivery device. We synthesize surface erosion polymers, investigate their chemical and physical properties, and develop advanced technologies to fabricate drug delivery devices, which are capable of long-term pulsatile and continuous drug release respectively. A series of technologies have been developed to tune the properties of the delivery systems as so to achieve optimal release kinetics.

Chapter 4 details the biological function of distinct PTH release kinetics in terms of the therapeutic effects on bone. PTH delivery devices were evaluated in a subcutaneous implantation model. With the capacity of the developed methodology and temporal controlled drug release, pulsatile and continuous PTH delivery devices were compared in terms of their potential to strengthen bone systemically. Long-term PTH pulsatile release was shown to be advantageous relative to continuous release. These results are published in *Advanced Healthcare Materials*[31].

Chapter 5 builds a bone defect model to exploit the therapeutic potential of PTH in healing local bone defect. A platform, which combines the biomimetic 3D NF scaffold and the PTH delivery device, has been established to enable PTH local delivery. For the first time we have repurposed PTH in a local repair scenario. These results are published in *Biomaterials*[39].

Chapter 6 develops a bioconjugation strategy to fabricate biodegradable microsphere to mimic apoptotic cells. Controlled surface conjugation and presentation of the "eat me signal" lipid molecule was achieved and the biomimetic BAM microspheres have demonstrated to target macrophages and manipulate the macrophage activity. Biomimetic NF scaffold loaded with BAM microspheres resulted in a drastic increase in endogenous mesenchymal stem/progenitor cell recruitment into the scaffold when compared with control microspheres. By targeting macrophage phagocytosis, the BAM/scaffold construct resulted in critical-sized bone defect repair.

The final chapter, chapter 7, summarizes the thesis work with major conclusions and discusses some possible future directions related to this dissertation.

CHAPTER 2

Drug Delivery Strategies in Bone Tissue Engineering

2.1 Introduction

A variety of signaling molecules have been identified and demonstrated to play a crucial role in regulating the cellular activity and microenvironment in bone tissue development and regeneration. The bioactive signal molecules are not only limited to growth factors, they also include small molecules[40, 41], peptides/proteins[42, 43], hormones[44], antibodies[45, 46], and nuclei acids[47, 48], which have been investigated for their ability to induce and accelerate bone regeneration (Figure 2.1.1). Different types of signal molecules contribute to the bone regeneration process using different mechanisms and therefore require specific delivery methods and kinetics. This chapter will review the types and mechanisms of the various bioactive signal molecules and the general considerations in drug delivery system (DDS) design. We will also discuss using the examples of recent research progress.

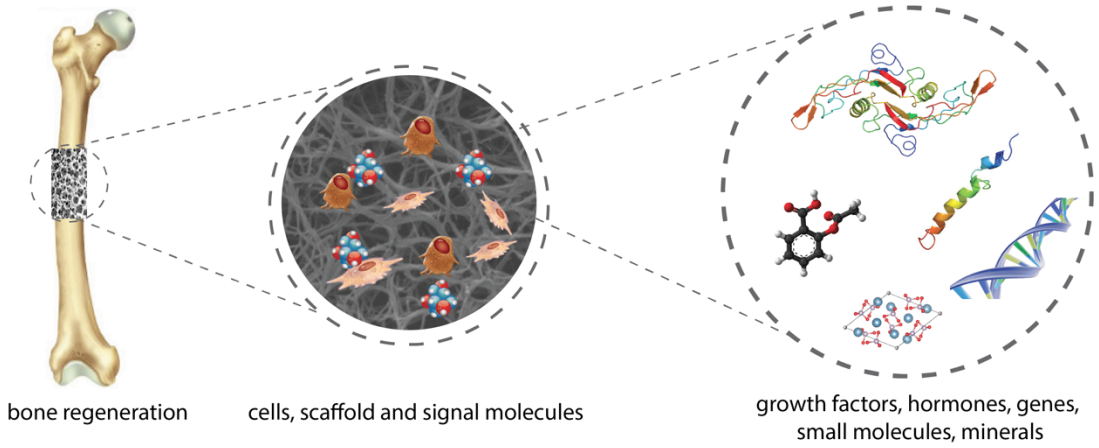

Figure 2.1.1 Bone tissue engineering involves cells, scaffold and signal molecules. Signal molecules can be incorporated into the scaffold to recapitulate the microenvironment and stimulate bone healing. While growth factors have been widely used, other types of signal molecules are under intense investigation to exploit their potential in promoting bone regeneration.

2.2 Bioactive Signal Molecules

Various biological signal molecules play important roles in regulating cellular activities and tissue development[49]. Traditionally the term "growth factor" refers to proteins or polypeptides capable of promoting tissue growth[50], but it does not accurately reflect other types and functions of bioactive signal molecules in certain situations. Besides the typical protein or polypeptide-based growth factors, many other types of signal molecules such as hormones and nucleic acids have also demonstrated great potential in promoting bone tissue regeneration. Each category of molecules possesses unique physiochemical properties and biological mechanisms, which require specific delivery system design strategies.

Growth factors

In this chapter the term “growth factor” refers to soluble, secreted signaling polypeptides or proteins, which can be synthesized by a wide variety of cells and play an important role in the regulation of cell proliferation, migration, differentiation and ECM synthesis[51]. Growth factors usually exhibit short-range diffusion through the ECM and act locally[52]. A multitude of growth factors are involved in regulating the bone regeneration process and some of these growth factors (such as bone morphogenetic protein-2 (BMP-2)[53, 54], BMP-7[43, 55, 56], vascular endothelial growth factor (VEGF)[57, 58] and fibroblast growth factors-2 (FGF-2)[59, 60]) have demonstrated great potential in numerous preclinical studies. Unfortunately, the promising results seen in animal models have yet to be translated successfully to human trials, mainly due to concerns over their side effects and safety. VEGF for example, has a strong tendency to induce vascular permeability, which may lead to systemic hypotension and edema[61, 62]. Most of the complications concerning BMPs are related to heterotopic bone formation[63] and BMP-2 is also known to increase risk of cancer development[64]. The majority of growth factors that are currently used in clinical settings are delivered at a high enough dose to ensure the local concentration reaches therapeutic levels. Negative side effects associated with growth factors derive from poorly controlled drug release and supra-physiological level dosage. Therefore, there is a strong need to develop a delivery system for growth factors that allows the effective low dose to be delivered through precisely controlled release kinetics and tight localization *in vivo*.

Endocrine secretion molecules (e.g. hormones) are a class of signaling molecules which are produced by glands in multicellular organisms and then transported by the circulatory

system to target distant organs to regulate physiology, including tissue growth, function, and development[65]. To reach their potential in promoting tissue regeneration, these molecules need to be delivered at specific time points and follow a certain pattern[66, 67]. For example, parathyroid hormone (PTH) is a hormone that is crucial to regulating bone remodeling, where bone tissue is alternately resorbed and rebuilt over time[68]. When given exogenously, pulsatile PTH administration promotes bone formation, whereas continuous PTH exposure results in bone resorption[29]. Currently, PTH is the only FDA approved anabolic (i.e. bone building) agent for the osteoporosis treatment in the US[30, 69] and its anabolic action has also been demonstrated to improve osseous healing[70, 71]. Although PTH has great potential as a regenerative agent to improve bone formation, its current administration via systemic injection is not suitable for localized defect regeneration. An engineered pulsatile system capable of delivering PTH to the local site to preserve its bioactivity and to induce the optimal anabolic action is highly desired[32].

Nucleic acids

Nucleic acids alter cellular function and modulate the tissue regeneration process at the genetic level. DNAs and mRNA encoding for growth and differential factors can enable protein expression for an extended period of time[72]. For example, genes encoding for BMPs[73, 74], FGF-2[75], insulin-like growth factors (IGFs)[76], TGF-β [77], platelet-derived growth factor (PDGF)[78], and VEGF[79] have been shown to induce bone regeneration. In addition, the use of non-coding genes such as siRNA[80, 81] and miRNA[47], which regulate gene expression and cell activity, have recently emerged as novel therapeutic agents and also demonstrated great potential in bone repair. Owing to

electrostatic repulsion, negatively charged nucleic acids (DNAs and RNAs) cannot easily cross the negatively charged cell membrane[82]. The rapid degradation of some RNAs *in vivo* presents another challenge*[83]*. For these reasons, gene vectors are usually used to protect and deliver genes *in vivo*. Viral and non-viral vectors have been used to deliver genes into the desired cells and each different vector has its advantages and disadvantages[84, 85], which will be discussed in detail in the next section.

Other bioactive agents

A series of antibiotics and anti-inflammatory drugs have been also considered in combination with scaffolds[86] for tissue engineering including bone repair[40]. The aim is to reduce the bacteria or inflammation in a wound to a level at which wound-healing processes can take place. It has been shown that sustained antibiotic release was effective in controlling infection at the bone defect caused by debridement, and supported bone tissue healing[87].

Minerals such as calcium-phosphonate (CaP) and hydroxyapatite have been widely used in a variety of orthopedic implants and scaffolds[88-90], and these minerals and the ions released have been demonstrated to promote pre-osteoblast proliferation and differentiation[91]. Uniform and controlled deposition of minerals throughout the implants can be achieved through various methods. Simulated body fluid (SBF) incubation was originally developed to achieve mineral deposition onto scaffolds but this process was time-consuming, taking several weeks to form ideal mineral deposition[92]. Subsequently, mineral electrodeposition has been developed and was able to rapidly generate mineralized CaP coating on the scaffold surface. This approach offers significant advantages over

conventional SBF mineralization in that a high quality mineral coating can be achieved within a short time (0.5-3 hours typically) and the surface topography of the deposits can be tailored by controlling the electrochemical process parameters[93].

2.3 General Considerations in Delivery System

Although different types of signaling molecules require specific delivery mechanisms, there are important universal considerations and factors in the design of delivery platforms. Specific strategies and examples will be discussed in the next section.

Spatial controlled release within the tissue

The concentration and spatial distribution of signal molecules play a key role in tissue regeneration and development[94]. The population of nearby cells sense the concentration gradient of signal molecules and responds in a concentration-dependent way[95]. The drug concentration and spatial distribution near the delivery vehicle is the major determinant of the drug efficacy and effects. For example, numerous studies have shown that there is a threshold dose of BMP for *in vivo* bone induction and the amount of bone formation is largely dependent on the BMP dose used. In a rat femur segmental defect model, 1.4 μg of BMP2 did not result in union, whereas a dose of 11μg was sufficient for complete union[96]. Therefore, it is crucial to deliver an effective amount of drug to the defect site. In general, the local drug concentration and spatial distribution is determined by both tissue physiology (i.e. drug diffusion rate and elimination rate) and properties of the delivery system properties (drug release rate and dosing).

Insufficient control over the spatial distribution of the drug can lead to potential side effects and toxicity in non-target tissues. For example, the most recognized side effect

related to BMP-2 use is ectopic bone formation, most likely due to BMP-2 leakage outside of the implant site[97]. After spinal fusion surgery, ectopic bone formation occurs in the patients who were administrated BMP-2 at a rate of nearly 6 times (70.1%) more than the control patients who were not administrated BMP-2 (12.9%)[98].

Biomimetic temporal controlled release

The bone healing process involves multiple phases: the initial inflammatory phase, soft callus formation, mineralization, and bone remodeling. Multiple factors are involved in the different phases in certain time-dependent or temporal patterns[99]. Biomimetic drug delivery strategies have been exploited to simultaneously or sequentially deliver multiple signals to mimic the natural healing process to enhance therapeutic effects synergistically and optimize the osteogenic outcome[27, 49]. It is known that natural osteogenesis is preceded by angiogenesis in the bone repair process. A combination of angiogenic (such as VEGF), cell recruiting (such as PDGF) and osteogenic (such as BMPs) growth factors has been designed and demonstrated a synergistic effect that is more beneficial to bone repair than any one growth factor delivered alone[100, 101].

Temporally controlled release is also critical for some drugs (e.g. endocrine secretion) that need to be delivered at specific time points and follow a certain pattern of distribution to be effective. Even given the same dose of a drug, distinct release patterns often lead to dramatic differences in the therapeutic outcome[31]. Therefore, precise control over the temporal distribution of the drug is essential to achieving the desired therapeutic effect[39].

Biocompatibility and safety issue

Biocompatibility and safety are required for DDSs and tissue engineering applications. Many different materials can be used to fabricate the delivery vehicles, including synthetic polymers, natural polymers and inorganic materials[102]. The materials and their degradation products must be safe and biocompatible to not cause excessive immune responses[103]. Typical synthetic polymers include poly(α-hydroxyester)s, polyanhydrides, polyorthoesters, poly(ethylene glycolide) (PEG), and poly(vinyl alcohol) (PVA)[103, 104]. The most commonly used poly(α-hydroxyester)s are homo- and copolymers of lactide and glycolide, because of their wide range of biodegradability and well-accepted biocompatibility[105]. Some natural polymers such as fibrin, collagen, chitosan, alginate, and hyaluronic acid have also been widely used as these materials have an innate capacity to interact with cells and undergo cell-mediated degradation[106]. Silica-based inorganic materials have been investigated as drug carriers in preclinical studies and while they show low cytotoxicity, most of them are non-degradable in the human body[107, 108].

Additionally some responsive drug delivery systems require external stimuli such as pH[109, 110], temperature[111, 112], light[113, 114], ultrasound[115, 116], electrical[117] and magnetic fields[118]. The safety issues associated with application of these stimuli also require careful investigations. Safe and less-invasive stimuli are more likely to translate into clinical applications.

2.4 Biomimetic Strategies in Drug Delivery

The importance and complexities of bioactive signal molecules in regulating cellular activities and bone healing suggests that sophisticated DDSs mimicking the natural healing

process are critical to achieve optimal therapeutic effects and thereby the desired bone regeneration outcome. Various methods and strategies have been exploited to enable spatiotemporal control over the drug release kinetics (Figure 2.4.1).

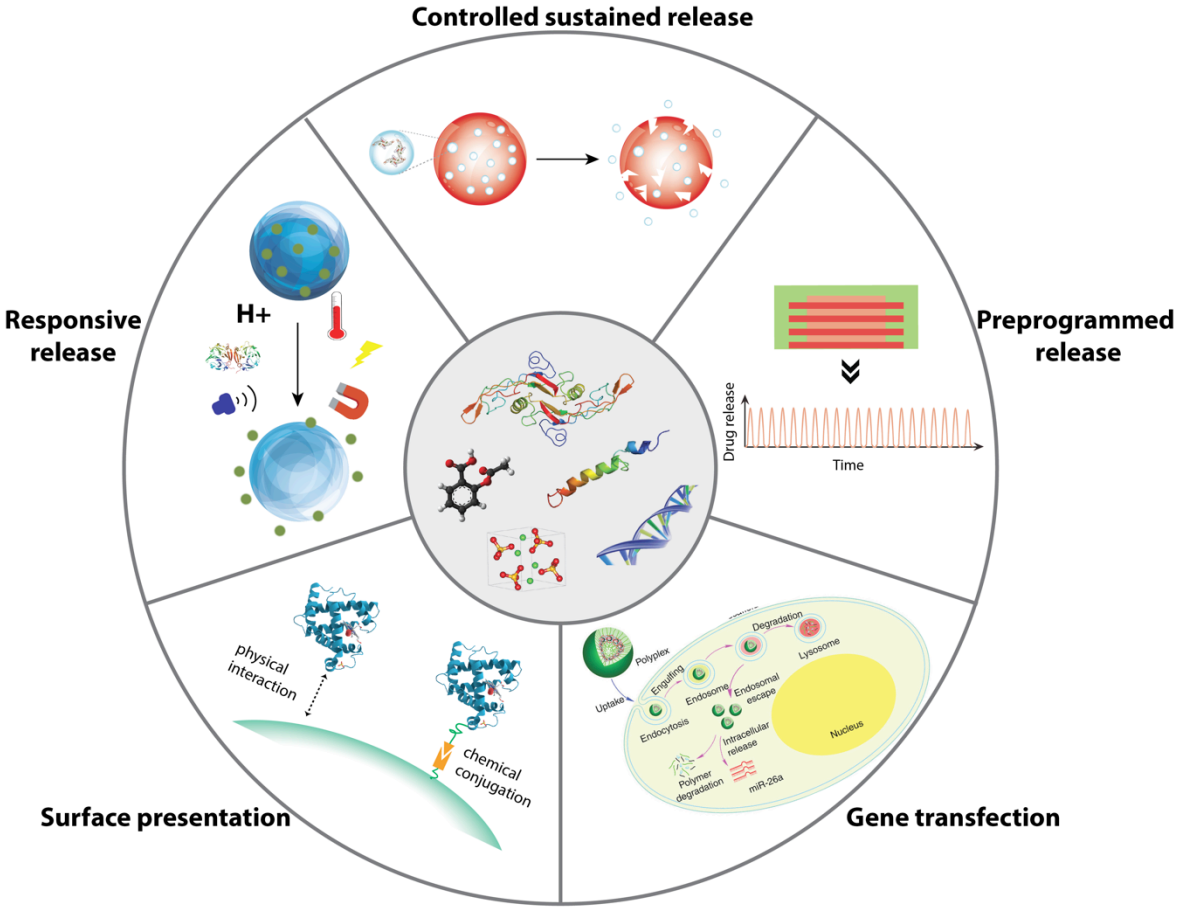

Figure 2.4.1 Various drug delivery strategies for signal molecules. Different types of signal molecules require specific delivery system to achieve the optimal therapeutic effects. Delivery systems, which have been developed and are currently used and/or are under investigation for bone tissue engineering applications, include surface presentation, controlled sustained release, preprogrammed release, responsive release and gene transfection. Copyright © 2016 by Nature Publishing Group, reprinted with permission of Nature Publishing Group, from Zhang et al

Surface presentation

Various techniques have been explored to present drug molecules on the surface of the scaffold, so that they are available for contact with cells migrating into the scaffold, acting

as localized biological cues to regulate cell behavior[119]. Surface presentation enables site-specific drug delivery and could reduce potential off-target side effects of the drugs. Physical adsorption and chemical conjugation are the two main methods for presenting drug molecules on the scaffold surface.

Physical adsorption usually relies on an interaction between the scaffold surface and the drug molecules, such as electrostatic interactions, hydrogen bonding, and hydrophobic interactions[120, 121]. The scaffold surface can be further modified to improve its affinity for drug molecules[122]. For example, heparin has often been used to modify the scaffold surface chemically or physically to improve binding of the growth factors to the scaffold. There are many studies that report the controlled release of BMPs, PDGF, VEGF and other growth factors in a heparin-modified scaffold[123-127]. While there are certain preferred features, the passive adsorption approach could be of limited control over drug retention and result in burst release or diminished bioactivity in some cases[119]. Physiological conditions such as temperature, acidity and mechanical movement could also interfere with the physical interactions, affecting the effectiveness of surface presentation.

Chemical conjugation, or covalent bonding, offers prolonged and more stable drug molecule presentation than the physical adsorption method. For this process, scaffold surface needs to be activated with functional groups, which can then conjugate with drug molecules through proper chemical reactions[128]. However, in many cases, commonly used polymeric materials for bone tissue engineering are biodegradable polyesters, which lack reactive functional groups. In these instances, there are various methods to activate the scaffold surface via post modification (such as plasma treatment, chemical etching, surface

coating) but it should be noted that the activation treatment conditions need to be properly adjusted to maintain scaffold integrity[129, 130]. Another approach involves functionalizing the matrix materials or blending functional molecules with the main matrix materials prior to the scaffold fabrication. A primary concern is that the conjugation reaction may lead to a change in the conformation of the drug molecule, especially for biologics and result in loss of the bioactivity. Therefore many drugs are pre-modified (e.g. conjugating to a PEG spacer)[131, 132] or drug mimics (growth factor peptide mimics)[133] are utilized. Various bioconjugation reactions have been investigated and the reactions conducted in aqueous solution or under mild reaction conditions are particularly favorable. Amidation, esterification and click reactions are among the most commonly used reactions[134]. For example, BMP2 mimicking peptide, P24, has been conjugated onto acrylic groups-bearing PLLA nanofibrous (NF) scaffold via the thiol-ene click reaction[135]. The scaffold decorated with BMP-mimicking peptide was able to retain its bioactivity and induce significant osteogenic differentiation of rabbit bone marrow-derived mesenchymal stem cells (BMSCs) compared to a non-modified scaffold, inducing ectopic bone formation in nude mice[133].

Controlled sustained release

Controlled sustained release of drug molecules is the prominent drug delivery strategy in bone tissue engineering and aims to provide the desired drug concentration at the local regeneration site. Physical encapsulation of the drugs into polymeric materials is the most commonly used method and the release kinetics can be controlled by the matrix degradation and drug diffusion rate[136]. The drugs can be either encapsulated inside the

scaffold matrix[137] or in separate delivery vehicle such as micro/nanoparticles[138], liposomes[139].

Direct loading of the drugs into the scaffold matrix is the simplest way to achieve sustained drug release and many techniques have been developed including solvent casting, in situ polymerization, phase separation, electrospinning, gas foaming and more[140-142]. The major challenge with this strategy is to protect the bioactivity of the drugs from the harsh scaffold fabrication process. Most growth factors and other type biologics cannot be dispersed directly in polymer solution as the solvent can temper their bioactivity. Another drawback of this strategy is the lack of control over the release kinetics. For example, growth factors have been electrospun into NF scaffolds but they usually aggregate on the outer surface, resulting in the burst release[119].

Encapsulating the drugs in separate delivery vehicles instead of directly within the scaffold matrix is a promising alternative strategy. Micro/nanospheres have long been used for drug encapsulation and various methods have been investigated to retain the drug bioactivity and achieve controlled release kinetics[43]. Additionally, a solvent annealing technique has been developed to immobilize the drug-loaded microspheres on the scaffold surface[143]. This method enables single or multiple drugs to be released in a spatially and temporally controlled fashion throughout the scaffold and also enables the drug release profiles to be individually designed without altering the scaffold structure. BMP7-loaded microspheres have been immobilized onto cell-free NF scaffolds, which were tested in subcutaneous implantation in rats[43]. BMP-7 was released from the scaffold-bound microspheres in a controlled fashion with high bioactivity and induced bone formation within the scaffold.

In contrast, the scaffolds with BMP-7 adsorbed were unable to induce osteogenesis, owing to the loss of bioactivity and short release duration of the BMP-7. In another study, such BMP-loaded microspheres mixed with an injectable scaffold and stem cells of apical papilla induced ectopic mineralized dentin formation[144].

Drug molecules can also be incorporated into liposomes, however, they are relatively unstable in a physiological environment, which results in short release duration[145, 146]. Sustained drug release can also be achieved using porous inorganic materials but safety and degradation issues limit their translational potential into clinical applications[147].

Preprogrammed release

While sustained delivery is a simple form of preprogrammed delivery, more sophisticated preprogrammed delivery systems are designed to utilize the spatiotemporal sensitivity of a patient to drugs to achieved optimal therapeutic effects[148, 149]. A common approach to achieve preprogrammed drug delivery involves multi-compartment constructs where drugs are pre-loaded in different compartments that have different release kinetics[42, 150]. Bulk- and surface-eroding polymers have been used as matrix materials for the compartments and can be engineered to achieve the desired release kinetics. Another strategy takes advantage of the development of nano/microfabrication techniques and functional materials to make drug delivery chips and responsive vehicles and the drug release can be either programmed in the chip or triggered by remote stimuli[151]. Preprogrammed DDSs are used to facilitate sequential release of multiple drugs to enhance bone regeneration. Instead of delivering single molecule at high doses, the safety and efficiency of the delivery system can be improved by delivering multiple signal molecules

at relatively low doses in a sequential manner. DDSs loaded with multiple osteogenic and /or angiogenic factors have shown improved osteogenic outcomes[55, 150, 152, 153].

For some drugs, different release patterns for the same drug can lead to distinct therapeutic outcomes, so achieving the specific drug release pattern is essential to achieve the desired therapeutic effects. As previously discussed, the anabolic or catabolic action of PTH highly depends on its delivery pattern. Pulsatile PTH administration improves bone microarchitecture, mineral density, and strength, whereas continuous exposure of PTH leads to bone resorption. A pulsatile delivery device has been developed and achieved PTH pulsatile delivery for 4 d but this its limited time frame, the device was not evaluated for its therapeutic function[154]. An electronic microchip based PTH delivery device has been fabricated and tested for long-term remote controlled PTH pulsatile release[151]. Although the microchip device demonstrated controlled pulsatile delivery, explanation surgery is needed after the drug release is complete and the fabrication costs and safety issue are also of great concern. A biodegradable pulsatile delivery device that degrades and is absorbed *in vivo* without the need to be surgically removed is highly desirable.

Responsive release

Responsive delivery systems that release drugs in response to local physiological signals or external stimuli have received increasing attention[155]. Such on-demand drug release could likely reduce side effects caused by excess drug dosing found in conventional administration[155, 156]. Commonly used stimuli include pH, temperature, electric or magnetic field, ultrasound, light irradiation and biomolecules. These responsive systems involve “smart” responsive materials, so that the materials undergo considerable changes

in response to the stimuli and thereby change the drug release kinetics (e.g. release rate, dosing and duration).

Responsive delivery systems have been used in systemic treatments, including most commonly cancer therapy[156, 157] but with limited success in tissue engineering applications. The regeneration process often requires long-term drug release, while most of the responsive systems suffer from the short release duration and irreversible responsive release[158]. Additionally, the biocompatibility and biodegradability of the functional materials and the safety concerns associated with the external stimuli limit their application in tissue engineering.

One promising class of responsive delivery systems for tissue engineering is the biomolecule-sensitive system[159]. This kind of bio-inspired system is triggered by the local environment and would not need external stimuli. A protease cleavage-based triggering mechanism has been developed to initiate local drug release. A metalloproteinase (MMP) is a protease that is upregulated in angiogenesis and cell invasion. A MMP-cleavable crosslinker has been incorporated into a PEG-based hydrogel for local rhBMP-2 delivery to the site of bone defects[160]. Prior to MMP exposure, BMP-2 remained as a precipitate within the PEG matrix and was not released over a period up to 5 d. After implantation in the bone defect, cells migrate and invade the hydrogel matrix resulting in MMP secretion and the degradation of the MMP-sensitive PEG network. This causes BMP-2 dissolution and release, leading to efficient bone regeneration. Similarly, cell-mediated release of VEGF has demonstrated local and controlled induction of angiogenesis[161].

Gene transfection

The goal of gene therapy is to deliver genes to the bone defect areas so they can regulate the expression of biomolecules (such as proteins) and cell activity to enhance proliferation and/or osteogenic differentiation. Gene transfection is often mediated by either a viral vector[85] (such as retrovirus, adenovirus, adeno-associated virus, herpesvirus) or a non-viral vector[162, 163] (such as polycations or liposomes). Viral vectors have shown high gene transfection efficiency, however, associated safety issues, immune response, and side effects are of serious concern and greatly limit the translation of this approach into clinical use. The main advantage of non-viral vectors over viral vectors is their superior safety with additional benefits including ease of fabrication and scale up. Liposome-based transfection vectors including Lipofectamine (a commercial non-viral vector) have been explored to transport genes into cells *in vitro* but most liposomes exhibit low stability in the physiological environment[164] . Polymeric non-viral vectors, including polyethylenimine (PEI), chitosan and other polycation-based vectors often suffer from low efficiency and considerable cytotoxicity[165, 166]. Moreover, both viral and non-viral transfection systems only allow for one-time or short-term delivery, whereas sustained release is typically required for bone regeneration. For this reason, there have been a limited number of gene therapies capable of *in vivo* bone regeneration reported[167].

New approaches are being actively pursued to overcome current limitations in gene delivery for bone tissue engineering. Recently a water-soluble hyperbranched polymeric vector was developed that can incorporate the desired genes when it assembles into a stable nanoshell structure[47]. This unique vector-gene complex, or polyplex, provides excellent

stability that polyplexes remained intact even after harsh sonication. Polyplexes loaded with miRNA-26a have been encapsulated in biodegradable polymer microspheres[47] to achieve long-term controlled miRNA-26a release. This delivery system enabled two-stage control over the gene release: sustained release of the polyplexes from the microspheres and efficient gene transfection into cells by the polyplexes. Microspheres loaded with the polyplexes were immobilized within the scaffold to provide spatially controlled distribution to prevent undesired off-target side effects. This study showed that the delivered miRNA-26a targets Gsk-3 β to increase osteoblast activity, resulting in the regeneration of critical-sized calvarial bone defects in both healthy and osteoporotic mice.

2.5 Conclusions

Significant progress has been made both in the understanding of the molecular mechanisms in tissue development and regeneration and in the design of biomimetic biomaterials. Various biomimetic DDSs have been developed to mimic the natural healing process and provide spatiotemporally controlled drug release. The integration of DDSs with bone implants or scaffolds could lead to advanced tissue engineering therapy for bone defect repair. Biomimetic DDS can also serve as a novel platform to study the basic biology of how signal molecules manipulate cell activity and tissue development.

A variety of biological and engineering challenges remain to be addressed in the future. Further qualitative and quantitative understanding of the complex interaction and cooperative signaling between the signal molecules, microenvironment and physiology could provide guidance to achieve precise spatiotemporal control and prediction of drug release and distribution. Development of more sophisticated delivery systems should rely

on multidisciplinary approaches that are based on biological principles and combine nanotechnology, advanced fabrication, and functional materials to deliver the required signals to the desired cells at the right time. Further research is needed to develop and optimize delivery systems for translation to clinical practice.

CHAPTER 3

Preprogrammed PTH Delivery Device

3.1 Introduction

PTH is currently the only FDA-approved anabolic agent for the treatment of osteoporosis in the US[69], however its anabolic or catabolic action depends on the pattern of PTH delivery. Intermittent (pulsatile) administration improves bone microarchitecture, mineral density, and strength, whereas continuous exposure of PTH leads to bone resorption[29, 68]. Current intermittent PTH treatment requires daily subcutaneous injection, which is neither a convenient nor a favorable choice of patients[154]. Thus, there is a clear clinical need for a patient-friendly alternative treatment capable of pulsatile PTH delivery, which would improve patients' compliance and thereby their therapeutic outcome.

A variety of delivery strategies have been explored to achieve controlled release in a pulsatile manner from various platforms such as micelles[168, 169], liposomes[170, 171], micro/nanoparticles[172, 173], hydrogel[174, 175], and microchips[176]. Based on the triggering mechanisms, these pulsatile delivery systems can be classified into stimuli-responsive pulsatile release systems and self-regulated pulsatile release systems. In stimuli-responsive systems, drug carriers release the loaded drug when triggered by external stimuli[177, 178] such as temperature[111, 112], pH[109, 110], light[113, 114], enzyme[179, 180], ultrasound[181, 182], biomolecules[183], and electric[117] or magnetic

fields[118]. These responsive systems can achieve pulsatile release but have also shown various limitations, such as an initial burst release, an irreversible triggered release, a short time interval (seconds to minutes), or a short release duration. Moreover, critical considerations have to be employed regarding the safety and biocompatibility of these responsive systems because many of the stimuli cannot be easily and safely utilized in patients and most of them are constructed with nondegradable polymers or inorganic materials[184]. Due to these limitations, few of them have been successfully implemented in patient care as a pulsatile PTH treatment. In self-regulated release systems, drugs are loaded in reservoirs sealed by a barrier material, which is usually composed of an erodible or biodegradable polymer[138, 154]. After the barrier material is eroded or degraded, drugs are rapidly released from the inner reservoir. The control over the pulsatile kinetics depends on the properties of the barrier materials and the design of the reservoir structure. In addition to the pulsatile releasing feature, the ability of long-term release is also critically important in developing a PTH delivery system. A series of studies indicate the beneficial effects of intermittent PTH administration on bone[185, 186], and its prominent anabolic action during three weeks of exogenous administration in an *in vivo* osteoregeneration mouse model[187]. Six-week systemic PTH administration was further demonstrated to be beneficial to osseous regeneration in a clinical human study[71]. Therefore, a delivery system capable of long-term release is needed to cover the effective therapeutic window. Previously, we developed a self-regulated pulsatile delivery device and achieved daily release of bioactive PTH for 4 d[154]. However, due to its limited time frame, the device was not evaluated for its therapeutic function. The challenge lies in the

structural design and fabrication techniques to enable a large number of controlled release pulses over a long duration. Ultimately, a biodegradable device that degrades and is absorbed *in vivo* without the need to be surgically removed is desirable.

Herein, the aim of this work was to develop an advanced patient-friendly delivery system, which would overcome the hindrances of the current treatment regimen (daily injection) and achieve the optimal anabolic effect with preprogrammed PTH delivery. We designed implantable and biodegradable polymeric devices using a surface erosion polyanhydride (PA) developed in our lab[188] and advanced fabrication techniques to achieve preprogrammed daily pulses for 21 d. We also developed a device, which achieved continuous PTH release over 21 d. Henceforth, the devices served as a platform that allowed us to study the distinct PTH delivery patterns (pulsatile vs continuous) and their therapeutic effects on bone.

3.2 Pulsatile Delivery Device Fabrication

We fabricated a multipulse PTH delivery device consisting of alternating drug layers and isolation layers via an electrostatic-assisted layer-by-layer stacking technique. The isolation layer was made of biocompatible PA, which is bio- degradable through surface erosion. Bovine serum albumin (BSA) (control protein) or PTH was mixed with alginate to form the drug layer. Alginate was used as the carrier because of its biocompatibility and processability. We first investigated the surface potential of the two layers using Kelvin probe force microscopy (KPFM)[189, 190]. A PA or alginate-PTH layer was coated onto a gold substrate. The relative surface potentials of the two polymeric layers were calculated using the gold surface as reference (0 mV) (Figure 2.2.1 A).

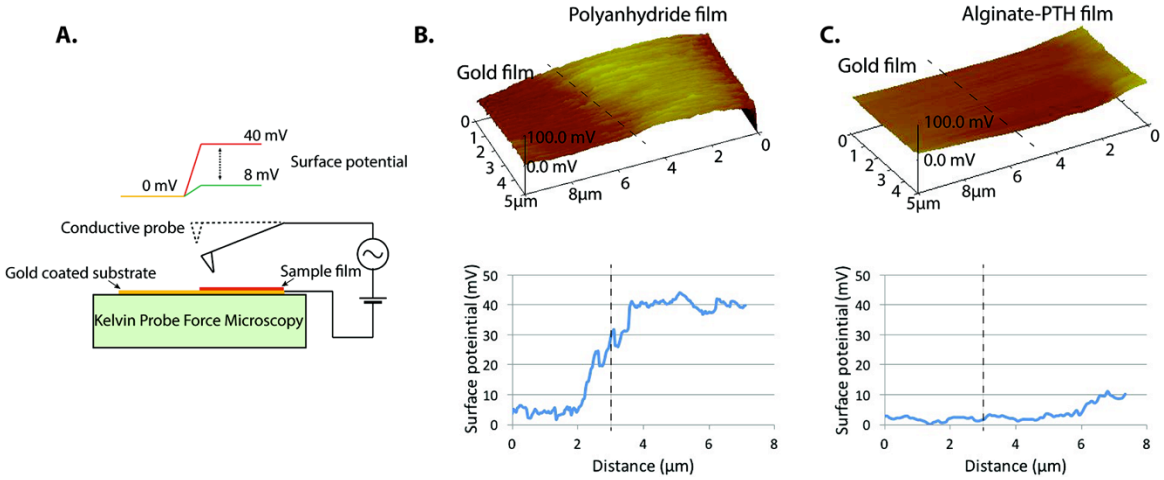

Figure 2.2.1 Surface characterization of the PA films and drug films: Schematic illustration of the KPFM used to measure the surface potential of the films (A); Surface potential map and the potential difference between gold substracte and a PA film (B) or alginate-PTH film (C).

We found that the PA layer was positive and the drug layer was nearly neutral. The surface potential of the PA layer (+40 mV) was about six times higher than that of the drug layer (+7 mV) (Figure 2.2.1 B and C). The intrinsic surface potential difference facilitated the generation of opposite electrostatic charges on the two layers. We generated positive charges on the PA layer by rubbing it with a Teflon film that has a strong tendency to gain electrons. Conversely, we generated negative charges on the drug layer by rubbing it with a glass slide that has a strong tendency to lose electrons (Figure 2.2.2 A).

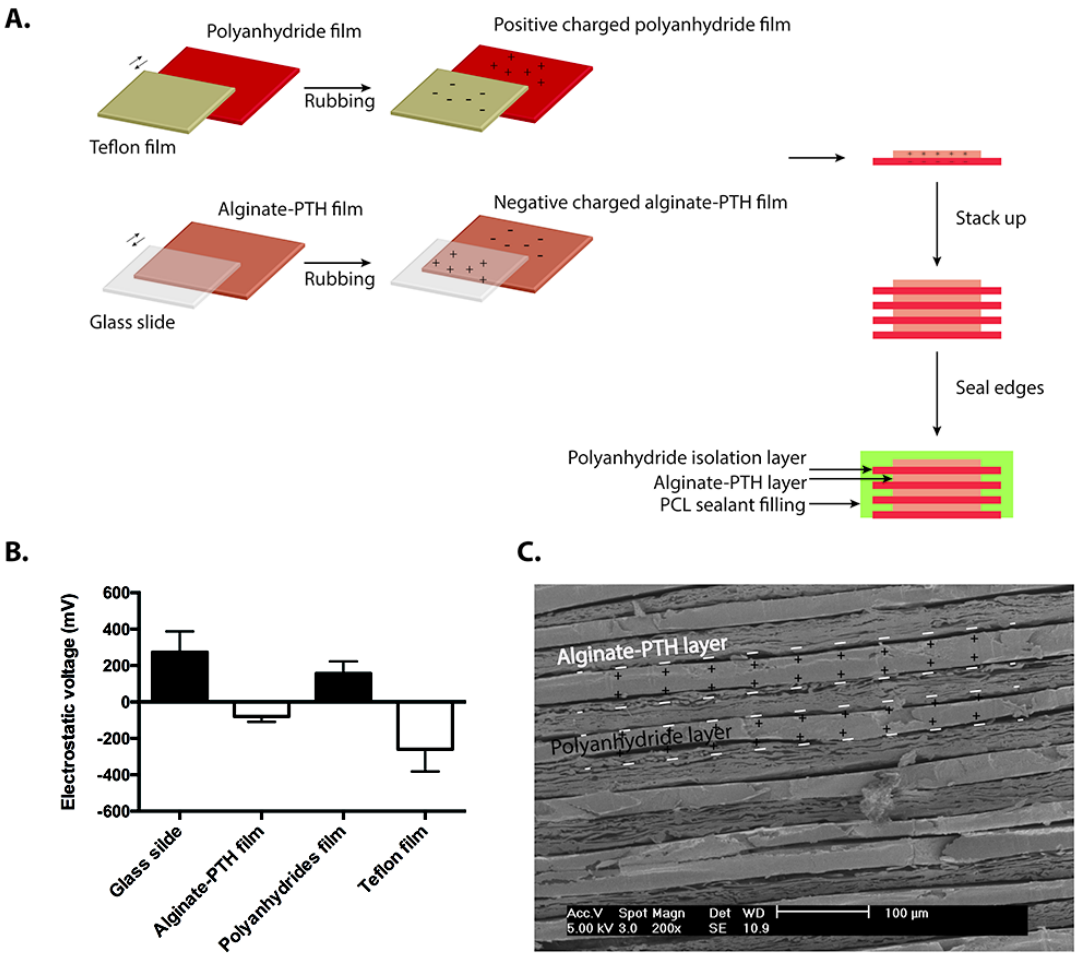

Figure 2.2.2 The illustration of the rubbing, stacking, and sealing process to fabricate the pulsatile release device. A) The fabrication process of a multi- pulse delivery device via electrostatic-assisted layer-by-layer stacking technique. B) The electrostatic potential of the different layers after the rubbing process. C) A cross-sectional SEM micrograph of the multilayer pulsatile release device.

The electrostatic voltages between the two different layers were measured with an electrostatic meter and the results indicated that we were able to generate opposite charges on the PA layer (+160 mV) and the drug layer (–80 mV) (Figure 2.2.2 B). One positive PA layer and one negative drug layer were attracted to each other and formed a bilayer structure. The bilayers were then stacked into a 21-bilayer structure. This technique

enabled close contact between drug layers and isolation layers and eliminated air gaps (Figure 2.2.2 C). Constructively, the drug layers were designed to be smaller than the isolation layers in diameter, preventing possible contact between adjacent drug layers, which could lead to leakage of drug between layers. The side and the bottom of the device were sealed with polycaprolactone (PCL), a slow biodegrading polymer[191], thus allowing unidirectional drug release from the top only.

3.3 Pulsatile Device Characterizations and Release Kinetics

The pulsatile release profile was preprogrammed by modulating the chemical composition and physical thickness of the isolation PA layer. The poly(SA-CPP) (sebacic acid (SA) and 1,3-bis (*p*-carboxyphenoxy) propane (CPP)) has been used as components of FDA-approved medical devices in human clinical application[192]. However, due to the hydrophobicity of the poly(SA-CPP), the hydrolytic degradation usually takes too long for an ideal pulsatile release profile. Therefore, we incorporated polyethylene glycol (PEG) segments into the poly(SA- CPP) and prepared a three-component PA (poly(SA-CPP-PEG)) by condensation polymerization as described previously[188]. Nuclear magnetic resonance (NMR) spectroscopy confirmed the successful synthesis as the spectrum showed a set of typical poly(SA-CPP-PEG) peaks (Figure 2.3.1).

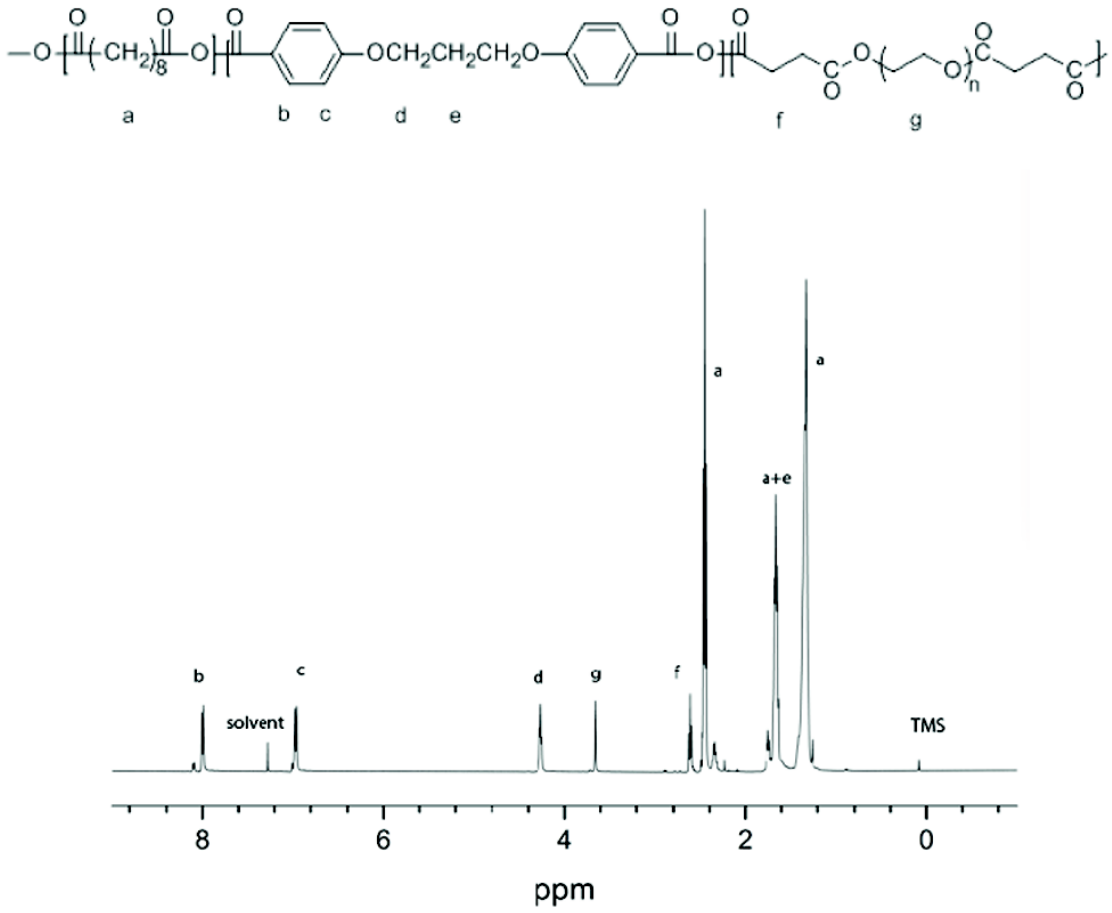

Figure 2.3.1 ^{1}H NMR (400 MHz, CDCl3) spectrum of an poly(SA-CPP-PEG).

Scanning electron microscopy (SEM) was used to examine the PA degradation. The cross section of the uneroded polymer was uniform, while there were evident pores in eroded portions of the treated samples (Figure 2.3.2). The erosion front moving with time was an indication of surface erosion. The PA containing more PEG segments exhibited a faster erosion rate than those containing fewer PEG segments. It was also observed that the eroded surface roughness increased with increasing PEG content of the PA. The new PEG-containing PA retained the surface erosion properties of the poly(SA-CPP) while imparting a large range of tunable erosion rate.

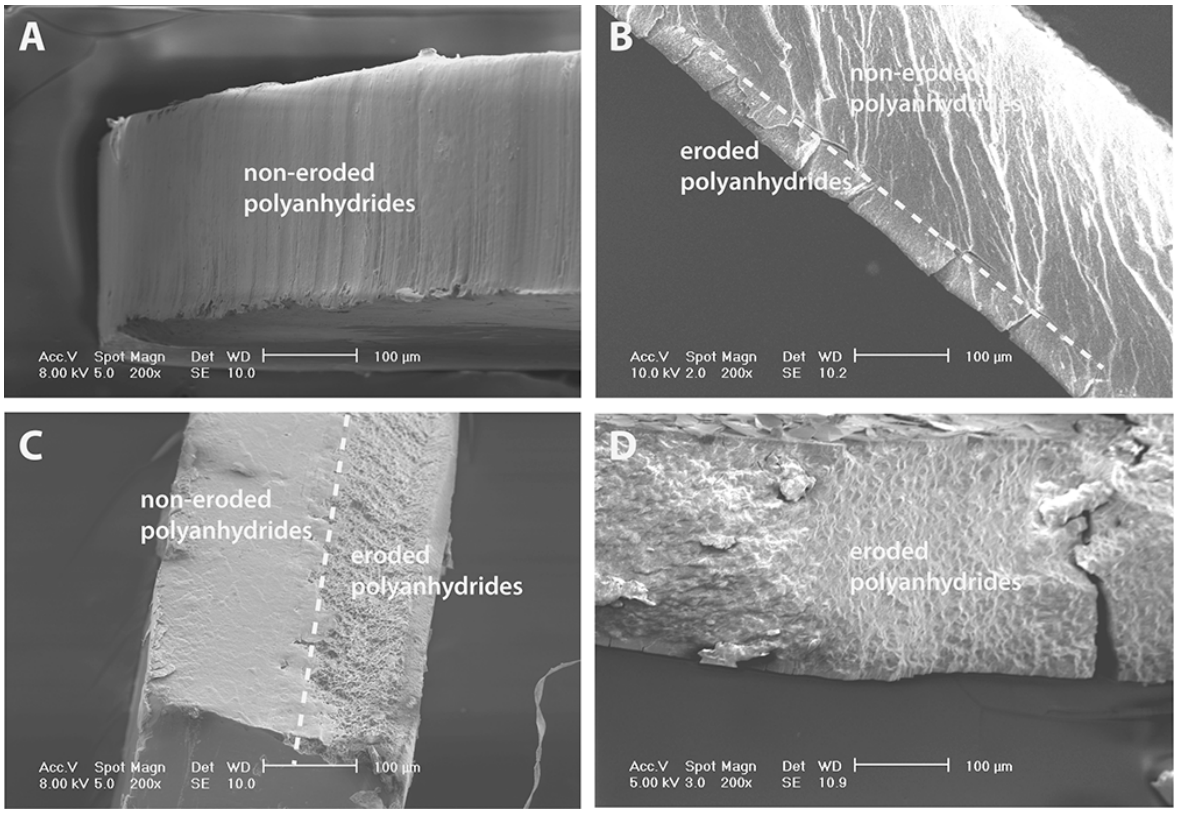

Figure 2.3.2 Degradation behavior of PA films. SEM micrographs of untreated PA stored under vacuum (A) and PA specimens with different compositions after erosion in 0.1M PBS at 37°C for 12 h: (B) SA/CPP/PEG=80/20/0, (C) SA/CPP/PEG=80/20/2, (D) SA/CPP/PEG=80/20/10.

The "dissolution time" of the surface erosion polymer layer is proportional to the thickness of the layer. Therefore, the thickness of each isolation layer can be adjusted to achieve desired time intervals between adjacent pulses of drug release. PA isolation layers of varying thickness (50, 100, and 200 µm) were used to assemble the multilayer devices, all of which were able to deliver 21 pulses of protein but with different durations (Figure 2.3.3). The average interval time be- tween two adjacent PTH peaks exhibited a linear relationship with the thickness of isolation layer and the linear regression equation is $\bar{T}(hour) = 0.26h(\mu m) + 7.5$ (Figure 2.3.3 D).

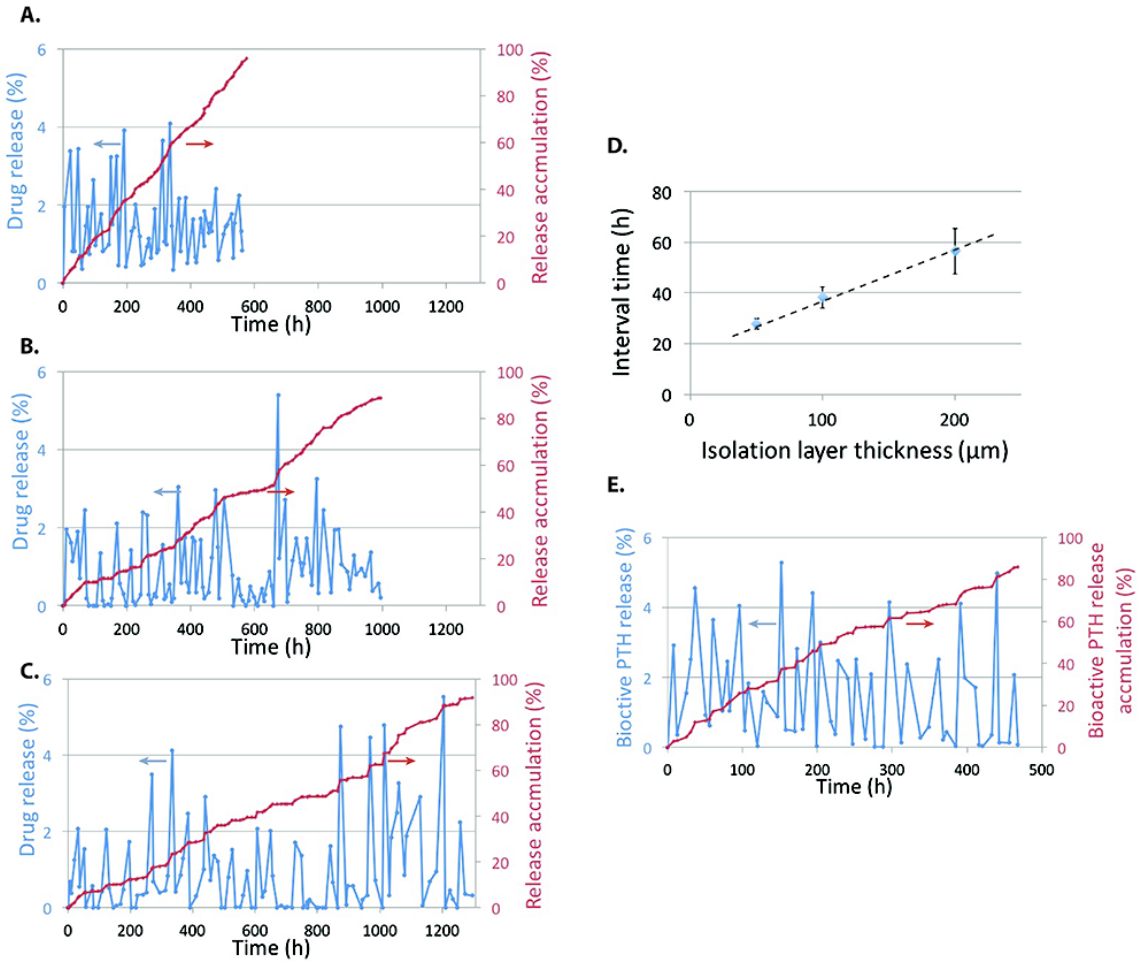

Figure 2.3.3 *In vitro* pulsatile drug release profiles. BSA release from devices of various isolation layer thickness. A) 50; B) 100; C) 200 μm. D) The average time interval between adjacent pulses exhibited linear relation with the thickness of isolation layer. E) Bioactive PTH released *in vitro* from a pulsatile drug delivery device with 50 μm thick isolation layers.

As also demonstrated, the degradation rate of the three- component PA escalated with increasing PEG content. Varying the chemical composition and the layer thickness allowed us to preprogram the release kinetics to target the entire three-week therapeutic window. The device made of 50 μm PA (weight ratio: SA-CPP-PEG = 80-20-2) could release 1 pulse per day and was therefore chosen for PTH–PTH loading. Release kinetics of bioactive PTH was determined using an adenylyl cyclase stimulation and cAMP-binding assay[193], which showed that 21 pulses of bioactive PTH were achieved over three

weeks, and that released PTH retained around 80% bioactivity (Figure 2.3.3 E)

3.4 Continuous Delivery Device Fabrication and Release Kinetics

Another device, with identical shape, size, and component materials to those of the pulsatile release device, was engineered to deliver the same total amount of PTH but in a continuous manner. This continuous device was designed to serve as a control device in order to determine the *in vivo* therapeutic effect in response to different PTH delivery patterns. We employed a double emulsion method to prepare drug-encapsulated PA microspheres, which were then compressed into a disk of the same shape and size as the pulsatile device (Figure 2.4.1 A).

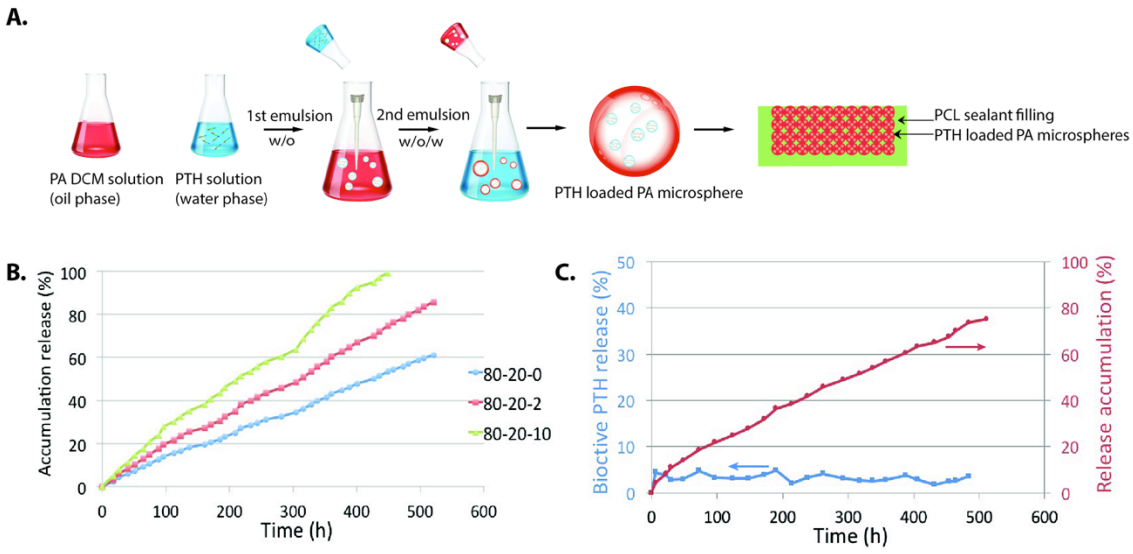

Figure 2.4.1 Continuous release device fabrication and release profiles. A) Schematic illustration of the fabrication process of the PA microspheres via double emulsion method and the construction of the continuous delivery device. B) *In vitro* release of BSA from continuous drug delivery device with different PAs. C) *In vitro* bioactive PTH released from continuous drug delivery device with PA (80/20/2).

We achieved linear continuous release of the model protein (BSA) (Figure 2.4.1 B). Interestingly, unlike most microsphere-based continuous delivery systems (such as

poly(lactic-co-glycolic acid), poly(lactic acid)[194, 195], there was no burst release and the sustained release of BSA from the new continuous release device was linear with release time. SEM observation showed that the uneroded PA particles were spherical in shape with smooth surfaces, and that during degradation in phosphate buffered saline (PBS), the size of the particles decreased, the particles lost the spherical shape, and fused together (Figure 2.4.2).

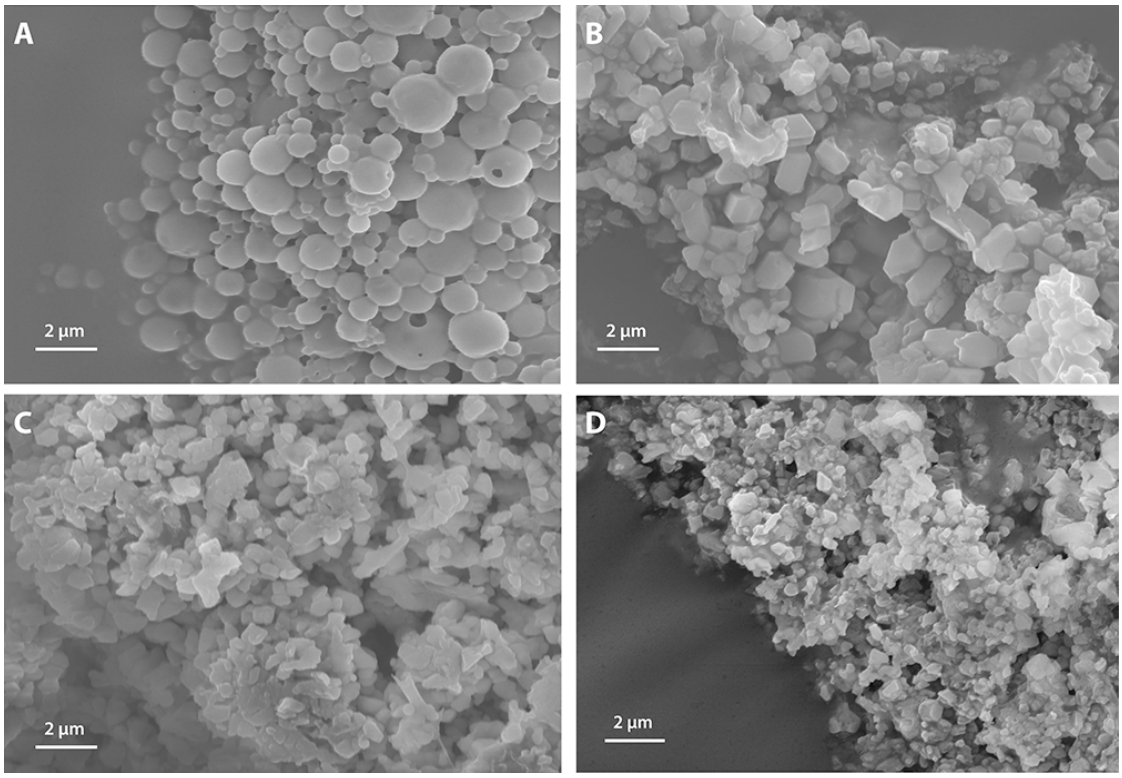

Figure 2.4.2 Degradation behavior of PA microspheres. SEM micrographs of untreated PA micrspheres stored under vacuum (A) and PA microspheres with different compositions after erosion in 0.1M PBS at 37°C for 12 h: (B) SA/CPP/PEG=80/20/0; (C) SA/CPP/PEG=80/20/2; (D) SA/CPP/PEG=80/20/10.

Instead of being porous throughout the particles, which would likely lead to a burst drug release, the surface erosion property of the PA resulted in the degradation only on the surface, thus enabling the steady linear drug release from the microspheres. In addition, the

unidirectional device design also contributed to the linear delivery kinetics, since the PBS only eroded spheres on the exposed disk surface and penetrated in a downward direction as the downmoving surface degraded.

The release kinetics of the linear release device could also be modulated by varying the chemical composition of the PA. The drug release profiles showed that the drug release rate increased with increasing hydrophilic PEG segments (Figure 2.4.1 B). The device made of the highest PEG content (10%) PA released 100% of the drug in 400 h, whereas the device made of no PEG content PA only released 50% of the drug in 400 h. The PA (80-20-2) device was able to release 90% of the drug in 21 d, which was the targeted three-week window of anabolic PTH treatment. Therefore, PTH was encapsulated into PA (80-20-2) microspheres and bioactive PTH was measured using the adenylyl cyclase stimulation and cAMP-binding assay. The bioactive PTH was released from the device following a linear release profile with bioactivity not statistically different from that of released PTH from the pulsatile device (Figure 2.4.1 C).

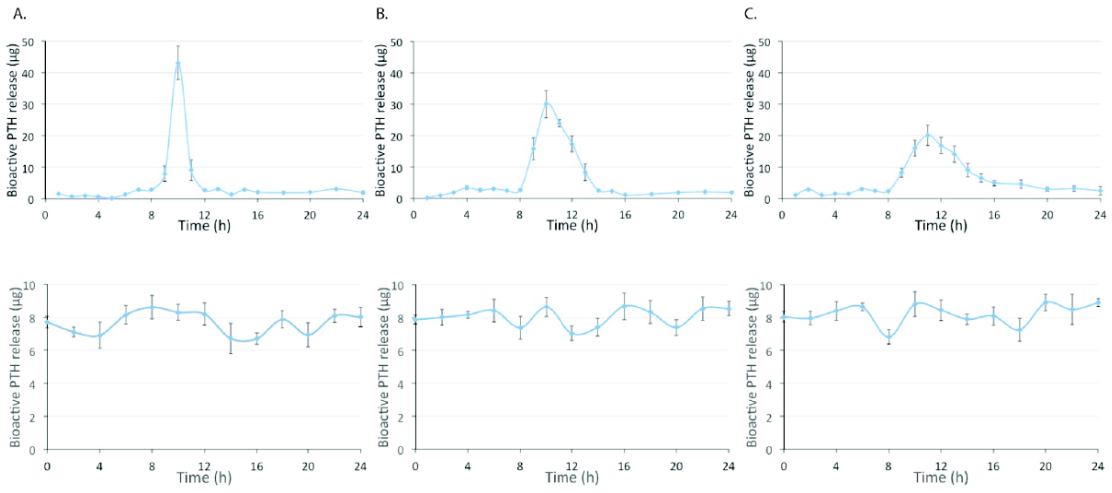

Figure 2.4.3 *In vitro* bioactive PTH release curves from the two different delivery devices. cAMP-binding assays were

used to determine the bioactive PTH amounts released from a pulsatile device (upper panel) and a continuous device (lower panel) at 3 time points: (A) day 1, (B) day 10, and (C) day 20 (n 1⁄4 3).

In addition, the released PTH from both types of devices was collected every hour on days 1, 10 and 20. The bioactivity of the released PTH was determined using the adenylyl cyclase stimulation and cAMP-binding assay. The released bioactive PTH data showed that pulsatile PTH release devolved from a sharp peak (day 1) to a relatively broader peak (day 20) over time (Figure 2.4.3 upper panel). This may be due to the increased diffusion distance of PTH through the residual PA layers. However, the pulsatile release feature was maintained over the 21 days. The bioactive PTH was released at a steady rate from the continuous device, which is consistent with the linear release behavior shown from the ELISA data (Figure 2.4.3 lower panel).

Both types of devices were constructed with the same components: the drug (PTH), isolation or encapsulation materials (PA), and sealant material (PCL) but the distribution of PTH in the devices was different, resulting in distinct release profiles. In the pulsatile device, PTH was isolated by PA in a layer-by- layer structure, whereas PTH was confined in microdomains that were uniformly distributed throughout the continuous device. The surface erosion property of the PA (SA-CPP-PEG) is essential to achieve the two types of the release kinetics. In the pulsatile device, it enabled the daily-pulsed release because the PBS could only erode one isolation layer before releasing one drug layer. In the continuous device, the surface erosion property enabled the PTH release from microspheres on the exterior surface then gradually from those inside the device, resulting in the linear continuous drug release. Moreover, the structural tunability of this three-component PA enabled a broad range of interval time in the pulsatile device or release duration time in the

continuous device.

3.4 Conclusion

Implantable and biodegradable long-term pulsatile and continuous PTH delivery devices were designed to investigate the effects of PTH delivery patterns on systemic bone therapy. The advanced materials and fabrication techniques developed in this work enable us to deliver daily pulses of bioactive PTH from a pulsatile device and to deliver bioactive PTH in a linear manner from a continuous device for three weeks. Beyond the PTH delivery application, we expect the platform (continuous and pulsatile devices) to be useful in fundamental and translational studies on how temporal effects and release patterns of biomolecules regulate cell fate, tissue development, and regeneration.

3.5 Experiment Section

Fabrication of the Pulsatile PTH Delivery Device

Three-component PAs composed of SA, CPP, and poly(ethylene glycol) (PEG, M_W = 1000) were synthesized as previously reported. ^{1}H NMR (400MHz, CDCl3) confirmed the synthesis of the PA: PEG (3.4–3.8 ppm), CPP (6.9 and 8.0 ppm), and SA (1.4–2.2 ppm). The PA was melted and compressed into layers of various thicknesses with error ≤10 μm. The PA layers were punched into disks of desired size (3 mm in diameter) as isolation films. BSA or PTH (1-34) (Bachem Bioscience Inc., Torrance, CA) was mixed with alginate in a 1:1.67 weight ratio. The mixture was dissolved in distilled water and the solution was cast into a film and freeze-dried for 1 d. The films were then punched into disks (2 mm in diameter). The PA films were rubbed with a Teflon film to generate positive surface charge and the alginate-PTH films were rubbed with a glass slide to

generate negative surface charge. One piece of the PA film and one piece of drug film attracted each other to form one bilayer. The 21 bilayers were stacked and then sealed using a 35% w/v PCL/dichloromethane (DCM) solution, leaving the top unsealed thus allowing one-direction erosion (from top to bottom). The device was vacuum dried for 3 d.

Film Surface Characterization

10% w/v PA/DCM solution or alginate-PTH aqueous solution was spin coated onto the gold substrate. KPFM (Bruker NanoMan atomic-force microscopy (AFM)) equipped with a conductive tip was used to map the surface potential in tapping mode and the data were analyzed with software (Nanoscope) equipped with the AFM. The drug layer was rubbed with a glass side and the PA was rubbed with a Teflon layer. The electrostatic voltages of the layers (Teflon, glass side, PA layer, and drug layer) were measured using a noncontact static meter (Electro-Tech Systems Static Meter Model 200).

Fabrication of Continuous PTH Delivery Device

To fabricate the continuous PTH release device, we employed the double emulsion method to prepare drug-encapsulated PA microspheres, which were then compressed into disks. Briefly, BSA (control protein) or PTH was dissolved in distilled water with 0.1% w/v gelatin. The drug solution was emulsified in a 10% w/v PA DCM solution, using a probe sonicator at an output power of 10 W (Virsonic 100, Cardiner, NY) for 10 s over an ice bath to first form a water-in-oil (w/o) emulsion. The w/o emulsion was then gradually added into 20 mL aqueous polyvinyl alcohol solution (1% w/v) under sonication at an output power of 20 W to form a water- in-oil-in-water (w/o/w) double emulsion. The solution was stirred at room temperature for 3 h to evaporate DCM and then centrifuged to

collect solid microspheres. The resultant microspheres were washed with distilled water three times and freeze dried. The microspheres were then compressed into disks and the bottoms and sides of the disks were sealed with a 35% w/v PCL/DCM solution, leaving only the top unsealed. The device was dried under vacuum for 3 d.

In vitro Drug Release and PTH Bioactivity

The protein-loaded devices were immersed in 1 mL PBS (0.1 m, pH = 7.4) and incubated at 37 °C. After designated times, the medium was collected and replaced with equal amount of fresh PBS. The collected medium was stored at −80 °C until analysis. The amount of released BSA was measured using a MicroBCA protein assay (Pierce, Rockford, IL). *In vitro* bioactivity of released PTH was determined using the adenylate cyclase stimulation assay and cAMP-binding protein assay. Briefly, human fetal osteoblasts were treated with PTH of known concentrations or with eluent from the PTH delivery devices for designated times in calcium- free and magnesium-free hanks' balanced salt solution containing 0.1% BSA and 1×10^{-3} m isobutylmethylxanthine. After incubation of the treated cells at 37 °C for 10 min, the cAMP in the cells was extracted with ice-cold perchloric acid. The cAMP extracts were then neutralized by adding KOH and centrifuged to remove the precipitates. (^{3}H)-cAMP was incubated with standards or unknowns and cAMP-binding protein for 90 min on ice. The unbound (^{3}H)-cAMP was removed by adding dextran-coated charcoal. The samples were then centrifuged and the supernatant of each tube was decanted to a scintillation tube. The radioactivity of the supernatants was determined using a liquid scintillation counter and cAMP levels were calculated using the standard curve.

CHAPTER 4

PTH Delivery Device in Systemic Delivery Application

4.1 Introduction

Current PTH administration relies on injection, but comparing different PTH release kinetics from a controlled delivery system has not yet been studied. PTH has been shown to promote bone formation *in vivo* via a net anabolic action, however it inhibits osteoblast differentiation and mineralization *in vitro*, indicating that the *in vivo* environment cannot be replicated using the *in vitro* model[196, 197]. Hence, *in vivo* models are a necessity to determine PTH's optimal delivery mode from the engineered devices in terms of anabolic action. In this chapter, we investigate the engineered PTH release from both pulsatile and continuous release devices *in vivo* and study their systemic therapeutic effects on bone in a mouse model (Figure 3.1.1).

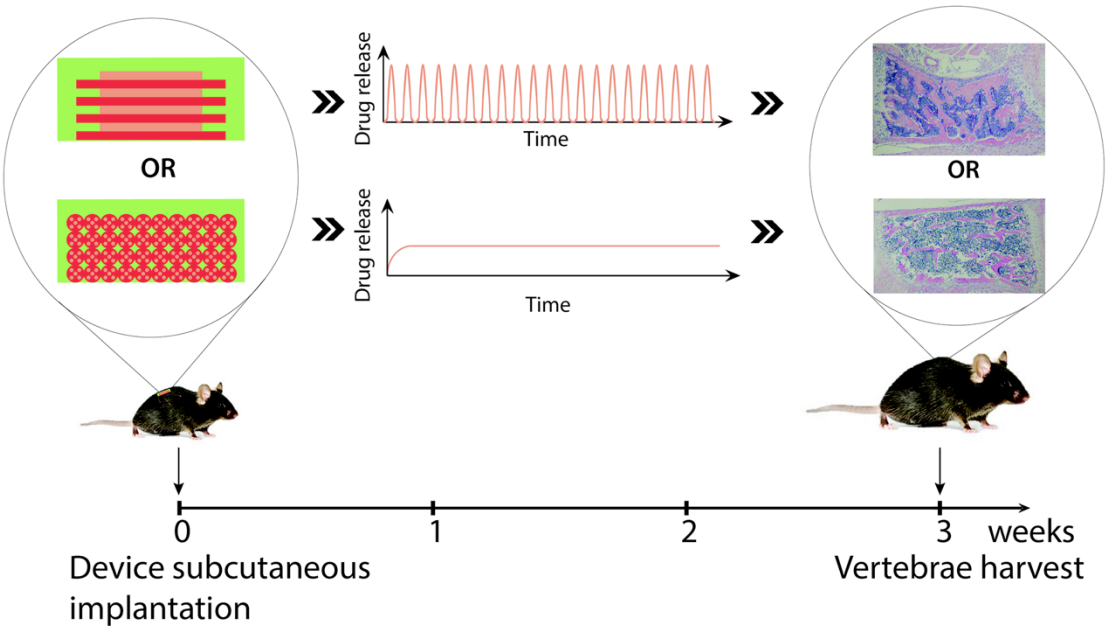

Figure 3.1.1 Experimental design used to investigate the therapeutic effects of PTH released from the pulsatile delivery device and the continuous delivery device. The PTH delivery devices were subcutaneously implanted in mice and bones and serum were collected three weeks later to examine the systemic effects of the two PTH release modes on bone.

4.2 PTH Delivery Device to Strengthen Bone

With the PTH release devices fabricated and function confirmed, the PTH devices were evaluated *in vivo* to compare the pulsatile and continuous release modes in terms of anabolic effects on bone. Both pulsatile and continuous devices (4 mm in diameter and around 1.6 mm in thickness) were loaded with equal amounts of PTH and implanted subcutaneously in mice. Three weeks later, the tibia, vertebrae, and blood serum were collected and analyzed.

MicroCT (μCT) evaluation showed that PTH released from the devices had obvious effects on the tibiae. The 3D reconstruction (Figure 3.2.1 A) and the quantitative analysis (Figure 3.2.1 B and C) showed that the pulsatile PTH release significantly increased trabecular bone volume and cortical bone thickness, while the continuous PTH release acted in the

opposite way and decreased both trabecular bone volume and cortical bone thickness.

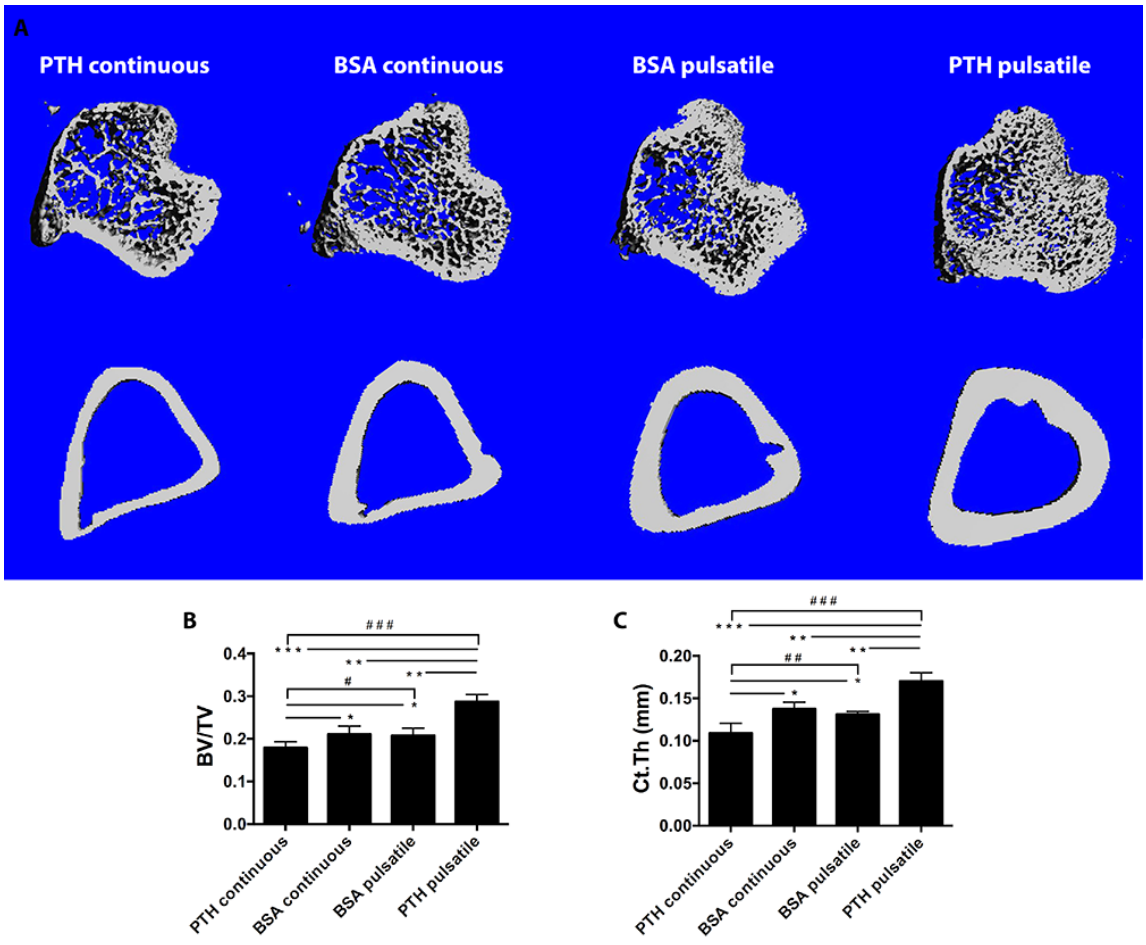

Figure 3.2.1 The mouse tibia bone analysis after PTH release using the pulsatile and continuous releasing devices, respectively. A) Representative μCT reconstruction of trabecular bone (top) and cortical bone (below) of the mouse tibias from different treatment groups. B) Trabecular bone volumes. C) Cortical bone thickness. n = 5–7 per group, *$P < 0.05$, **$P < 0.005$, ***$P < 0.001$, #$P < 0.05$, ##$P < 0.005$, ###$P < 0.001$.

Vertebral bone turnover and the osteoclastic response were examined using hematoxylin and eosin (H&E) staining and tartrate-resistant acid phosphatase (TRAP) staining (Figure 3.2.2 A). Quantitative analysis of the bone area ratio showed that pulsatile PTH significantly increased bone area, while continuous PTH significantly decreased bone area compared to controls (Figure 3.2.2 B). The serum bone formation marker (pro-collagen I

intact N-terminal propeptide (PINP)) level was measured using an enzyme-linked immunosorbent assay (ELISA) and showed that the PINP levels were significantly elevated in the pulsatile PTH group (Figure 3.2.2 C).

Interestingly, TRAP staining of the vertebrae showed that both PTH pulsatile and continuous delivery led to an increased number of TRAP-positive osteoclasts (OSCs) per bone perimeter (Figure 3.2.2 D and E), but the serum bone resorption marker TRAP 5b level was signi cantly higher only for continuous PTH release (Figure 3.2.2 F).

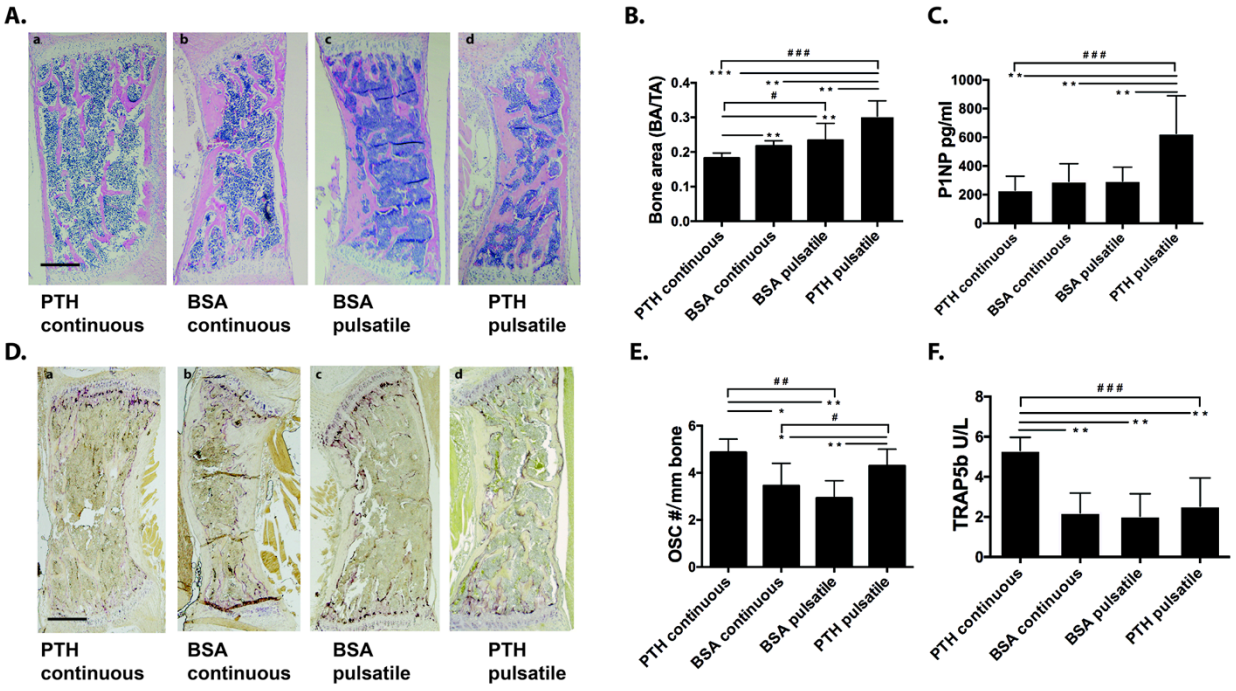

Figure 3.2.2 Mouse vertebral bone response to pulsatile and continuous PTH releases. A) Representative H&E staining of vertebrae of different PTH delivery groups. B) Vertebral bone area/tissue area analyzed by histomorphometry. C) Serum PINP level measured by PINP ELISA. D) Representative TRAP staining of vertebrae of different PTH delivery groups. E) Osteoclast (OSC) numbers per bone perimeter. F) Serum TRAP5b level measured by ELISA; pulsatile groups: n = 9–12 per group, continuous groups: n = 6–9 per group, *P < 0.05, **P < 0.005, ***P < 0.001, #P < 0.05, ##P < 0.005, ###P < 0.001. Scale bar: 0.5 mm (A) and (D).

These *in vivo* results indicated that while delivering the same amount of PTH, the pulsatile

release device enhanced bone growth through increasing bone remodeling evidenced by an increase in bone formation marker PINP and enhanced osteoclast numbers, while continuous release induced bone resorption through enhanced osteoclast activity. The systemic pulsatile PTH release was found to be superior in terms of anabolic action in bone and significantly increase bone volume systemically after three weeks, so such delivery method could potentially reduce the treatment duration from two years to a significantly short duration.

4.3 Biocompatibility and Biodegradability of the Devices

It has always been a critical concern in implantable products whether degradation byproducts (such as monomers, acids) of a biodegradable polymer result in toxicity and negative effects. The components (SA-CPP and PEG) of PA used in this study have been used as components of FDA-approved medical devices in the human body. The degradation products of the PA copolymer are similar to those of the two components, which potentially have similar biocompatibility.

To help determine biocompatibility, we examined the pH value change during the degradation of the PA devices *in vitro* and the body response to the implants *in vivo*. The pH value of the PBS medium, in which devices were immersed, remained about 6.8, close to neutral pH 7, over time as the devices degraded. There was no significant difference between pulsatile and continuous devices (Figure 3.3.1 A) since the same amounts of PA were used to fabricate the two types of devices. The *in vivo* body response to the devices was evaluated using histological analysis of the devices explanted three weeks after subcutaneous implantation. Most parts of the devices had been degraded, leaving the slow

degrading sealant shell of PCL (Figure 3.3.1 B), which would degrade eventually as reported earlier. H&E staining was performed to assess inflammation at the implant sites *in vivo* (Figure 3.3.1 C and E). The devices were mainly surrounded by granulation tissue composed mostly of macrophages and lymphocytes and partial encapsulation by a fibrovascular connective tissue wall was noted. The inflammatory infiltrate was localized to the area surrounding the devices with limited extension into the adjacent adipose tissue. Overall, all the materials (alginate, PA, and PCL) used to construct the delivery devices are biocompatible and biodegradable. Subcutaneous implanted devices degraded *in vivo* and resulted in an encapsulation of the materials with minimal acute inflammation.

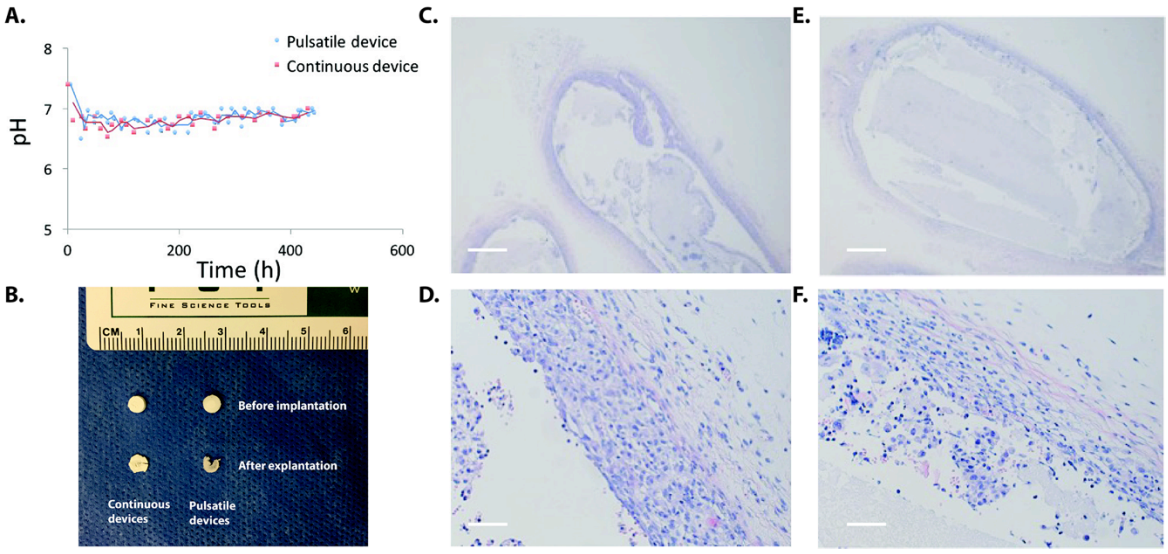

Figure 3.3.1 The degradation of pulsatile and continuous release devices *in vitro* and *in vivo*. **(**A) Change of solution pH value over time (drug delivery devices were immersed in 1 ml 0.1M PBS at 37°C). N=3 (B) Drug delivery devices before implantation and after 3-week implantation. H&E staining of pulsatile device at low (C), and high (D) magnification. H&E staining of continuous release device at low (E) and high (F) magnification. Scale bar: 1mm (C and E) and 50 μm (D and F).

4.4 Conclusion

Implantable and biodegradable long-term pulsatile and continuous PTH delivery devices were designed to investigate the effects of PTH delivery patterns on systemic bone therapy. The pulsatile device was preprogrammed to deliver daily pulses of bioactive PTH and the continuous device to deliver bioactive PTH in a linear manner for three weeks. We demonstrated that systemic pulsatile PTH release was able to increase bone via enhancing bone remodeling, whereas the continuous PTH release resulted in bone resorption via elevated osteoclast resorption activity. The biodegradable pulsatile PTH delivery device has the potential to be a patient-friendly PTH therapy, which could be administered only once (implantation) instead of daily injection. In addition, the device is biodegradable and resorbable *in vivo*, eliminating the need of removal surgery. Beyond the PTH delivery application, we expect the platform (continuous and pulsatile devices) to be useful in fundamental and translational studies on how temporal effects and release patterns of biomolecules regulate cell fate, tissue development, and regeneration.

4.5 Experiment Section

Subcutaneous Implantation

All animal procedures were carried out under the guidelines of and were approved by the Institutional Animal Care and Use Committee of the University of Michigan. Pulsatile or continuous PTH delivery devices were implanted into subcutaneous pockets created from a midline incision on the backs of C57B6 mice (The Jackson Laboratory, Bar Harbor, ME) at postnatal d 10. Three weeks after implantation, the mice were euthanized and whole blood was obtained by intracardiac blood draw, serum separated and kept frozen until

biochemical assays were performed.

Micro CT analysis

3D analyses of mice tibiae were performed using μCT as previously described[198]. Briefly, formalin fixed tibiae were embedded in 1% agarose and placed in a 19 mm diameter tube and scanned over their entire length using a μCT system (μCT100 Scanco Medical, Bassersdorf, Switzerland). Scan settings were 12 μm voxel size, medium resolution, 70 kVp, 114 μA, 0.5 mm AL filter, and an integration time of 500 ms. Trabecular bone parameters were measured over 50 slices using an 180 mg cm^{-3} hydroxyapatite (HA) threshold beginning 15 slices distal to the growth plate; cortical bone parameters were measured over 30 slices beginning 250 slices proximal to the tibia–fibular joint using a 280 mg cm^{-3} HA threshold. The trabecular bone volume and cortical bone thickness (Ct.Th) were quantified using the manufacturer's evaluation software (Scanco μCT 100).

Bone histological and histomorphometric analysis

The Mice vertebrae samples were fixed with 4% formalin, decalcified with 10% EDTA for 2 weeks and subsequently embedded in paraffin. Hematoxylin & eosin (H&E) and Trichrome staining of the coronal sections (5 mm thick) were performed by the histology core at the University of Michigan School of Dentistry. Tartrate-resistant acid phosphatase (TRAP) staining was performed using the Leukocyte Acid Phosphatase Assay (Sigma) following the manufacturer's protocol. Bone static histomorphometric analyses for bone area and osteoclast number were performed using a computer-assisted histomorphometric analyzing system (Image-Pro Plus version 4.0; Media Cybernetics, Inc., Silver Spring,

MD).

Serum biomarker analysis

The whole blood was obtained by intracardiac blood draw. After centrifugation for 10 min at 13000 rpm, serum was separated and kept frozen until biochemical assays were performed. Serum procollagen I N-terminal propeptide (P1NP) (MyBioSource, Inc) and TRAP5b (Novatein Biosciences, MA) ELISA immunoassays were performed following the manufacturer's protocols.

Statistical analysis

All numerical data are presented as mean ± SD. All P values were two-tailed and $P < 0.05$ was considered statistically significant. One-way ANOVA test was applied to compare different groups using GraphPad InStat software (GraphPad).

CHAPTER 5

PTH Delivery Device in Local Delivery Application

5.1 Introduction

In the previous chapter, we demonstrated systemic PTH delivery from the delivery device and the pulsatile delivery could promote bone formation systemically. However, extending PTH utilization from systemic treatment to localized application for bone defect regeneration has not been achieved. The major drawbacks of repurposing PTH as a therapeutic for local defect repair include its systemic side effects and its administration via daily injection, which is inconvenient for patient compliance. Many different drug delivery strategies have been investigated but most of them center on systemic administration[32]. Successful systems to deliver PTH to the local site, to preserve PTH bioactivity and to induce the optimal anabolic action are lacking.

In this work, we developed a novel acellular biomaterial strategy to promote bone regeneration by incorporating local PTH delivery in a 3D biomimetic scaffold (Fig. 1). Biodegradable drug delivery devices were designed to preprogram the delivery of PTH in either a pulsatile or continuous manner for 21 days using the surface erosion PA. We investigated the effects of the two distinct kinetics, pulsatile and continuous, in a local calvarial defect regeneration model. This platform allowed us to explore the potential of PTH for the treatment of localized bone defects (Figure 4.1.1).

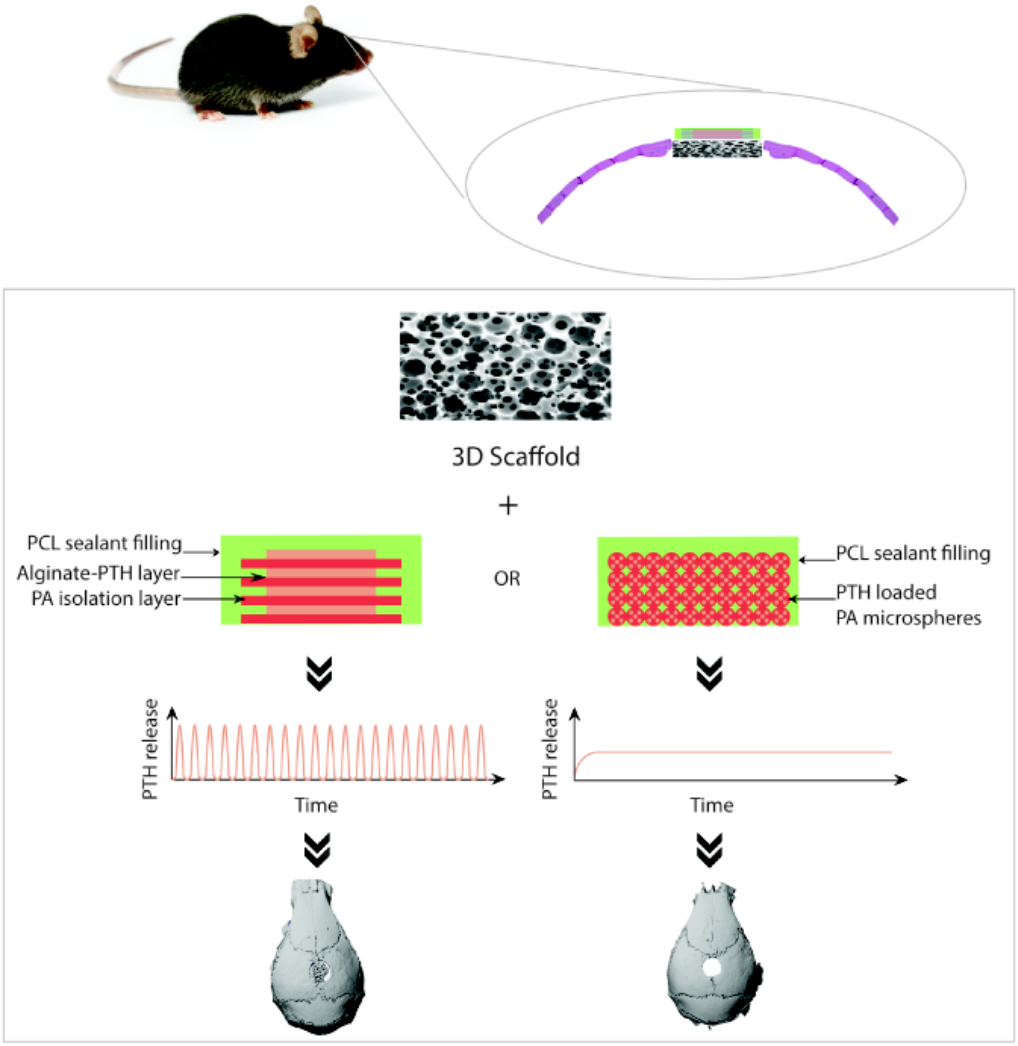

Figure 4.1.1 Experimental design of using a 3D cell-free scaffold and a PTH deliver device (pulsatile or continuous) to repair calvarial bone defect in a mouse model.

5.2 PTH Delivery Device to Repair a Bone Defect

First of all, 3D scaffolds were prepared, which plays an important role in defining the 3D micro- environment for regenerative cells. Pore size, porosity and surface architecture are important parameters to design an ideal scaffold for regeneration[14]. In this work, we combined the sugar spheres leaching technique with the thermal induced phase separation technique to fabricate NF PLLA scaffolds with inter-connected spherical pore network

(Figure 4.2.1 A and B). The spherical pores of the scaffold ranged from 250 mm to 420 mm and the porosity was as high as 98.5%. The major organic component of bone is collagen, which self-assembles into nanofibers ranging from 50 to 400 nm in diameter[199] and the PLLA scaffold surface (inset in Figure 4.2.1 B) had the similar NF feature of collagen.

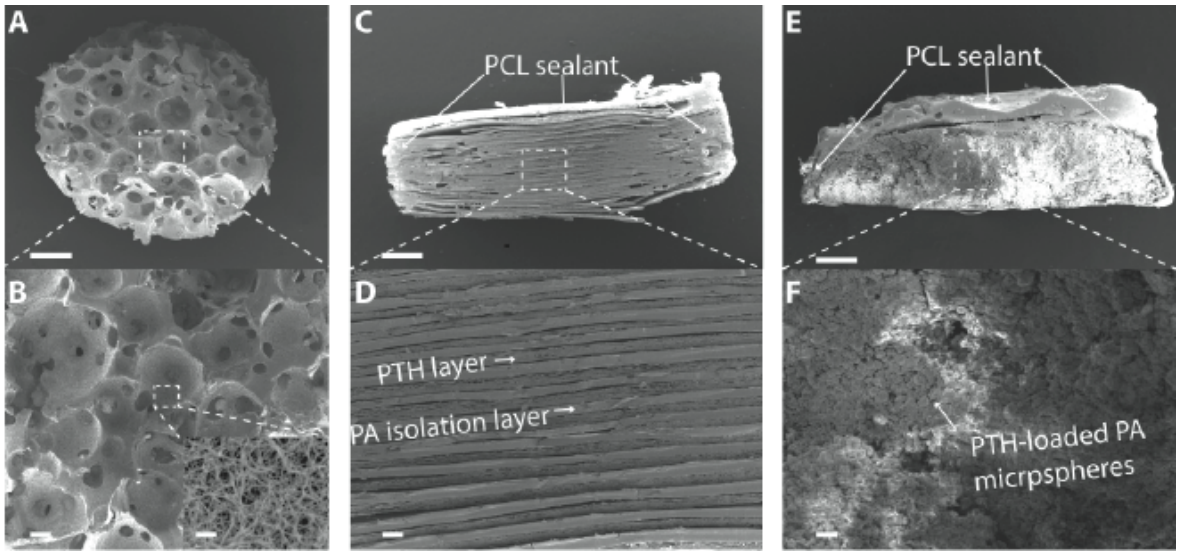

Figure 4.2.1 Scanning electron microscopy (SEM) images of scaffold and PTH delivery devices. (A, B) NF PLLA scaffold with interconnected spherical pore network; (C, D) the pulsatile PTH release device; and (E, F) the continuous PTH release device. Scale bars: 400 mm in A, C, E and 50 mm in B, D, F. Inset in B shows the NF architecture of the scaffold at a higher magnification (scale bar: 2 mm).

To determine the optimal PTH release mode to ensure desired PTH anabolic action in bone regeneration, the pulsatile device (21 layers) and the continuous device (21 days) were compared in identical experimental set ups to access the outcomes of bone regeneration in a round defect (2.3 mm in diameter) created in the mouse skull (Figure 2.1 C and E). BSA loaded pulsatile devices were used as vehicle controls. In the positive control group, we injected PTH for 3 weeks using a standard systemic administration dose (40 mg/ kg/d), which showed notable anabolic effects as reported before. Both the pulsatile devices and

continuous devices were loaded with the same amount of PTH as the total standard injection amount.

Eight weeks after implantation, μCT reconstruction of the skulls (Figure 4.2.2 A) showed that local pulsatile PTH release resulted in the best regeneration outcome among all groups; whereas continuous PTH release resulted in less bone compared to the BSA control group.

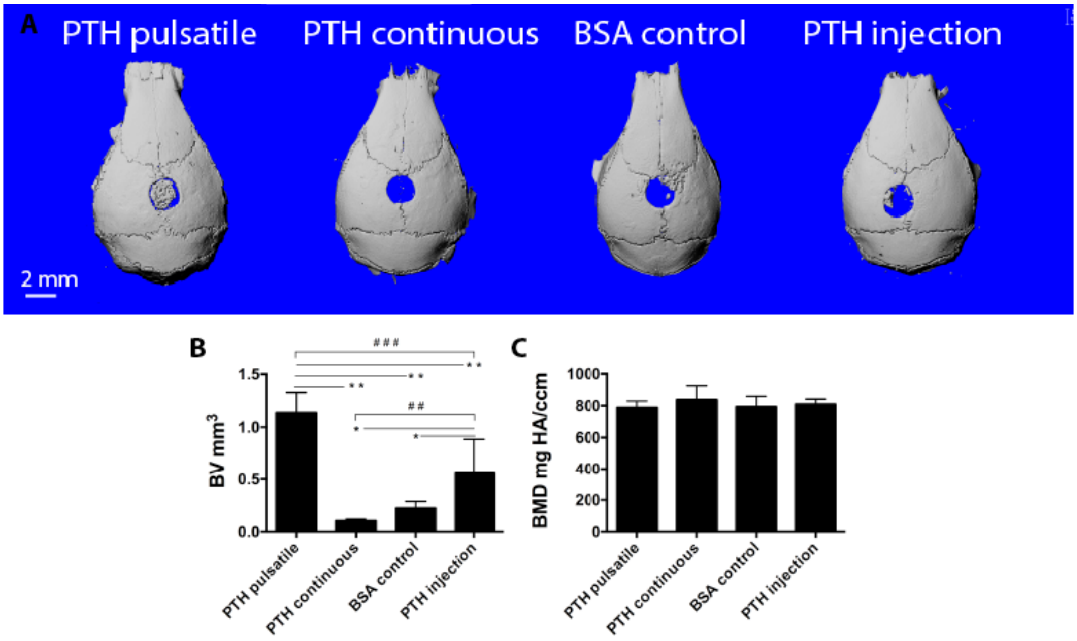

Figure 4.2.2 μCT characterization of the local defect repair in 8 weeks. (A) Representative μCT reconstructions of mouse calvarial defects in different PTH delivery groups. (B) The new bone volume; and (C) The new bone mineral density. n =6-9 per group, *P < 0.05, **P < 0.005, #P < 0.05, ##P < 0.005, ###P < 0.001.

H&E (Figure 4.2.3 A) and Trichrome staining (Figure 4.2.3 B) showed that in the pulsatile PTH group, collagen-rich bone tissue (stained pink in H&E staining and dark blue in Trichrome staining) was formed throughout the scaffold, whereas only fibrous tissue was present in the continuous PTH group. Areas and volumes of newly formed bone were quantitatively analyzed using μCT and histomorphometry, revealing that the PTH injection

significantly promoted bone growth in the NF scaffold compared to the control BSA group. Further, local pulsatile PTH release significantly increased bone volume and connected bone tissue regeneration even compared to systemic PTH injection (Figures. 4.2.2 and 4.2.3).

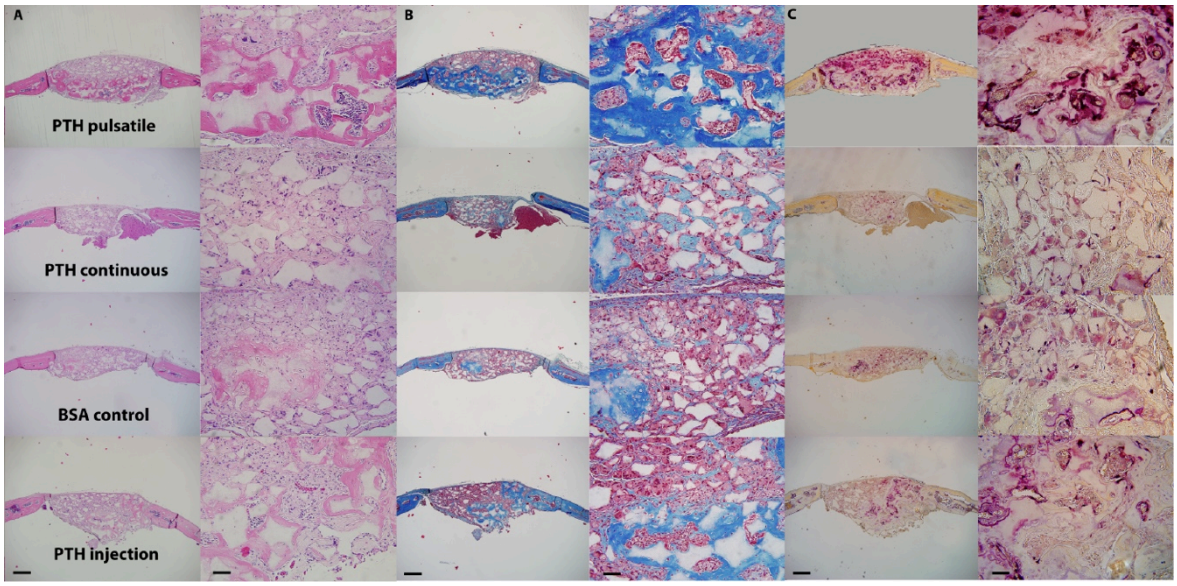

Figure 4.2.3 Histological characterization of the bone defect repair 8 weeks after implantation. (A) H&E staining, (B) Trichrome staining, and (C) TRAP staining of different PTH delivery groups. Scale bars: 0.5 mm in the left column and 0.2 mm in the right column.

TRAP staining (Figure 4.2.3 C) and the resultant osteoclast analysis (Figure 4.2.4 B and C) showed that both pulsatile and continuous PTH release devices increased the number of osteoclasts compared to BSA controls. Over 60% of the osteoclasts were aligned along the new bone tissue in the pulsatile PTH group, while most of the TRAP positive cells (over 85%) in the continuous PTH group were found distributed throughout the fibrous tissue inside the scaffold. The osteoclast distribution in the local pulsatile and the systemic injection groups were similar, but local delivery recruited significantly more osteoclasts.

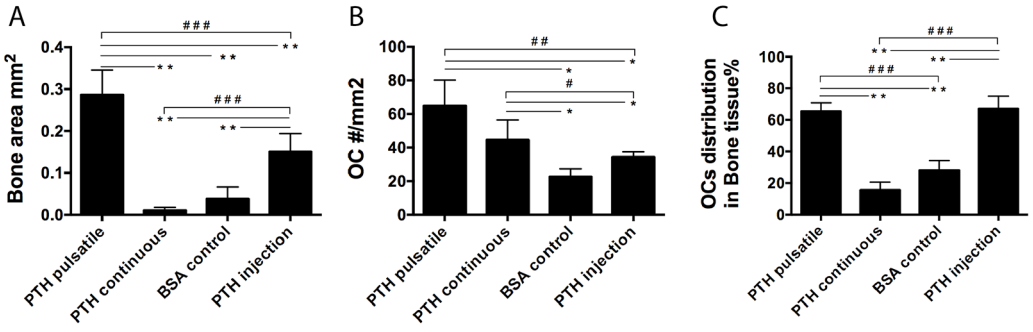

Figure 4.2.4 Quantitative analysis of the bone repair using histomorphometry. (A) Newly formed bone areas, (B) TRAP positive osteoclasts numbers, and (C) the distribution of the osteoclasts in the bone area and scaffold area quantified using histomorphometry. n=6-9 per group, *P < 0.05, **P < 0.005, #P < 0.05, ##P < 0.005, ###P < 0.001.

Moreover, as the components of the devices were biodegradable and biocompatible polymers, the devices degraded/eroded over time and minimum immune reaction and inflammation were observed.

5.3 Reduced Systemic Side Effects

Mouse tibiae from the different groups were examined using μCT to assess the potential systemic side effects of the local PTH releases. As expected, 3 weeks of PTH injection significantly increased trabecular bone volumes[200]. PTH released from the local device, both pulsatile and continuous, however, did not affect the trabecular bone, such that the volume of the trabecular bone remained unchanged compared to the BSA control group (Figure 4.3.1 A and B). Serum was isolated at the end of the 3-week treatment regimen and ELISA analyses were employed to evaluate the levels of bone biomarkers. Serum P1NP (bone formation marker) and TRAP5b (bone resorption marker) suggested that the intermittent systemic injection of PTH increased systemic bone turnover, as the levels of P1NP and TRAP5b in the blood were significantly elevated compared to the local delivery groups (Figure 4.3.1 C and D).

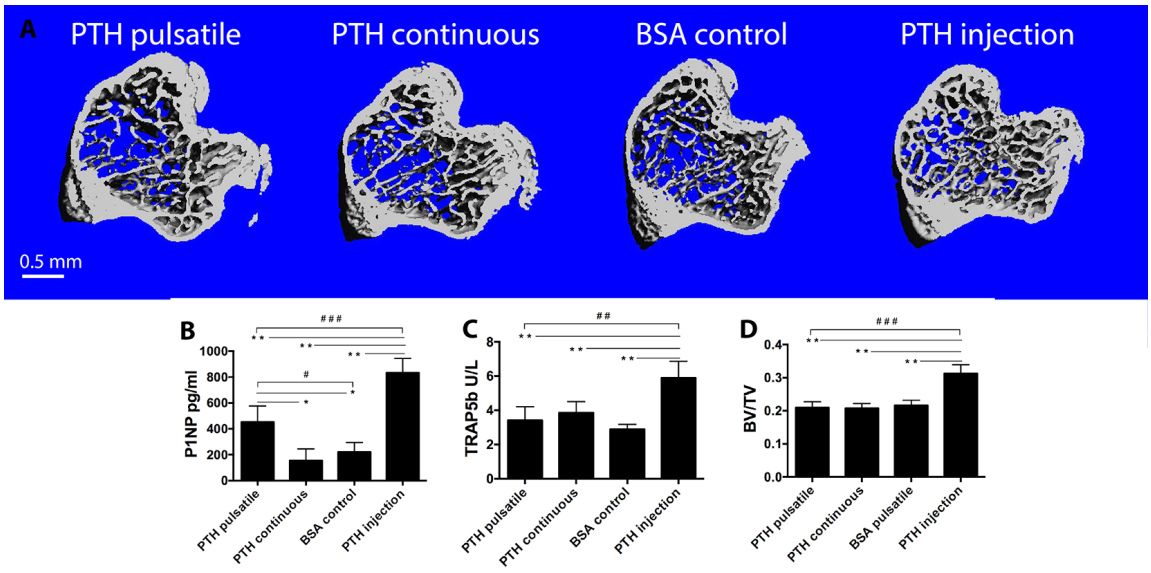

Figure 4.3.1 Analysis of the systemic effects of PTH release from the local delivery devices. (A) Representative mCT reconstructions of the tibiae from different treatment groups; (B) Trabecular bone volume; (C) Serum P1NP level and (D) TRAP5b level measured using ELISA kits. n=6-9 per group, *P < 0.05, **P < 0.005, #P < 0.05, ##P < 0.005, ###P < 0.001.

5.4 Discussion

PTH is the only FDA approved anabolic agent for the treatment of osteoporosis and its efficacy in stimulating bone remodeling, with net promotion of bone formation and few side effects, has been well established[29, 68, 201]. The unique anabolic action of PTH implies its potential in bone regeneration, yet studies have been lacking in this type of administration for local regenerative application[202, 203].

In this chapter, we achieved bone defect repair using local pulsatile PTH delivery. The success of repurposing PTH from osteoporosis to bone regeneration was achieved by developing a novel long-term pulsatile PTH delivery device to accurately deliver PTH to the defect sites to induce local anabolic effects.

Current PTH treatment which relies on systemic administration, was shown to be less

effective in enhancing local defect repair and to have unintended systemic side effects. Local treatment, in contrast, has advantages such as maintaining relatively higher local bioactive agent levels, reducing dose concentration or number of dosages, and circumventing possible adverse side effects resulting from systemic administration[119, 204].

The anabolic actions of PTH are also highly dependent on intermittent delivery and a specific temporal profile. Current treatment requires daily injections, which is cumbersome for both patients and physicians. A self-regulated pulsatile delivery system capable of long-term delivery would be desirable. Although that various delivery strategies have been developed, none has achieved successful and patient-friendly pulsatile delivery. Electrically controlled drug release microchips were fabricated to realize controlled PTH daily pulse release but such a device would require secondary surgery for removal[184]. In the present study, patient-friendly drug delivery devices were utilized to expand PTH application and to determine optimal PTH release kinetics, pulsatile or continuous, in a local bone regeneration model. The pulsatile delivery device, made of alternating PA isolation layers and PTH drug layers, was preprogrammed to deliver daily PTH pulses for 21 days. The PTH/alginate blend was freeze-dried, cut into drug layers and then packed into the pulsatile device. This method enabled high drug loading efficiency and capacity and the bioactivity of the PTH was well preserved during the 3 weeks of PTH release. The continuous device, with identical shape and polymeric materials to that of pulsatile device, was loaded with the same amount of total PTH and delivered within the same time period (21 days). The difference between these two types of devices is the PTH distribution,

where PTH is distributed in a layered structure to achieve pulsatile release or PTH is more uniformly distributed in the matrix within microspheres to achieve continuous release.

A highly porous NF scaffold was used to evaluate the two engineered PTH release modes for regeneration application. The PLLA scaffolds, with NF surface feature, were demonstrated to selectively enhance the adsorption of cell-adhesion proteins including fibronectin and vitronectin, increasing osteoblast adhesion[205]. Besides, such NF scaffolds enhance the osteoblastic differentiation of a variety of stem cells, including BMSCs, which are integral for bone defect healing[206, 207]. Here, the histological cross-section of the control group (scaffold with BSA delivery) also supported the conclusion that the NF structure alone could induce certain level of bone formation *in vivo* (Figure 4.2.2). Furthermore, with different PTH release kinetics incorporated, distinct osteogenic outcomes in the NF scaffolds were observed. Local pulsatile PTH delivery significantly improved the defect repair, generating connected and robust new bone tissue throughout the scaffold, whereas local continuous delivery resulted in less bone in the NF scaffold versus the BSA control group.

From the TRAP staining data (Figure 4.2.3 C), we noticed that both PTH releases, pulsatile and continuous, were able to increase osteoclast numbers. Pulsatile PTH release induced stronger bone remodeling with enhanced numbers of the osteoclasts aligned along the formed bone tissue, while continuous PTH release resulted in reduced bone, with increased osteoclasts, not lining the bone, but throughout the fibrous tissue inside the scaffold. The results indicate that the local pulsatile PTH release was able to induce beneficial catabolic actions by stimulating osteoclasts to realize the needed bone remodeling activity in this

specific bone-regeneration scenario.

As has been shown 3 weeks systemic PTH injection is also able to increase bone turnover and generate notable anabolic effects. Thus, we also compared the local pulsatile PTH release device with the standard systemic PTH injection treatment, and found that local release was advantageous over the systemic injection in improving the defect repair. This local strategy may have benefitted from the more localized higher bioactive PTH level and the longer action time in the local defect sites. Given the 8 min half-life of PTH[208], only a part of the total bioactive PTH could reach the defect sites considering the bioactivity loss during circulation time when PTH is given systemically. On the contrary, the local delivery strategy is more likely to maintain bioactive PTH level within an effective range for the needed period of time.

In addition to enhancing local defect repair, local PTH release led to little undesired systemic effects, whereas PTH systemic injection resulted in clear systemic effects as expected. μCT and serum data showed that PTH injection significantly increased tibiae trabecular bone volume and serum bone formation biomarkers, while PTH local release did not affect tibiae trabecular bone and exerted only minor effects on serum bone formation biomarkers. These results indicate that PTH release from the device was likely to be delivered and act more locally.

The polymeric materials used in this system, PLLA, PA, PCL and alginate, have been used as components of FDA-approved devices for certain medical applications[209]. The biodegradable and biocompatible devices developed in this study elicited minimum immune response and inflammation, which are particularly advantageous for the defect

repair application. In addition, this approach needs only a one-time administration (implantation) instead of daily injection for 3 weeks and there is no need for retrieval of the empty devices after the drug release is complete. Therefore, the implantable device is more patient-friendly and is promising for clinical translation.

5.5 Conclusion

In summary, PTH, a FDA-approved anabolic agent for osteoporosis, was repurposed to repair local bone defects. Current PTH treatment requires daily injection, while in this work PTH was incorporated into a novel biodegradable device, which was capable of delivering PTH to the defect area in a preprogrammed pulsatile manner. It was found that local continuous PTH release inhibited, while local pulsatile PTH release promoted bone regeneration. In addition, the local pulsatile delivery strategy significantly improved the osteogenic outcome and reduced the systemic side effects compared to the standard PTH injection treatment. This acellular therapy provides a novel strategy to improve bone defect repair by integrating a biomimetic scaffold and an anabolic local delivery strategy to maximize the regenerative effects within the intended areas of interest. This biomaterial technology holds promise for bone defect regeneration without addition of external cells, the burden of daily PTH injections, or the need for device removal surgery. The technology could also be readily employed to deliver other therapeutics or their combinations in a tailored manner to maximize their therapeutic effects.

5.6 Experiment Section

Materials

Three-component PA was synthesized by polymerizing sebacic acid (SA), 1,3-bis (p-

carboxyphenoxy) propane (CPP), and poly(ethylene glycol) (PEG, MW=1000 Da) as previously reported. Poly(l-lactic acid) (PLLA, Resomer L207S) with an inherent viscosity of 0.8-1.2 dl/g (0.1% in chloroform, 25 ^{o}C) was purchased from Boehringer Ingelheim (Ingelheim, Germany). PTH (1-34), was obtained from Bachem Bioscience Inc (Torrance, CA). SA, CPP, PEG, polycaprolactone (PCL), polyvinyl alcohol (PVA), bovine serum albumin (BSA), alginate, gelatin, fructose, mineral oil, tetrahydrofuran (THF) and dichloromethane (DCM) were purchased from Sigma-Aldrich Company (USA) and used as received. Phosphate- Buffered Saline (PBS) was purchased from Life Technologies Company (USA).

3D nanofiberous (NF) scaffold fabrication

3D NF PLLA scaffolds with inter-connected spherical pores were fabricated as previously described[92]. Briefly, fructose sugar spheres were made by emulsion technique. 50 g fructose was melted at 130 ^{o}C into clear light yellowish liquid and the liquefied sugar was gradually added into 50 mL mineral oil with 1.5 mL Span 80 under vigorous stirring for 3 min to create emulsion. The mixture was cooled down in an ice-bath to solidify the sugar spheres and sifted with standard sieves to separate them by size.

Spheres of desired-size (250-420 mm) were collected, washed with hexane for three times, and added to a Teflon mold. The mold was heat-treated at 37 ^{o}C for 15 min to achieve the desired inter- connected pore structure. After bonding the sugar spheres, hexane was removed under vacuum. PLLA/THF (10% w/v solution) was then cast into the sugar sphere assembly and the whole construct was stored at 80 ^{o}C over night to induce phase separation. The phase- separated samples were immersed into distilled water to extract the

solvent and leach away the sugar spheres. Last, the polymer scaffolds were freeze-dried and punched into desired size (2.3 mm in diameter and 1.5 mm in thickness).

Calvarial bone-defect repair model construction

All animal procedures were performed following a protocol approved by the University of Michigan Institutional Animal Care and Use Committee. C57BL/6 mice were randomly divided into four groups. Animals were anaesthetized with isoflurane (2%) inhalation. A 2.3 mm craniotomy defect centered on the parietal calvarial bone was created using a trephine. A blank scaffold was placed to fill in the defect and a delivery device (pulsatile PTH, continuous PTH or BSA control) was placed adjacent to the scaffold with the opening side facing the scaffold. The PTH injection group did not receive PTH delivery devices; instead subcutaneous injection of PTH (40 mg/kg/d) was administrated for 21 days. The mice were euthanized 8 weeks after implantation. The skull and tibiae were harvested

Micro CT analysis

For the calvarial bone analysis, the skulls were scanned with a fixed global threshold of 20%. 3D reconstruction of the skull and quantitative analyses were performed. A 2.3 mm-round region of interest centered on the defect was determined and the bone volume (mm^3) (BV) and bone mineral density (BMD) in the area were measured using manufacturer's software (Scanco μCT 100).

For the tibiae analyses, tibiae were scanned over the entire length. A fixed global threshold of 18% (180 on a grayscale of 0-1000) was used to segment trabecular bone from non-bone areas. A region of 0.75 mm right below the growth plate was analyzed to quantify the

trabecular bone volume.

Bone histological and histomorphometric analysis

The calvarial samples were fixed with 4% formalin, decalcified with 10% EDTA for 2 weeks and subsequently embedded in paraffin. Hematoxylin & eosin (H&E) staining of the coronal sections (5 mm thick) were performed by the histology core at the University of Michigan School of Dentistry. Tartrate-resistant acid phosphatase (TRAP) staining was performed using the Leukocyte Acid Phosphatase Assay (Sigma) following the manufacturer's protocol. Bone static histomorphometric analyses for bone area and osteoclast number were performed using a computer-assisted histomorphometric analyzing system (Image-Pro Plus version 4.0; Media Cybernetics, Inc., Silver Spring, MD).

Serum biomarker analysis

Three weeks after implantation, the mice were anaesthetized with inhalation of isoflurane (2%) and blood was collected by tail blood draw. After centrifugation for 10 min at 13000 rpm, serum was separated and kept frozen until biochemical assays were per- formed. Serum procollagen I N-terminal propeptide (P1NP) (MyBioSource, Inc) and TRAP5b (Novatein Biosciences, MA) ELISA immunoassays were performed following the manufacturer's protocols.

Statistical analysis

All numerical data are presented as mean ± SD. All P values were two-tailed and $P < 0.05$ was considered statistically significant. One-way ANOVA test was applied to compare different groups using GraphPad InStat software (GraphPad).

CHAPTER 6

Biodegradable Apoptotic-Cell Mimicking Microspheres

6.1 Introduction

Macrophages are often associated with diseases and inflammatory immune responses[210] and have been generally considered negative for tissue homeostasis. However, recent studies have revealed diverse functions of macrophages, which are emerging as not only key players in the orchestration of inflammation resolution and tissue regeneration[211-213], but also as crucial participants in maintaining tissue homeostasis[214, 215]. Pettit, et al. coined the term 'osteomacs' as macrophages which are located in close proximity to osteoblasts *in vivo* and support osteoblasts function[216]. Depletion of macrophages leads to a reduction in cortical and trabecular bone mass[217]. Macrophages are also critical to the fracture healing process. They are responsible for the clearance of damaged tissue and the initiation and progression of early endochondral ossification[215, 218]. The secretion of cytokines and growth factors stimulated by macrophage engulfment of apoptotic cells (termed efferocytosis) could regulate osteoblasts and mesenchymal stem cells and fuel the bone turnover and remodeling process. Indeed, following efferocytosis, the secretion of C-C motif chemokine ligand 2 (CCL2), aka monocyte chemotactic protein 1 (MCP1), and transforming growth factor-ß 1(TGF-ß1) were increased[219]. Both have been known to enhance the recruitment of mesenchymal progenitor cells and play key roles in bone

repair[219-221]. These findings show that modulation of the macrophages efferocytosis process has great potential in therapeutic bone repair. The efferocytosis process is initiated and mediated by the macrophages' recognition of the signal molecules released or presented by apoptotic cells.[222-224] One important category of signal molecules is termed the "eat me" signals, which are expressed on the surface of apoptotic cells[225, 226].

Phosphatidyserine (PS) lipid, a well-recognized "eat me" signal, has been incorporated into liposomes to regulate inflammation and promote tissue repair via systemic injection.[227] Herein, we hypothesize that biodegradable apoptotic-cell mimicking microspheres (BAM) could mimic the apoptotic cells, attract macrophages, initiate efferocyctosis and subsequent marrow stromal cells (MSCs) recruitment and benefit new bone regeneration. To test this hypothesis, we developed BAM, which are biodegradable polymeric microspheres (MS) with the PS lipid conjugated on their surface and then seeded these BAM onto a porous and nanofibrous (NF) tissue-engineering scaffold. We then examined the potential of BAM in enhancing bone regeneration in the 3D space defined by the scaffold in a calvarial bone defect model.

6.2 BAM Microsphere Fabrication

To immobilize PS lipids onto polymeric MS, we selected the avidin-biotin conjugation because of this strategy's high efficiency and versatility[228]. We synthesized MS-biotin (Figure 6.2.1 A) and PS-biotin (Figure 6.2.2 A) respectively and used avidin to link MS-biotin and PS-biotin to yield BAM.

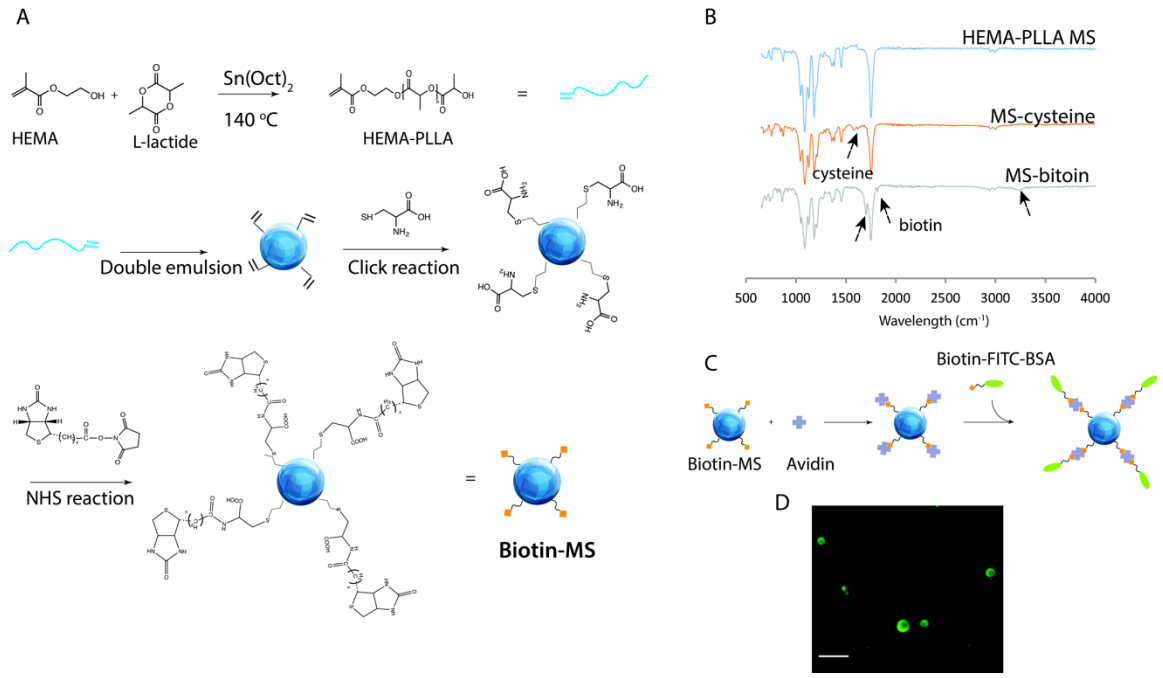

Figure 6.2.1 Synthesis of MS-biotin. (A) Synthesis route of MS-biotin. (B) FTIR spectrum of HEMA-PLLA MS before and after functionalization, showing the peaks corresponding to conjugated molecules (arrowed). (C) A schematic picture of the conjugation between MS-biotin and FITC-BSA-biotin via avidin. (D) Confocal images of FITC-BSA conjugated MS-biotin (scale bar: 5μm).

MS were made from biodegradable, biocompatible polyesters to ensure that they were safe in biological systems[31, 43]. However, a majority of polymers which belong to this category lack functional groups for conjugation reactions.[133] Therefore, we first initiated PLLA polymerization with HEMA to form HEMA-PLLA, and then used HEMA-PLLA to formulate MS of desired size (in the range of 1-5μm). Amine groups were modified onto the particle surface through click reaction between thiol groups of cysteine and alkene groups of HEMA-PLLA MS. The amine groups were then functionalized into biotin by reacting with NHS-biotin (Figure 6.2.1 A). FTIR spectrums confirmed the intended surface chemistry changes (Figure 6.2.1 B). To further demonstrate the success of biotin modification and visualize the conjugation sites, fluorescent moieties (FITC-BSA-biotin)

were conjugated to the prepared MS-biotin through avidin conjugation (Figure 6.2.1 C). Confocal imaging showed that fluorescent signal was emitted only from the surface of MS-biotin (Figure 6.2.1. D). No fluorescent signal was detected from the unmodified MS.

PS lipids, like most lipid molecules, are hydrophobic. An organic chloroform-methanol mixture was used as a solvent to dissolve the PS lipids. PS were modified with NH_2-PEG-NH_2 through EDC/NHS mediated Steglich esterification in order to increase the PS hydrophilicity and then reacted with NHS-biotin to obtain PS-biotin. The PS-biotin chemical structure was confirmed using both FTIR (Figure 6.2.2 B) and NMR (Figure 6.2.2 C).

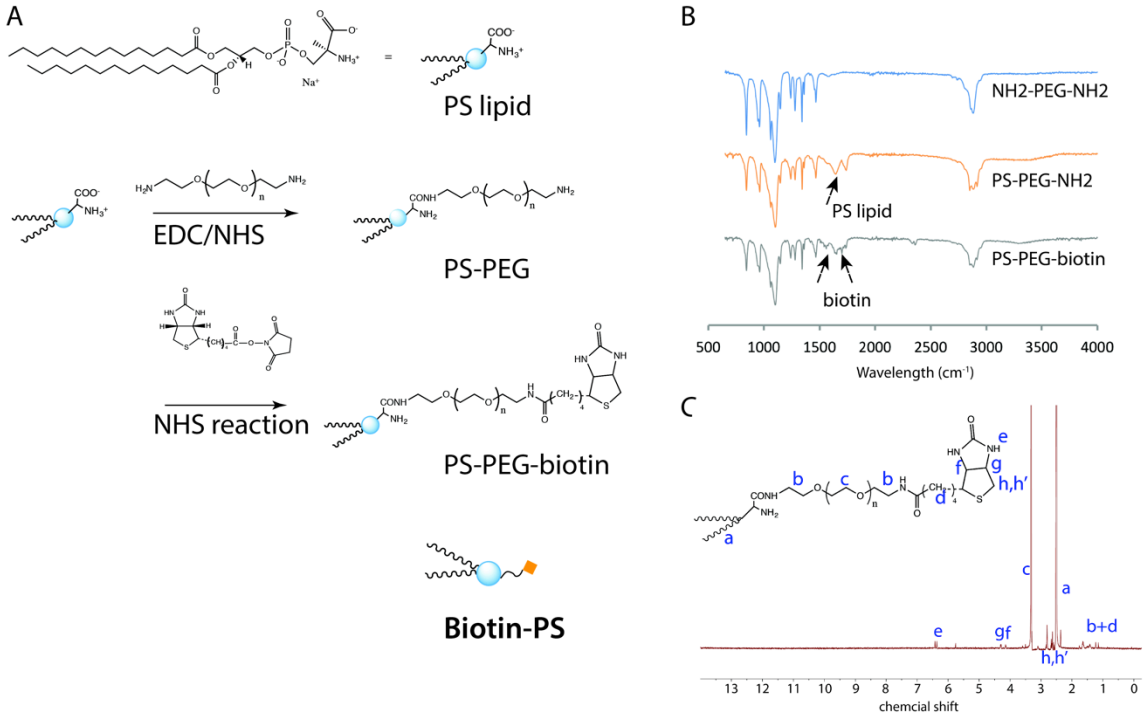

Figure 6.2.2 Synthesis of PS-biotin. (A) Synthesis route of PS-biotin. (B) FTIR spectrum of PS before and after functionalization, showing the peaks corresponding to biotin molecule (arrowed). (C) 1HNMR spectrum of the synthesized PS-PEG-biotin.

To prepare BAM via the avidin-biotin conjugation, we first added avidin to an aqueous MS-biotin suspension so that the avidin bound to MS-biotin to form MS-avidin, and then added PS-biotin into the MS-avidin to form MS-PS, henceforth termed BAM. Immunofluorescence staining visualized the successful conjugation of PS onto the MS. We labeled the MS with FITC (green fluorescence) in both control MS and BAM groups and incubate them with Annexin V-TRITC (red fluorescence)[229], an antibody that shows high affinity for PS lipids. We found that the red fluorescence was specifically bound to BAM but not to the control MS, indicating that PS presentation on the surface of the prepared BAM (Figure 6.2.3 A).

The avidin-biotin interaction enables well-controlled and highly efficient conjugation under mild reaction conditions. We eluted the PS-biotin from the BAM and measured the amount of PS-biotin in the supernatant to determine the conjugation efficiency[230]. The results showed that as much as 85% PS-biotin was conjugated at various feeding amounts (Figure 6.2.3 B), indicating a high conjugation efficiency.

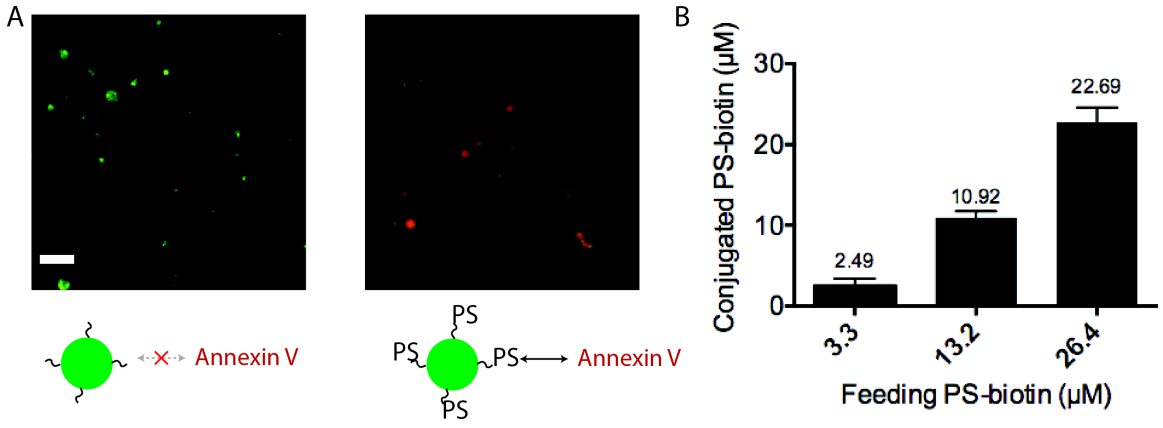

Figure 6.2.3 Conjugation between MS-biotin and PS-biotin. (A) Confocal images of FITC-tagged control MS and BAM after incubation with Annexin V (a red fluorescence PS binding protein. Scale bar: 10 μm. (B) Amount of PS conjugated on the surface of BAM at different feeding amounts. N=3.

6.3 BAM Microspheres Enhanced Macrophage Phagocytosis *in vitro*

Microspheres (BAM or control MS) were co-cultured with macrophages to study efferocytosis *in vitro*. TEM showed that both types of microspheres were engulfed by macrophages and that they kept their original spherical shape inside macrophages (Figure 6.3.1). Qualitative confocal microscopy imaging revealed that macrophages engulfed more BAM than control MS (Figure 6.3.2 A, B & C). Quantitative FACS data confirmed that macrophages internalized significantly more BAM than control MS at 0.5 and 1 h in the co-culture. This indicates that the PS modification mimicked apoptotic cells and enhanced macrophage efferocytosis (Figure 6.3.2 D).

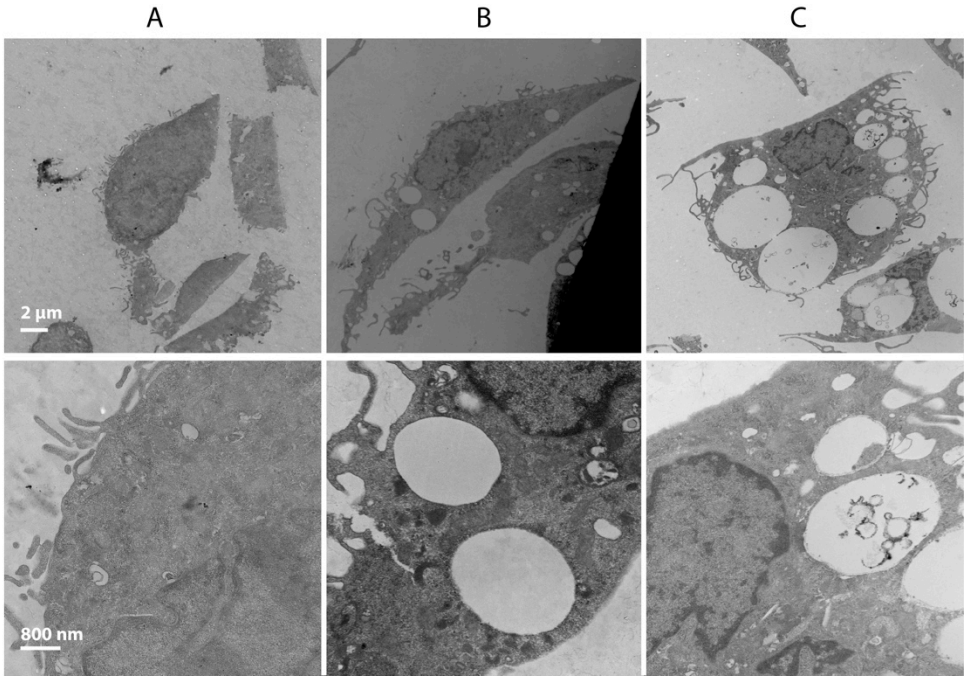

Figure 6.3.1 TEM observation of the macrophages (A) and engulfment of control MS (B) and BAM (C) at low magnification (top panel) and high magnification (bottom panel).

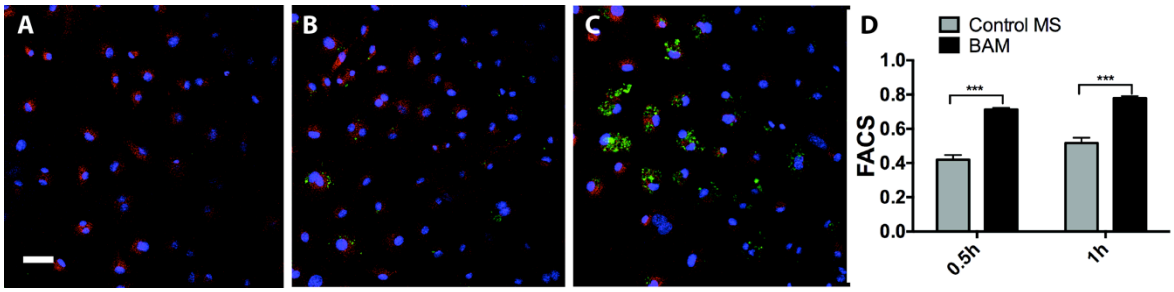

Figure 6.3.2 Macrophage phagocytosis *in vitro*. Confocal images of macrophages alone (Deep red stained) (A), and FITC-tagged control MS (B) or BAM (C) engulfed by macrophages 1 h after incubation. Scale bar: 10 μm. (D) Flow cytometry analysis demonstrated that BAM were more efficiently internalized by F4/80 positive macrophages at 30 min and 60 min compared to control MS. N=4 per group, ***P<0.0005.

To study the macrophages response after efferocytosis of BAM, macrophages were cultured alone or co-cultured with microspheres (BAM or control MS). Cells were harvested for gene expression analysis at multiple time points and supernatants were collected after 24 h for analysis of secreted proteins. Gene level expression results revealed that control MS and BAM had insignificant influence on BMP2, BMP7 and TGF-β1 gene expressions at both 6 h and 24 h time points (Figure 6.3.3 A, B & C). The osteogenic BMP genes (BMP2 & BMP7) were expressed at levels more than 2 orders of magnitude lower than those in BMSCs. Control MS significantly increased CCL2 gene expression at 6 h compared to macrophages alone group. BAM further increased CCL2 gene expression by 20 times or higher than control MS for all time points (Figure 6.3.3 D). Consistent with the gene expression data, protein level analysis showed significantly increased CCL2 secretion in BAM-macrophage co-cultures. No significant protein secretion difference was observed between control MS-macrophage co-culture and macrophage alone groups (Figure 6.3.3 E).

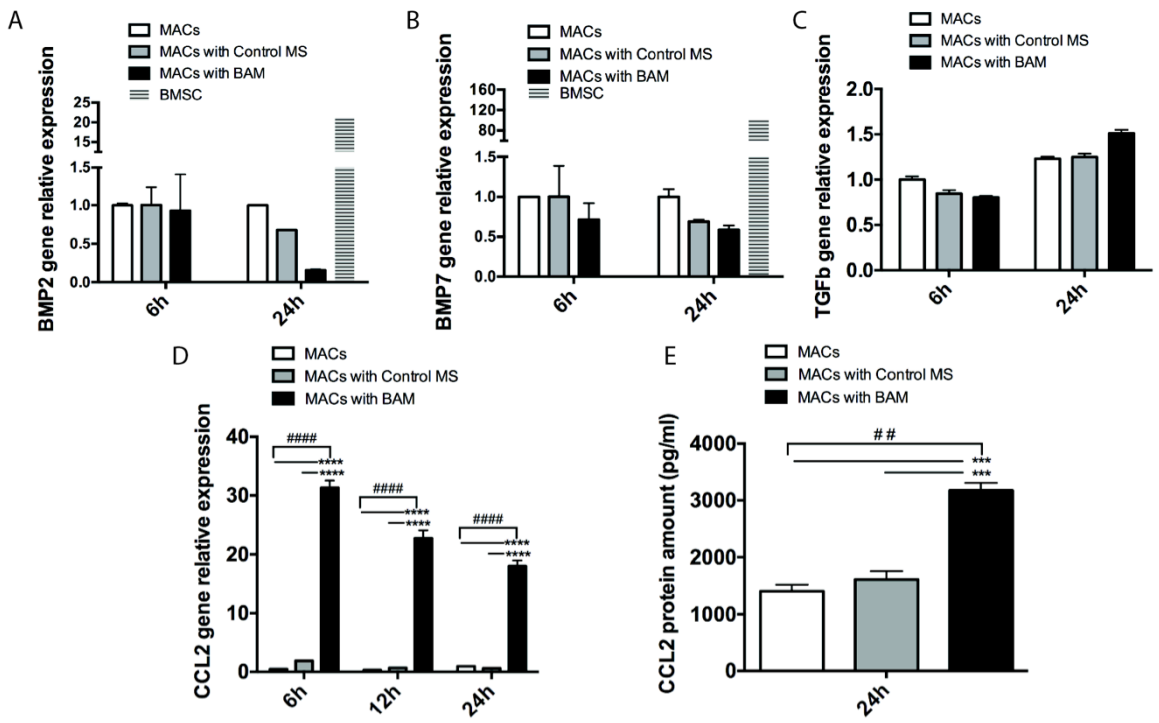

Figure 6.3.3 *In vivo* macrophage response to BAM. Phagocytosis of BAM did not modulate the BMP2 (A), BMP7 (B) and TGF-β1 (C) gene expression but significantly increased CCL2 production by macrophages at both gene expression (D) and protein (E) level. N=4, ##P<0.01, ####P<0.0001 for ANOVA test, and ***P<0.0005, ****P<0.0001 for post t-test.

6.4 BAM Microspheres Promoted Cell Migration

A transwell assay was used to investigate the ability of the conditioned medium collected from the experimental culture groups to induce the migration of BMSCs (Figure 6.4.1 A). Conditioned medium collected from macrophages alone doubled BMSC migration compared to the control medium alone. Conditioned medium from the BAM-macrophage co-cultures resulted quadrupled BMSC migration compared to control medium (Figure 6.4.1 B). Different concentrations of recombinant CCL2 were also examined to determine CCL2 effects on BMSC migration. Results showed that a concentration of 10 ng/ml CCL2 increased BMSCs migration by about 70% when compared with control medium.

However, CCL2 concentration up to 100 ng/ml did not cause any further increase in BMSC migration. These results suggest that BAM stimulated macrophages to secrete cytokines, such as CCL2, which could contribute to the enhanced BMSCs migration.

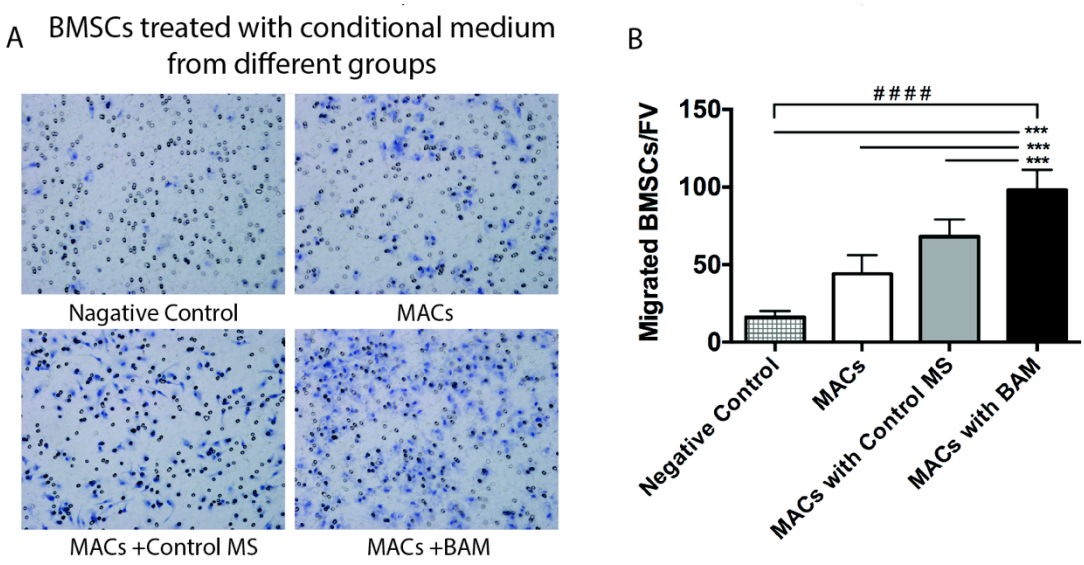

Figure 6.4.1 (A) Transwell migration assay of mouse BMSCs cultured for 8 hours in conditioned media from macrophages alone, co-culture of macrophages with control MS, and BAM. (B) Numbers of cells migrated were counted after fixation and hematoxylin staining. N=8, ####P<0.0001 for ANOVA test and ***P<0.0005 for post t-test.

Control MS or BAM were immobilized onto NF PLLA scaffolds and implanted in mice subcutaneously to investigate the *in vivo* response to the different microspheres. The scaffold constructs were harvested at day 4 and day 7. Trichrome staining showed that higher numbers of cells were seen surrounding and infiltrating BAM-scaffold constructs compared to the control MS-scaffold constructs (Figure 6.4.2 A & B). F4/80 immunohistological staining[214] also indicated that BAM (green) could recruit more F4/80 positive (red) macrophages than control MS into the scaffolds (Figure 6.4.2 C & D).

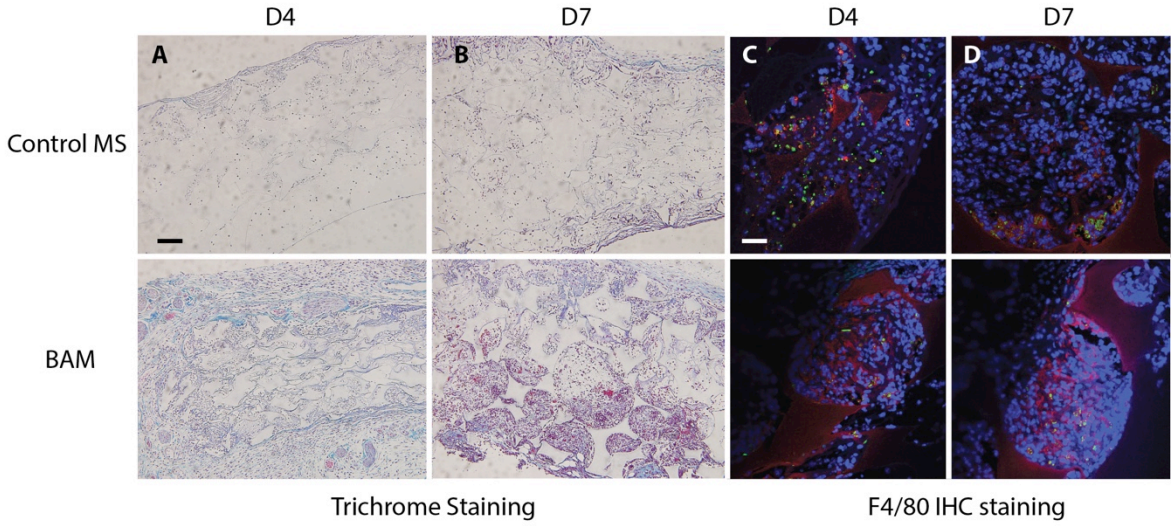

Figure 6.4.2 Scaffolds loaded with control MS and BAM 4 days and 7 days after subcutaneous implantation. Trichrome staining (A, B) and F4/80 immunohistological staining (C,D) of control MS (top panel) and BAM (bottom panel) scaffold at different time points. Particles were labeled with FITC green and F4/80 positive cells stained deep red. Scale bar: 50μm.

6.5 BAM Microspheres Promoted Bone Regeneration

Cell-free scaffolds (alone, loaded with control MS or loaded with BAM) were used to fill critical-sized calvarial bone defects in C57BL/6 mice.

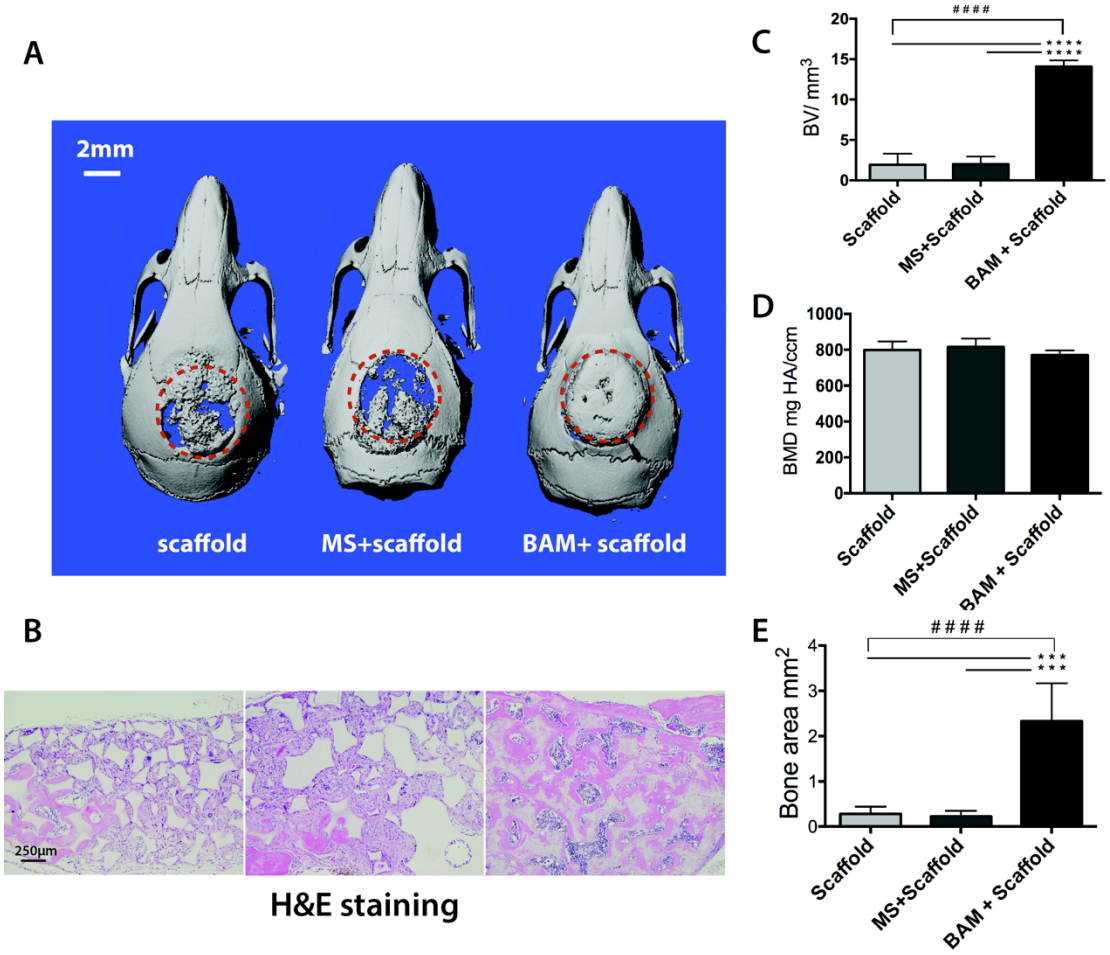

Figure 6.5.1 μCT and histological characterization of critical-sized defect repair after 8 weeks. Representative μCT reconstructions (A) and H&E staining (B) of mouse calvarial defects in scaffold groups. New bone volume (C) and new bone mineral density (D) was quantified by μCT and newly formed bone areas (E) were measured by histomorphometry. N =6 per group, ####P < 0.0001 for ANOVA test and ***P<0.005, ****P < 0.0001 for post t-test.

Cell-free scaffolds (alone, loaded with control MS or BAM) were used to fill critical-sized calvarial bone defects in C57BL/6 mice. Eight weeks after implantation, similar amounts of bone formed in the plain scaffold and the control MS-scaffolds, indicating that the biomimetic NF scaffold could promote bone repair via enhanced osteoblasts differentiation and biomineralization, corroborated by our previous observation[231]. Control MS did not appreciably enhance the bone repair. Excitingly, the bone defect was completely filled in

the BAM-scaffold group (Figure 6.5.1). To better evaluate the bone repair process and investigate the reasons which lead to the osteogenic outcome differences between the control MS group and BAM group, a time course study was conducted to examine the implanted constructs (control MS-scaffold and BAM-scaffold) at different time points (3 days, 1, 2, 4 and 8 weeks). NF scaffolds loaded with control MS were able to regenerate a very small amount of mineral tissue in 4 weeks, whereas a significant amount of mineral tissue started to form after 2 weeks implantation of BAM-scaffold (Figure 6.5.2) and substantial amount of bone was regenerated at 4 weeks and eventually the bone defect was

fully repaired at 8 weeks.

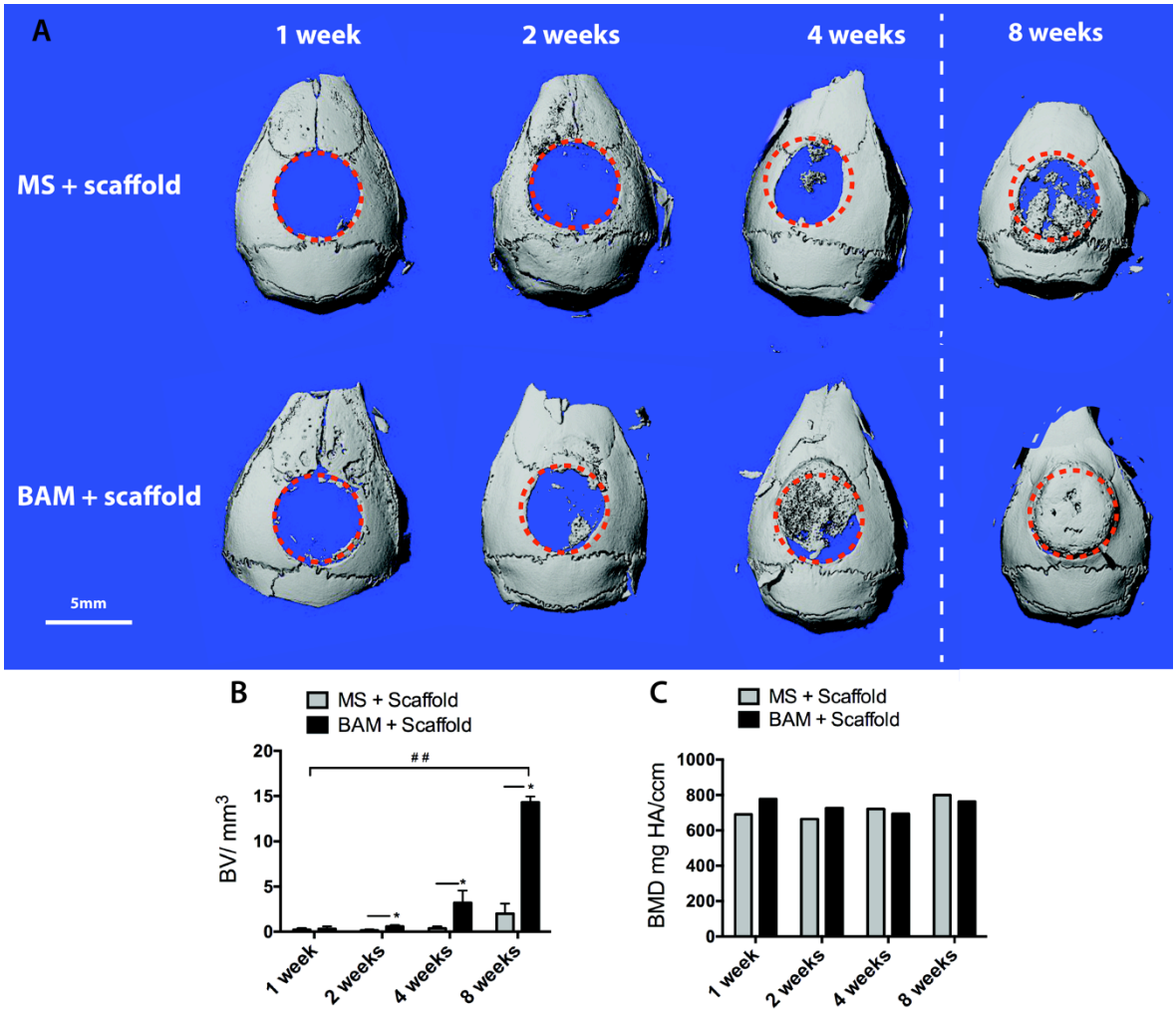

Figure 6.5.2 µCT characterization of the critical-sized defect repair over time. (A) Representative µCT reconstructions of mouse calvarial defects at 1, 2, 4 & 8 weeks, (B) New bone volume, and (C) new bone mineral density were quantified. N =6 per group, *P < 0.05.

F4/80 staining showed that the population of F4/80 positive macrophages remained at a stable and low level over 4 weeks within the control MS-scaffold. However, in BAM group, the population of F4/80 macrophages was significantly increased at day 3 post implantation and remained significantly higher than the level of MS-scaffold at day 7, but at the later time points the population was statistically indistinguishable from the MS-

scaffold group (Figure 6.5.3 C & D). We also noticed that the macrophages were distributed throughout the scaffold at the early stage and then aligned along the scaffold and mineral tissue edges at the late stage, likely acting as the bone supporting macrophages. CCL2 expression was significantly increased at all time points within BAM-scaffold, with the highest level expression exhibited at day 3 (Figure 6.5.3 E & F). Consistent with the *in vitro* transwell study, MSC population within the BAM-scaffold construct was higher than in the control MS-scaffold construct at all time points, especially at the early stage, evidenced by the increased double $CD73^+$ & $CD105^+$ expression (Figure 6.5.3 I & J), which are two well-recognized MSC biomarkers. Following the early influx of MSCs, osteogensis was evaluated by monitoring osteocalcin (OCN) expression, an important late stage biomarker of osteogenesis[232, 233]. OCN expression was gradually and slightly elevated over time in the control MS group. OCN expression was significantly higher over time in the BAM group than in the MS group and increased with time (Figure 6.5.3 G & H). Taken together, BAM enhanced bone healing via promoted MSCs recruitment into the scaffold, initiated by the efferocytosis of BAM, which led to the increased macrophage population and CCL2 secretion.

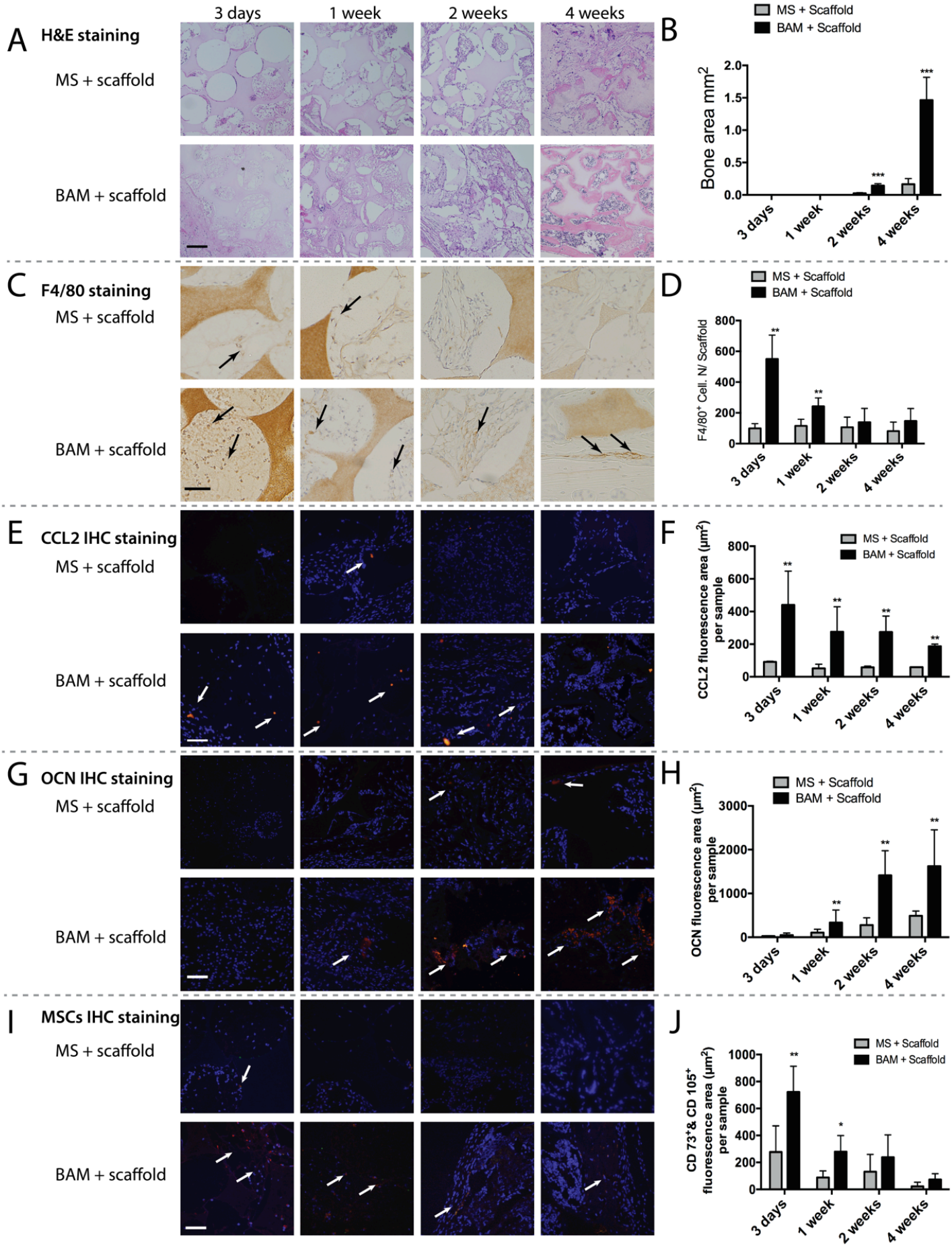
A
H&E staining
MS + scaffold
BAM + scaffold
3 days
1 week
2 weeks
4 weeks
B
MS + Scaffold
BAM + Scaffold
Bone area mm2
C
F4/80 staining
D
F4/80+ Cell. N/ Scaffold
E
CCL2 IHC staining
F
CCL2 fluorescence area (µm2) per sample
G
OCN IHC staining
H
OCN fluorescence area (µm2) per sample
I
MSCs IHC staining
J
CD 73+& CD 105+ fluorescence area (µm2) per sample

Figure 6.5.3 Histological characterization and histomorphometric analysis of the defect area over time. Representative pictures of (A) H&E staining, scale bar 150μm, (C) F4/80 staining, scale bar 125μm, (E) Immunofluorescence staining for CCL2 (red), DAPI staining for nuclei (blue), scale bar 100μm, (G) Immunofluorescence staining for OCN (red), DAPI staining for nuclei (blue), scale bar 100μm, (I) Immunofluorescence staining for CD73 (green), CD105 (red) DAPI staining for nuclei (blue), scale bar 200μm of mouse calvarial defects with either MS-scaffold or BAM-scaffold at different time points. Quantitative analysis of the defect area using histomorphometry. (B) Newly formed bone areas, (D) F4/80 positive cells numbers, (F) CCL2, (H) OCN expression and (J) double $CD73^+$ and $CD105^+$ expression in the defect areas. N=6~9 per group, *P < 0.05, **P < 0.01.

To further confirm the essential role of CCL2 in the BAM mediated bone regeneration, we compared the BAM-scaffold construct in both WD and CCR2 (the CCL2 receptor) KO mice. Four weeks bone repair data showed that the bone regeneration was greatly impaired in the CCR2 KO mice, with limited response to BAM (Figure 6.5.4). Reduced F4/80 cells, MSCs and CCL2 expression were also observed compared to the WD mice group (Figure 6.5.5).

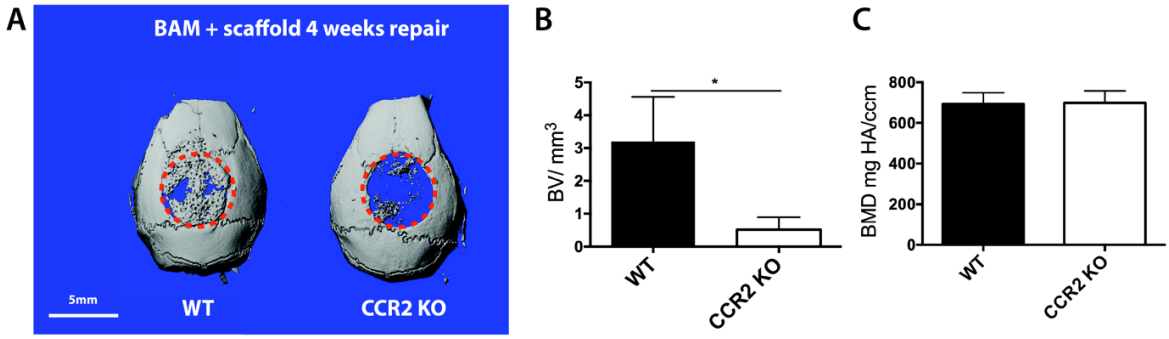

Figure 6.5.4 μCT characterization of the critical-sized defect repair in WT mice and CCR2 KO mice after 4 weeks. (A) Representative μCT reconstructions of mouse calvarial defects. (B) New bone volume, and (C) new bone mineral density were quantified. N =5 per group, *P < 0.05.

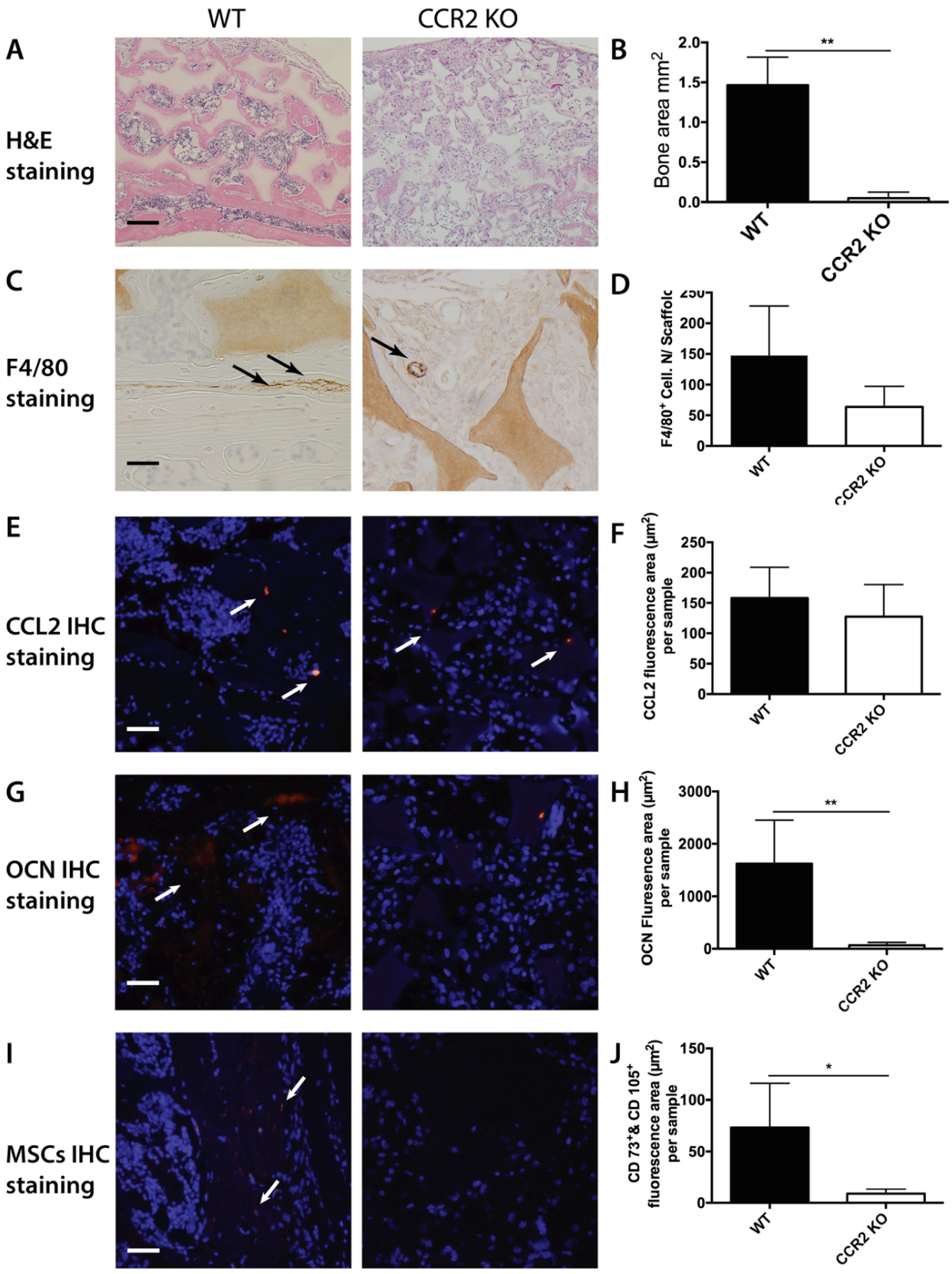
WT
CCR2 KO
A
H&E staining
B
Bone area mm2
2.0
1.5
1.0
0.5
0.0
**
WT
CCR2 KO
C
F4/80 staining
D
F4/80+ Cell. N/ Scaffold
250
200
150
100
50
0
WT
CCR2 KO
E
CCL2 IHC staining
F
CCL2 fluorescence area (μm2) per sample
250
200
150
100
50
0
WT
CCR2 KO
G
OCN IHC staining
H
OCN Fluresence area (μm2) per sample
3000
2000
1000
0
**
WT
CCR2 KO
I
MSCs IHC staining
J
CD 73+& CD 105+ fluorescence area (μm2) per sample
150
100
50
0
*
WT
CCR2 KO

Figure 6.5.5 Representative pictures of (A) H&E staining, scale bar 150µm, (C) F4/80 staining, scale bar 125µm, (E) Immunofluorescence staining for CCL2 (red), DAPI staining for nuclei (blue), scale bar 100µm, (G) Immunofluorescence staining for OCN (red), DAPI staining for nuclei (blue), scale bar 100µm, (I) Immunofluorescence staining for CD73 (green), CD105 (red) DAPI staining for nuclei (blue), scale bar 200µm of mouse calvarial defects with either MS-scaffold or BAM-scaffold. Quantitative analysis of the defect area using histomorphometry. (B) Newly formed bone areas, (D) F4/80 positive cells numbers, (F) CCL2, (H) OCN expression and (J) double $CD73^+$ and $CD105^+$ expression in the defect areas. N=6~9 per group*P < 0.05, **P < 0.01.

6.6 Discussion

Macrophages were originally known for their protective role in eliminating undesired pathogens, foreign bodies, and mediating inflammation and infection[234]. However, tissue resident macrophages have been found to hold a unique and vital role in maintaining tissue homeostasis and promoting tissue regeneration. Osteoclasts are classically considered resident macrophages in the bone tissue. They are known to play an important role in bone tissue homeostasis and repair, but recent studies suggest that non-osteoclast macrophages also play diverse and significant roles[216, 235].

Case in point, macrophages play an important role in bone fracture healing, which involves both the removal of damaged tissue and the initiation of prolonged regenerative response. It has been reported that while a certain number of osteoblasts matured into osteocytes, 40% to 70% of osteoblasts underwent apoptosis and were subsequently cleared by macrophages[236]. Recent studies suggest that efferocytosis of these apoptotic osteoblasts could trigger the secretion of key factors that are capable of inducing an influx of stem and/or progenitor cells[219, 237]. Indeed, CCL2 and TGF-ß1 levels increased after the macrophage engulfment of apoptotic bone cells. These macrophages initiate a cascade of events that result in the recruitment of mesenchymal stromal cells via various growth

factors, cytokines, and chemokines secretion. It has been shown that depletion of macrophages at the time of bone injury results in catastrophic failure of bone regeneration[238]. Macrophages have also demonstrated the ability to promote osteogenic differentiation and participate in both anabolic and remodeling phases[217, 239]. Because of these findings, macrophages have become attractive targets for bone regeneration therapy. Various genetic and pharmacological[240-243] approaches have been developed to modulate macrophages and can significantly regulate macrophage phenotypes, plasticity, and function.

An important "eat me" signal expressed on the surface of apoptotic cells is the PS lipid, which link to the integrins on macrophages for recognition and resultant efferocytosis[225]. Most PS lipids have been formulated into liposome systems for systemic administration[227] and PS liposome treatment has shown promising effects in resolving inflammation and benefiting tissue repair[35, 36, 244]. However, liposome systems have several disadvantages, including instability in the blood stream[37], short half-lives,[38, 245] and off-target effects[135, 246], and are therefore not suitable for regenerating localized bone defects, where spatially-controlled and prolonged presentation of the biological factors and signal cues are required.

In this work we hypothesize that engineered particles bearing "eat me" signals present a unique approach to target macrophages and harness macrophage beneficial effects in bone regeneration. We have designed a biomimetic biomaterials strategy, biodegradable MS with PS lipids immobilized on their surfaces. Biodegradable HEMA-PLLA was synthesized and fabricated into MS of sizes that mimicked those of apoptotic cells (1-5μm)

and the microsphere surfaces were then functionalized with biotin groups. Hydrophobic PS lipids were modified with PEG to increase the hydrophilicity and were further functionalized with biotin groups. Conjugation between the MS-biotin and PS-biotin was achieved by the addition of avidin and this process provided a versatile and highly efficient (~85%) conjugation to yield BAM.

Our *in vitro* efferocytosis assay revealed that macrophages engulfed more BAM than control MS. This supported our hypothesis that macrophage efferocytosis is enhanced by the microsphere surface presentation of PS lipid, the "eat me" signal. We also found significantly increased CCL2 secretion when macrophages were co-cultured with BAM *in vitro* at both the gene and protein levels. Recent studies have shown that CCL2 functions to recruit mesenchymal progenitor cells during early phases of bone fracture healing[221] and the stimulation of CCL2 production could also result in TGF-β1-mediated recruitment of bone marrow cells and bone marrow-derived mesenchymal stem cells[220]. Our *in vitro* trans-well cell migration assay data confirmed that CCL2 promoted BMSC migration, consistent with published data. Conditioned medium collected from the co-culture of macrophages and BAM or control MS demonstrated that BAM induced migration of significantly more BMSCs than the control MS. This difference can be partially explained by the enhanced CCL2 secretion of macrophages after engulfment of BAM. Due to the ability to mediate macrophage efferocytosis, CCL2 secretion, and ultimately BMSC recruitment and migration, BAM have demonstrated the ability to orchestrate bone defects repair.

NF scaffolds that mimic the fine fibrous structure of bone extracellular matrix have been developed and shown to promote osteogenesis and biomineralization[205, 247]. However, it remains a critical challenge to achieve critical-sized bone defect repair without the addition of cells to the scaffolds[39, 248]. We hypothesized that the macrophage engulfment of BAM loaded in the NF scaffold would induce an influx of stem and progenitor cells from the surrounding native bone, marrow and periosteum to the scaffold and thereby would enhance and maximize the osteogenic effects of these scaffolds. We tested the BAM-scaffold construct in a critical-sized calvarial defect repair model. Eight weeks after the implantation, we found that a certain amount of bone was regenerated in both plain scaffolds and control MS-scaffolds, demonstrating the degree of osteogenesis promoted by the advantageous biomimetic NF feature of the scaffolds. Excitingly, the whole calvarial defect was repaired in the BAM-scaffolds. In order to understand the dynamic process how the BAM enhanced the osteogenic effect of the NF scaffold, we monitored and compared the bone regeneration process at different time points between the MS-scaffold and the BAM-scaffold. The μCT and histologic data showed that the osteogenic outcomes of the two groups started to differentiate since 2 weeks and BAM group significantly increased the mineral tissue formation. The histologic examination of the defect areas between the control MS and BAM allowed us to uncover the events at early stage (prior to 2 weeks), which led to the resultant bone formation cascade. F4/80 staining revealed that BAM, as hypothesized, recruited significantly more macrophages in the first week (Figure 6.5.3 C & D), which subsequently elevated CCL2 secretion (Figure 6.5.3 E & F). The increased CCL2 level

in the initial phase contributed to the influx of bone forming cells including MSCs (Figure 6.5.3 I & J) to the injury site and differentiated into osteoblasts or their precursors, promoted by the NF scaffold, evidenced by the increased OCN expression levels (Figure 6.5.3 G & H). The control MS-scaffold relied on the passive cell migration and thus resulted in limited bone regeneration similar to the scaffold alone group. The impaired bone repair in CCR2 KO mice in response to the BAM-scaffold treatment further confirmed the critical role of CCL2 in recruiting MSCs for bone regeneration. This biomimetic BAM strategy took advantage of the macrophage efferocytosis and resultant CCL2 secretion that recruited stem cell into the osteogenic NF scaffold microenvironment, maximizing bone tissue formation.

6.7 Conclusion

Recent studies have shown the important role of macrophages in supporting bone formation, fracture healing and remodeling and most of work focus on genetic and pharmacological approaches to modulate macrophages. In this study, we developed a biomimetic strategy to attract macrophages and utilize their therapeutic potential in bone regeneration. Specifically, polymeric microspheres were surface modified with PS lipid, an "eat me" signal, to mimic apoptotic cells. Such BAM significantly enhanced the macrophage efferocytosis and recruited BMSCs via increased CCL2 secretion. Cell-free NF PLLA scaffolds loaded with BAM substantially promoted bone regeneration in a critical-sized calvarial bone repair model. The recruited and enriched osteogenic stem/progenitor cells in the NF scaffold microenvironment, likely further differentiate into mature osteoblasts/ osteocytes to produce and maintain mineralized bone locally. This

biomaterial design presents a novel tissue engineering approach to the repair of critical-sized bone defects without the addition of cells, and may be utilized in other macrophage-targeting therapeutics.

6.8 Experiment Section

Materials: (3s)-cis-3, 6-dimethyl-1, 4-dioxane-2, 5-dione (L-lactide or LLA) and Bovine serum albumin (BSA) were obtained from Sigma–Aldrich Inc. (St. Louis, MO) and purified by recrystallization from toluene. Stannous 2-ethylhexanoate (Sn(Oct)2), 2-hydroxyethyl methacrylate (HEMA), tris(2-carboxyethyl) phosphine hydrochloride (TCEP), 1-Ethyl-3-(3-dimethylaminopropyl)carbodiimide (EDC), N-hydroxysuccinimide (NHS), triethylamine (TEA), poly(ethylene glycol) diamine (NH2-PEG-NH2), fluorescein isothiocyanate (FITC), cysteine, polyvinyl alcohol (PVA), dichloromethane (DCM), dimethyl sulfoxide (DMSO), chloroform, methanol and albumin from bovine serum were purchased from Sigma–Aldrich Inc. (St. Louis, MO) and used as received. Biotin-NHS was purchased from Chem-Impex Int'l Inc. (Wood Dale, IL). 1,2-dipalmitoyl-sn-glycero-3-phosphoserine, sodium salt (DPPS) was purchased from Echelon Biosciences Incorporated (Salt Lake City, UT). Avidin, Egg White was purchased from EMD Millipore Corporation (USA).

Preparation of microsphere-biotin: The synthesis of HEMA-PLLA copolymer was outlined in a previous paper[133]. HEMA was used as initiator and $Sn(Oct)_2$ was used as catalyst to induce the ring opening polymerization of LLA. LLA (40 mmol, 5.760 g), HEMA (4 mmol, 0.464 g), and $Sn(Oct)_2$ (0.4 mmol, 0.162 g) were well-mixed in a 25 mL round-bottom flask under nitrogen purge and kept at 140°C for 2 h. The product was

cooled down and dissolved in 20 mL DCM. The polymer was precipitated out in 50 mL cold methanol, and then vacuum dried.

HEMA-PLLA was formulated into microspheres (MS) using the double emulsion method. One ml 10 % w/v HEMA-PLLA/ DCM solution was emulsified into 20 ml PVA aqueous solution (1% w/v) using a probe sonicator at an output power of 10 W (Virsonic 100, Cardiner, NY) for 20 s to create an oil-in-water emulsion. The solution was stirred at room temperature for 3 hours to evaporate DCM, and then centrifuged at 6000 rpm for 6 minutes to collect solid microspheres. The microspheres were washed with distilled water three times and freeze dried.

Excess cysteine (5 equiv), HEMA-PLLA MS (containing 1 equiv HEMA-PLLA), and TCEP (1 equiv) were dissolved in deionized water, then purged with N_2 for 10 min and stirred for 2 h at room temperature. This induces click reactions between thiol groups of cysteine and surface alkene groups on MS. MS-cys were then washed extensively using deionized water and lyophilized for 2 d.

Excess NHS-Biotin (5 equiv) was dissolved in DMSO, and then added into a MS-cys aqueous dispersion. The mixture was stirred for 3 h at room temperature, then washed 3 times and freeze-dried.

Preparation of PS-biotin: PS (1 equiv) and NH2-PEG-NH2 (1 equiv) were dissolved in a solution of chloroform and methanol (65:35). EDC (1 equiv) and NHS (1 equiv) were added to the solution and the reaction mixture was stirred at room temperature for 24 h. After the reaction mixture was filtered, 4 ml water was added and the mixture was

concentrated in a rotary evaporator to remove chloroform and methanol. The remaining PS-PEG aqueous solution was then freeze-dried.

Excess NHS-Biotin (5 equiv) was first dissolved in DMSO and added into a PS-PEG aqueous solution. The mixture was stirred for 3 h at room temperature, transferred into a dialysis bag (molecular weight cut-off (MWCO) 1000 Da, Fisherbrand regenerated cellulose), and dialyzed against a continuous flow of deionized water for 2 days, then freeze-dried.

Conjugation between microspheres and PS lipids: MS-biotin was first dispersed in water, then avidin was added and the mixture was stirred for 10 min. Varying amounts of PS-biotin were then added. The ratio of avidin to PS-biotin was 1 mg avidin to 10 µg biotin. The mixture was stirred for additional 40 mins, and then centrifuged. The microspheres were washed extensively with water 5 times, and then freeze-dried.

Evaluation of PS-biotin conjugation efficiency: The BAM were incubated in nonionic water at 70 C° for 5 mins to break PS-biotin bonds from the MS surfaces, then centrifuged. The PS-biotin amount in the supernatant was determined using Biotin Quantitation Kits (ThermoFisher, USA). MS conjugated with NH_2-PEG-NH_2 were used as control MS to minimize hydrophilicity difference between the control MS and BAM groups. PS to MS weight ratio was fixed at 1:20 in BAM experimental groups for the following experiments in the subsequent studies.

NMR characterization: ^{1}H spectra of the PS-biotin were obtained with an Inova 400 NMR instrument operating at 400 MHz at room temperature using deuterated chloroform (CDCl3) as the solvent.

FTIR characterization: The FTIR spectrums of MS and PS lipid before and after biotin functionalization were recorded with a Perkin Elmer 1800 FTIR spectroscopy, in the wavelength range from 600 to 4000 cm^{-1}.

Scanning Electron Microscopy (SEM) Observation: The microspheres were coated with gold using a sputter coater (DeskII, Denton vacuum Inc) and the surface morphology was examined using SEM (JEOL 7800FLV, USA) with an acceleration voltage of 15kVe.

In vitro cell culture: Primary bone marrow cells were collected from 4 to 8-week old C57BL/6J mice. Bone marrow-derived macrophages (BMMs) were differentiated *in vitro* from bone marrow flush in α-MEM medium (10% FBS, Pen/Strep, glutamine) with murine M-CSF (30 ng/mL eBioscience) for 6 days. At day 7, macrophages were plated in 3×10^5 cells/well in 12-well plates (for efferocytosis assays) or 1.0×10^6 cells/well in 6-well plates (for protein/RNA). Bone marrow stromal cells (BMSCs) were derived from bone marrow flush, cultured in α-MEM medium (20% FBS, Pen/Strep, glutamine) and used at passage 1.

Confocal Imaging: BMMs were plated in 1.5-mm coverglass chambers (8×10^4 cells/well) and stained with CellTracker DeepRed for 1 hr before efferocytosis study. Microspheres were then added into the wells (microspheres/macrophages=6:1). After 0.5 and 1 h co-cultures, BMMs were fixed with ice-cold methanol for 20 mins. Cells were then washed with PBS and covered with ProLong® Gold antifade reagent with DAPI (Life Technologies). Confocal microscopy images were analyzed using the Leica inverted SP5X confocal microscope system with two-photon film and Leica software (Leica Microsystems).

Transmission electron microscopy (TEM) imaging: Transmission electron microscopic images of the BMMs were taken for both the cellular ultrastructural analysis and the assessment of microsphere internalization. The macrophages (1.0×10^6 cells/mL) were plated in 6-well plates. The BMMs were then allowed to adhere for 24 h. Next, the cell medium was withdrawn and replaced with α-MEM medium supplemented with 0.2 % FBS. Different microspheres (microspheres/macrophages=5:1) were separately added to the plate and incubated for 1 h. After the incubation period, the cellular medium was replaced by a fixative solution containing 2.5 % glutaraldehyde (0.1 mol /L), sodium cacodylate buffer (0.1 mol /L, pH 7.4), and calcium chloride (3 mmol /L) for 5 min at room temperature, followed by 1 h in an ice bath. Next, the cells were rinsed with cacodylate buffer/calcium chloride and were post-fixed with 1 % osmium tetroxide, cacodylate buffer (0.1 mol/L), calcium chloride (3 mmol/ L), and potassium ferrocyanide solution (0.8%) for 30 min on ice. The cells were scraped off from the plate and washed with deionized (DI) water, then dehydrated in an ascending series of ethanol (20, 50, 70, 80%, and twice at 100%). The cells were embedded in Epon 812 resin for 72 h and placed in an oven for polymerization at 60°C. The monolayer culture ultra-thin sections were stained with uranyl acetate and lead citrate, then transferred to uncoated copper grids and examined in a Zeiss LEO 902 transmission electron microscope at an accelerating voltage of 60 kV.

Efferocytosis assay: Macrophages were stained using CellTracker DeepRed before adding microspheres. A total of 1.8×10^6 microspheres (microspheres/macrophages=6:1) were added into each well of the macrophage seeded 12-well plate (α-MEM medium, 0.2% FBS). After 0.5 and 1 h, BMMs co-cultured with microspheres were harvested and stained

with F4/80-PE (Abd Serotec, CI:A3-1). The co-cultures were fixed with 1% formalin and efferocytosis was assessed via flow cytometric (FACs) analyses (BD FACSAriaTM III) for double labeled cells ($FITC^+$ PE^+) reflecting engulfment. Macrophages cultured alone without microspheres were used as the control.

Gene expression and QRT-PCR: Gene expression was compared among the groups of BMM alone, BMM-control MS, and BMM-BAM. After 2, 6, 12, 24 h of co-culture, RNA was isolated using the Qiagen RNeasy Mini Kit. Reverse transcription PCR was conducted and the cDNA products were amplified and detected using TaqMan Universal PCR master mix (Applied Biosystems) and TaqMan probes. Mouse BMP2 (Mm01340178_m1), BMP7 (Mm00432102_m1) and CCL2 (Mm00441242_m1) were used as an endogenous controls. Realtime PCR was analyzed on ABI PRISM 7700 (AppliedBiosystems).

CCL2 enzyme-linked immunosorbent assay (ELISA): Supernatants were collected from 24 h co-cultures of BMM alone, BMM-control MS, and BMM-BAM groups. CCL2 protein levels in culture supernatants were measured with the Quantikine mouse CCL2 ELISA (R&D systems) per manufacturer's instructions. The absorption values were measured using an EZ Read 400 microplate reader (Biochrom).

In vitro transwell BMSC migration study: Migration assays were performed as described in previous studies with minor modifications[249]. Cell migration was assessed in 24-well plate transwells (Corning, Inc.) with a diameter of 6.5 mm and a pore size of 8 μm coated with 0.2 mg/mL collagen type I (EMD Millipore). BMSCs were placed in the upper chambers. Conditioned media from macrophage and either BAM or MS co-culture or α-MEM medium containing CCL2 protein and 0.2% FBS were added to the lower chambers.

After 8 hours, cells were fixed with 2.5% glutaraldehyde for 15 minutes. Cells, which remained on top of transwell membranes, were removed with cotton swabs. Cells that had migrated through the pores to the lower surface were stained with Gill's Hematoxylin (Sigma-Aldrich). Four fields at 200X magnification were selected at random, photo micrographic images obtained, and the cells in each image counted.

BAM immoblized scaffold preparation: 3D NF PLLA scaffolds with inter-connected spherical pores were fabricated as previously described[92]. Sugar spheres of desired-size (250-420 μm) were collected, washed with hexane three times, and added to a Teflon mold. The mold was heat-treated at 37 °C for 15 min to achieve the desired inter-connected pore structure, then placed under vacuum to remove the hexane. PLLA/THF (10% w/v solution) was cast into the sugar sphere assembly and the whole construct was stored at -80 °C overnight to induce phase separation. The phase-separated samples were immersed in distilled water to extract the solvent and leech away sugar spheres, leaving behind the NF PLLA scaffolds which were then freeze-dried and cut into thin disks (5 mm diameter and 1 mm thickness). BAM or control MS were immobilized onto the scaffolds via a solvent annealing method. Briefly, the BAM or control MS suspension was seeded onto the prefabricated NF PLLA scaffold, then subjected to a mixed solvent of hexane/THF (volume ratio of 90/10) which immobilized the BAM or control MS on the scaffold. The scaffolds were vacuum dried for 3 days to remove the solvent.

Calvarial bone-defect repair: All animals were maintained in accordance with institutional animal care and use guidelines. Experimental protocols were approved by the Institutional Animal Care and Use Committee of the University of Michigan. C57BL/6J mice were

purchased from the Jackson Laboratory, Bar Harbor, ME and CCR2 knockout (CCR2 KO) mice were received from Prof. Beth Moore lab, University of Michigan. Mice were randomly divided into experimental groups. Animals were anesthetized with isoflurane (2%) inhalation. A 5-mm craniotomy defect centered on the parietal calvarial bone was created using a trephine. A scaffold was placed to fill the defect (blank, control MS and BAM). The mice were euthanized at designated time points after implantation and the skulls were harvested.

μCT reconstruction and analysis: The skulls were placed in a 34 mm diameter specimen holder and scanned using a microCT system (μCT100 Scanco Medical, Bassersdorf, Switzerland). Scan settings were: voxel size 18 μm, 70 kVp, 114 μA, 0.5 mm AL filter, and integration time 500 ms. Analysis was performed using the manufacturer's evaluation software, and a fixed global threshold of 18% (180 on a grayscale of 0–1000) was used to segment bone from non-bone. 3D reconstruction of the skull and quantitative analyses were performed. A 5-mm round region of interest centered on the defect was determined and the bone volume (mm^3) (BV) and bone mineral density (BMD) in the area were measured using manufacturer's software (Scanco μCT 100).

Bone histologic and histomorphometric analysis: Calvarial samples were fixed with 4% formalin, decalcified with 10% EDTA for 2 weeks and subsequently embedded in paraffin. Hematoxylin & eosin (H&E) staining of the coronal sections (5 μm thick) were performed by the histology core at the University of Michigan, School of Dentistry. To visualize F4/80 positive cells, the de-paraffinized slides were incubated overnight at 4 °C with a mouse polyclonal primary antibody to F4/80 (1:100, ab6640 Abcam) and staining was

performed using the standard Anti-Rat HRP-DAB Cell & Tissue Staining Kit (R&D) following the manufacturer's protocol. For immunofluorescence visualization of OCN and CCL2 expression within the defect areas, the slides were de-paraffinized and heat treated in the citrate buffer (2.1 M citric acid, pH 6.0) at 100 °C for 30 min for antigen retrieval. After blocking in 3% BSA/PBS solution, sections were then incubated overnight at 4 °C with a rabbit polyclonal primary antibody to OCN (1:100, ab93876 Abcam) or a rabbit polyclonal primary antibody to MCP1 (1:100, ab25124 Abcam). After three washes in PBS, the sections were incubated with TRITC-conjugated donkey antibody to rabbit IgG (1:400, Santa Cruz) for 1 h. To visualize the CD73 and CD105 expressing cells, slides were incubated overnight at 4 °C with Polyclonal Sheep antibody to Mouse 5'-Nucleotidase/CD73 (1:100, AF4488
, R&D system) and Polyclonal Goat antibody to Mouse Endoglin/CD105 (1:100, AF1320, R&D system), after de-paraffinized, blocked in 3% BSA/PBS solution. After three washes in PBS, the sections were incubated with TRITC-conjugated donkey antibody to goat IgG (1:400, sc3885, Santa Cruz) and FITC-conjugated rabbit antibody to sheep IgG (1:400, #31627, ThermoFisher) for 1 h. The sections were mounted with the medium containing DAPI (Vector Laboratories) and then examined under a confocal microscope (Eclipse C1 Plus, Nikon).

Static histomorphometric analyses for F4/80 positive cell number and CCL2 and OCN expression were performed using computer-assisted histomorphometric analyzing software (Image-Pro Plus version 4.0; Media Cybernetics, Inc., Silver Spring, MD and NIS-Elements AR, Nikon.).

Statistical Analysis: All numerical data are presented as mean ± SD. All P values were two-tailed and $P < 0.05$ was considered statistically significant. One-way ANOVA test was applied to compare different groups using GraphPad InStat software (GraphPad).

CHAPTER 7

Conclusion and Outlook

7.1 Conclusion

In this thesis, we have developed two biomimetic systems and use them as platform technologies to explore the regenerative potential of PTH delivery and apoptotic-cell mimicking microspheres in bone tissue engineering applications.

Preprogrammed PTH delivery system

Implantable preprogrammed drug delivery devices have been developed with the ability to release PTH in pulsatile and continuous fashions. For the pulsatile delivery device, surface erosion polymer has been synthesized and advanced fabrication techniques have been developed to enable us to fabricate the pulsatile delivery device capable of delivering multiple pulses of PTH. The release kinetics can be modulated via tuning the both chemical and physical properties of the device. We achieved 21-pulse PTH release with different time intervals (ranging from 24 hours to 60 hours) and over 90% drug bioactivity can be maintained. For the continuous delivery device, we prepared surface-erosion microspheres capable of sustained PTH release in a linear manner, which has not been demonstrated with other types of biodegradable polymers. The release rate can be controlled via adjusting the properties of the surface erosion polymer. We demonstrated linear drug release for 3 weeks with over 85% drug bioactivity retained.

Both pulsatile and continuous delivery device loaded with same amount of PTH were first

tested in a subcutaneous implantation model. We examined the systemic therapeutic effects of the engineered PTH release on vertebrae and tibia and the results showed that pulsatile PTH release was able to increase bone via enhancing bone remodeling, whereas the continuous PTH release resulted in bone resorption via elevated osteoclast resorption activity. The devices were biodegradable and biocompatible *in vivo*, eliminating the need for removal surgery. Therefore the biodegradable pulsatile PTH delivery device has demonstrated the potential to be a patient-friendly PTH therapy, which could be administered only once (implantation) in contrast to the current daily injection treatment. Further, we repurpose PTH in a local bone defect model to expand the application of PTH from systemic osteoporosis treatment to local bone defect repair. The delivery device locally releases PTH to a cell-free biomimetic NF scaffold. This combination system (PTH delivery device and scaffold) enabled us to determine the optimal release kinetics (pulsatile vs continuous) in terms of osteogenic outcome. We found that local continuous PTH release inhibited, while local pulsatile PTH release (daily pulse for 21 days) promoted bone regeneration. In addition, the local pulsatile delivery strategy advantageously achieved higher quality regenerated bone and reduced the systemic side effects compared to the standard PTH injection treatment. This is the first time local pulsatile PTH delivery has been achieved to promote bone regeneration via enhanced bone remodeling. This acellular therapy provides a novel strategy to improve bone defect repair by integrating a biomimetic scaffold and an anabolic local delivery to maximize the regenerative effects within the intended areas of interest. This technology holds promise for bone defect repair without addition of external cells, the burden of daily PTH injections, and the need for device removal surgery.

Biodegradable Apoptotic-cell Mimicking Microspheres

The unique role of macrophages in supporting bone formation, fracture healing and bone remodeling has drawn a lot of attention. In this study, we developed a biomimetic strategy

to target macrophages and enhance their therapeutic functions in promoting bone regeneration. Specifically, biodegradable polymeric microspheres were surface modified with "eat me signal" lipid molecules, to mimic apoptotic cells. A novel bioconjugation strategy has been developed to enable efficient and controlled conjugation between the functionalized microsphere surface and the PS lipids. This strategy overcomes the drawbacks of the conventional lipid liposome formulation and achieved controlled surface presentation of the lipid signal molecules. Several significant advantages of this strategy also include that the fabrication was conducted in mild aqueous and RT conditions; chemicals involved in these reactions have already been used in FDA-approved products. We evaluated BAM microspheres biological function and their interaction with macrophages both *in vitro* and *in vivo*. We found that BAM microspheres significantly enhanced the macrophages phagocytosis and induced BMSCs migration via increased secretion of CCL2. Cell-free NF PLLA scaffolds loaded with BAM microspheres substantially promoted bone regeneration in a critical-sized calvarial bone repair model. BAM enhanced macrophage-mediated stem cells recruitment to the NF scaffold microenvironment and helped induce osteoblast differentiation and biomineralization, thereby enhancing the osteogenic outcome in the NF scaffold.

7.2 Future Work and Outlook

There are numbers of future directions these systems developed here could lead to.

Preprogrammed delivery system

In this thesis, we demonstrated long-term preprogrammed PTH release for both systemic and local delivery applications. Besides PTH, more therapeutics (small molecule drugs and biologics) could be readily incorporated into these devices. The preprogrammed systems could enable delivery of multiple molecules in a simultaneous or sequential manner to

better replicate and regulate the natural healing process, which often involves sequential signaling of multiple types of biomolecules. Therefore these systems could provide more qualitative and quantitative understanding of the complex interaction and cooperative signaling between the signal molecules, microenvironment and physiology. The information and the drug delivery toolbox could further provide guidance to design optimal personalized treatment. Beyond the tissue engineering application, we expect the platform (continuous and pulsatile devices) to be useful in other fundamental and translational studies on how temporal effects and release patterns of biomolecules regulate cell activity, tissue development, and physiology.

Biodegradable Apoptotic-cell Mimicking Microspheres

Novel chemical modification and conjugation methods have been developed to functionalize biodegradable microsphere with lipid signal molecules. Besides lipids conjugation, the functional microspheres would be readily modified with other types of molecules (like peptides, proteins, and antibodies). Therapeutics can be readily loaded into the BAM microspheres so that BAM microspheres can also serve as drug vehicle targeting macrophages. As we have demonstrated the BAM microspheres could promote BMSCs migration and further benefit the bone defect repair. We expect in the future this biomimetic immunomodulatory strategy opens a novel avenue to bone and potential other tissue regeneration without the need for exogenous cells.

BIBLIOGRAPHY

[1] M.M. Martino, P.S. Briquez, K. Maruyama, J.A. Hubbell, Extracellular matrix-inspired growth factor delivery systems for bone regeneration, Advanced Drug Delivery Reviews, 94 (2015) 41-52.

[2] R. Marsell, T.A. Einhorn, The biology of fracture healing, Injury, 42 551-555.

[3] T.N. Vo, F.K. Kasper, A.G. Mikos, Strategies for Controlled Delivery of Growth Factors and Cells for Bone Regeneration, Advanced drug delivery reviews, 64 (2012) 1292-1309.

[4] Bone Grafts And Substitutes Market Analysis By Material (Natural - Autografts, Allografts; Synthetic - Ceramic, Composite, Polymer, Bone Morphogenetic Proteins (BMP)), By Application (Craniomaxillofacial, Dental, Foot & Ankle, Joint Reconstruction, Long Bone, Spinal Fusion) Forecasts To 2024, in: Bone Grafts And Substitutes Market Size, Share Report, 2024, 2016, pp. 80.

[5] C.G. Finkemeier, Bone-Grafting and Bone-Graft Substitutes, JBJS, 84 (2002).

[6] C. Laurencin, Y. Khan, S.F. El-Amin, Bone graft substitutes, Expert Review of Medical Devices, 3 (2006) 49-57.

[7] D.H. Kim, R. Rhim, L. Li, J. Martha, B.H. Swaim, R.J. Banco, L.G. Jenis, S.G. Tromanhauser, Prospective study of iliac crest bone graft harvest site pain and morbidity, The Spine Journal, 9 886-892.

[8] M.K. Sen, T. Miclau, Autologous iliac crest bone graft: Should it still be the gold standard for treating nonunions?, Injury, 38 S75-S80.

[9] H.C. Pape, A. Evans, P. Kobbe, Autologous Bone Graft: Properties and Techniques, Journal of Orthopaedic Trauma, 24 (2010).

[10] K.U. Gomes, J.L. Carlini, C. Biron, A. Rapoport, R.A. Dedivitis, Use of Allogeneic Bone Graft in Maxillary Reconstruction for Installation of Dental Implants, Journal of Oral and Maxillofacial Surgery, 66 (2008) 2335-2338.

[11] S. Stevenson, Enhancement of Fracture Healing With Autogenous and Allogeneic Bone Grafts, Clinical Orthopaedics and Related Research, 355 (1998).

[12] M. Yildirim, H. Spiekermann, S. Biesterfeld, D. Edelhoff, Maxillary sinus augmentation using xenogenic bone substitute material Bio-Oss® in combination with venous blood, Clinical Oral Implants Research, 11 (2000) 217-229.

[13] J. Wiltfang, O. Zernial, E. Behrens, A. Schlegel, P.H. Warnke, S.T. Becker, Regenerative Treatment of Peri-Implantitis Bone Defects with a Combination of Autologous Bone and a Demineralized Xenogenic Bone Graft: A Series of 36 Defects, Clinical Implant Dentistry and Related Research, 14 (2012) 421-427.

[14] P.X. Ma, Biomimetic materials for tissue engineering, Advanced Drug Delivery Reviews, 60 (2008) 184-198.

[15] X. Liu, P.X. Ma, Polymeric scaffolds for bone tissue engineering, Ann Biomed Eng, 32 (2004) 477-486.

[16] S. Neuss, C. Apel, P. Buttler, B. Denecke, A. Dhanasingh, X. Ding, D. Grafahrend, A. Groger, K. Hemmrich, A. Herr, W. Jahnen-Dechent, S. Mastitskaya, A. Perez-Bouza, S. Rosewick, J. Salber, M. Wöltje, M. Zenke, Assessment of stem cell/biomaterial combinations for stem cell-based tissue engineering, Biomaterials, 29 (2008) 302-313.

[17] J.R. Porter, T.T. Ruckh, K.C. Popat, Bone tissue engineering: A review in bone biomimetics and drug delivery strategies, Biotechnology Progress, 25 (2009) 1539-1560.

[18] K.J.L. Burg, S. Porter, J.F. Kellam, Biomaterial developments for bone tissue engineering, Biomaterials, 21 (2000) 2347-2359.

[19] A.I. Caplan, Adult mesenchymal stem cells for tissue engineering versus regenerative medicine, Journal of Cellular Physiology, 213 (2007) 341-347.

[20] W.-J. Li, R. Tuli, C. Okafor, A. Derfoul, K.G. Danielson, D.J. Hall, R.S. Tuan, A three-dimensional nanofibrous scaffold for cartilage tissue engineering using human mesenchymal stem cells, Biomaterials, 26 (2005) 599-609.

[21] R.S. Tuan, G. Boland, R. Tuli, Adult mesenchymal stem cells and cell-based tissue engineering, Arthritis Res Ther, 5 (2002) 32.

[22] S. Gronthos, S.O. Akintoye, C.-Y. Wang, S. Shi, Bone marrow stromal stem cells for tissue engineering, Periodontology 2000, 41 (2006) 188-195.

[23] E.M. Bueno, J. Glowacki, Cell-free and cell-based approaches for bone regeneration, Nat Rev Rheumatol, 5 (2009) 685-697.

[24] J.A. Burdick, R.L. Mauck, J.H. Gorman, R.C. Gorman, Acellular Biomaterials: An Evolving Alternative to Cell-Based Therapies, Science Translational Medicine, 5 (2013) 176ps174.

[25] A.R. Derubeis, R. Cancedda, Bone Marrow Stromal Cells (BMSCs) in Bone Engineering: Limitations and Recent Advances, Ann Biomed Eng, 32 (2004) 160-165.

[26] H. Shin, S. Jo, A.G. Mikos, Biomimetic materials for tissue engineering, Biomaterials, 24 (2003) 4353-4364.

[27] M.M. Stevens, Biomaterials for bone tissue engineering, Materials Today, 11 (2008) 18-25.

[28] S. Bose, M. Roy, A. Bandyopadhyay, Recent advances in bone tissue engineering scaffolds, Trends in Biotechnology, 30 (2012) 546-554.

[29] D.W. Dempster, F. Cosman, M.A.Y. Parisien, V. Shen, R. Lindsay, Anabolic Actions of Parathyroid Hormone on Bone, Endocrine Reviews, 14 (1993) 690-709.

[30] D.W. Dempster, F. Cosman, E.S. Kurland, H. Zhou, J. Nieves, L. Woelfert, E. Shane, K. Plavetić, R. Müller, J. Bilezikian, R. Lindsay, Effects of Daily Treatment with Parathyroid Hormone on Bone Microarchitecture and Turnover in Patients with Osteoporosis: A Paired Biopsy Study*, Journal of Bone and Mineral Research, 16 (2001) 1846-1853.

[31] M. Dang, A.J. Koh, T. Danciu, L.K. McCauley, P.X. Ma, Preprogrammed Long-Term Systemic Pulsatile Delivery of Parathyroid Hormone to Strengthen Bone, Advanced Healthcare Materials, 6 (2017) 1600901-n/a.

[32] H.L. Chan, L.K. McCauley, Parathyroid Hormone Applications in the Craniofacial Skeleton, Journal of Dental Research, 92 (2013) 18-25.

[33] K. Lauber, E. Bohn, S.M. Kröber, Y.-j. Xiao, S.G. Blumenthal, R.K. Lindemann, P. Marini, C. Wiedig, A. Zobywalski, S. Baksh, Y. Xu, I.B. Autenrieth, K. Schulze-Osthoff, C. Belka, G. Stuhler, S. Wesselborg, Apoptotic Cells Induce Migration of Phagocytes via Caspase-3-Mediated Release of a Lipid Attraction Signal, Cell, 113 (2003) 717-730.

[34] C. Grimsley, K.S. Ravichandran, Cues for apoptotic cell engulfment: eat-me, don't eat-me and come-get-me signals, Trends in Cell Biology, 13 (2003) 648-656.

[35] M.-L.N. Huynh, V.A. Fadok, P.M. Henson, Phosphatidylserine-dependent ingestion of apoptotic cells promotes TGF-β1 secretion and the resolution of inflammation, The Journal of Clinical Investigation, 109 (2002) 41-50.

[36] G.C. Ramos, D. Fernandes, C.T. Charão, D.G. Souza, M.M. Teixeira, J. Assreuy, Apoptotic mimicry: phosphatidylserine liposomes reduce inflammation through activation of peroxisome proliferator-activated receptors (PPARs) in vivo, British Journal of Pharmacology, 151 (2007) 844-850.

[37] R.W. Malone, P.L. Felgner, I.M. Verma, Cationic liposome-mediated RNA transfection, Proceedings of the National Academy of Sciences of the United States of America, 86 (1989) 6077-6081.

[38] M.L. Immordino, F. Dosio, L. Cattel, Stealth liposomes: review of the basic science, rationale, and clinical applications, existing and potential, International Journal of Nanomedicine, 1 (2006) 297-315.

[39] M. Dang, A.J. Koh, X. Jin, L.K. McCauley, P.X. Ma, Local pulsatile PTH delivery regenerates bone defects via enhanced bone remodeling in a cell-free scaffold, Biomaterials, 114 (2017) 1-9.

[40] V. Mouriño, A.R. Boccaccini, Bone tissue engineering therapeutics: controlled drug delivery in three-dimensional scaffolds, Journal of The Royal Society Interface, (2009).

[41] C.T. Johnson, A.J. García, Scaffold-based Anti-infection Strategies in Bone Repair, Ann Biomed Eng, 43 (2015) 515-528.

[42] F. Buket Basmanav, G.T. Kose, V. Hasirci, Sequential growth factor delivery from complexed microspheres for bone tissue engineering, Biomaterials, 29 (2008) 4195-4204.

[43] G. Wei, Q. Jin, W.V. Giannobile, P.X. Ma, The enhancement of osteogenesis by nano-fibrous scaffolds incorporating rhBMP-7 nanospheres, Biomaterials, 28 (2007) 2087-2096.

[44] H.L. Chan, L.K. McCauley, Parathyroid Hormone Applications in the Craniofacial Skeleton, Journal of Dental Research, 92 (2012) 18-25.

[45] A.D. Taut, Q. Jin, J.-H. Chung, P. Galindo-Moreno, E.S. Yi, J.V. Sugai, H.Z. Ke, M. Liu, W.V. Giannobile, Sclerostin antibody stimulates bone regeneration after experimental periodontitis, Journal of Bone and Mineral Research, 28 (2013) 2347-2356.

[46] A.S. Virdi, M. Liu, K. Sena, J. Maletich, M. McNulty, H.Z. Ke, D.R. Sumner, Sclerostin Antibody Increases Bone Volume and Enhances Implant Fixation in a Rat Model, The Journal of Bone and Joint Surgery. American volume, 94 (2012) 1670-1680.

[47] X. Zhang, Y. Li, Y.E. Chen, J. Chen, P.X. Ma, Cell-free 3D scaffold with two-stage delivery of miRNA-26a to regenerate critical-sized bone defects, Nat Commun, 7 (2016).

[48] Y. Gafni, G. Pelled, Y. Zilberman, G. Turgeman, F. Apparailly, H. Yotvat, E. Galun, Z. Gazit, C. Jorgensen, D. Gazit, Gene Therapy Platform for Bone Regeneration Using an Exogenously Regulated, AAV-2-Based Gene Expression System, Molecular Therapy, 9 (2004) 587-595.

[49] F.-M. Chen, M. Zhang, Z.-F. Wu, Toward delivery of multiple growth factors in tissue engineering, Biomaterials, 31 (2010) 6279-6308.

[50] J.E. Babensee, L.V. McIntire, A.G. Mikos, Growth Factor Delivery for Tissue Engineering, Pharmaceutical Research, 17 (2000) 497-504.

[51] J.K. Tessmar, A.M. Göpferich, Matrices and scaffolds for protein delivery in tissue engineering, Advanced Drug Delivery Reviews, 59 (2007) 274-291.

[52] P. Tayalia, D.J. Mooney, Controlled Growth Factor Delivery for Tissue Engineering, Advanced Materials, 21 (2009) 3269-3285.

[53] C. Li, C. Vepari, H.-J. Jin, H.J. Kim, D.L. Kaplan, Electrospun silk-BMP-2 scaffolds for bone tissue engineering, Biomaterials, 27 (2006) 3115-3124.

[54] D.H.R. Kempen, L. Lu, T.E. Hefferan, L.B. Creemers, A. Maran, K.L. Classic, W.J.A. Dhert, M.J. Yaszemski, Retention of in vitro and in vivo BMP-2 bioactivities in sustained delivery vehicles for bone tissue engineering, Biomaterials, 29 (2008) 3245-3252.

[55] P. Yilgor, K. Tuzlakoglu, R.L. Reis, N. Hasirci, V. Hasirci, Incorporation of a sequential BMP-2/BMP-7 delivery system into chitosan-based scaffolds for bone tissue engineering, Biomaterials, 30 (2009) 3551-3559.

[56] A. Berner, J.D. Boerckel, S. Saifzadeh, R. Steck, J. Ren, C. Vaquette, J.Q. Zhang, M. Nerlich, R.E. Guldberg, D.W. Hutmacher, M.A. Woodruff, Biomimetic tubular nanofiber mesh and platelet rich plasma-mediated delivery of BMP-7 for large bone defect regeneration, Cell and Tissue Research, 347 (2012) 603-612.

[57] H. Eckardt, M. Ding, M. Lind, E.S. Hansen, K.S. Christensen, I. Hvid, Recombinant human vascular endothelial growth factor enhances bone healing in an experimental nonunion model, Journal of Bone & Joint Surgery, British Volume, 87-B (2005) 1434.

[58] J. Kleinheinz, U. Stratmann, U. Joos, H.-P. Wiesmann, VEGF-Activated Angiogenesis During Bone Regeneration, Journal of Oral and Maxillofacial Surgery, 63 (2005) 1310-1316.

[59] R. Kigami, S. Sato, N. Tsuchiya, T. Yoshimakai, Y. Arai, K. Ito, FGF-2 Angiogenesis in Bone Regeneration Within Critical-Sized Bone Defects in Rat Calvaria, Implant Dentistry, 22 (2013).

[60] H. Maehara, S. Sotome, T. Yoshii, I. Torigoe, Y. Kawasaki, Y. Sugata, M. Yuasa, M. Hirano, N. Mochizuki, M. Kikuchi, K. Shinomiya, A. Okawa, Repair of large osteochondral defects in rabbits using porous hydroxyapatite/collagen (HAp/Col) and fibroblast growth factor-2 (FGF-2), Journal of Orthopaedic Research, 28 (2010) 677-686.

[61] N. de Jesus-Gonzalez, E. Robinson, J. Moslehi, B.D. Humphreys, Management of Antiangiogenic Therapy-Induced Hypertension, Hypertension, 60 (2012) 607-615.

[62] Y.-S. Ng, P.A. D'Amore, Therapeutic angiogenesis for cardiovascular disease, Current Controlled Trials in Cardiovascular Medicine, 2 (2001) 278-285.

[63] C.A. Tannoury, H.S. An, Complications with the use of bone morphogenetic protein 2 (BMP-2) in spine surgery, The Spine Journal, 14 552-559.

[64] E.J. Carragee, G. Chu, R. Rohatgi, E.L. Hurwitz, B.K. Weiner, S.T. Yoon, G. Comer, B. Kopjar, Cancer Risk After Use of Recombinant Bone Morphogenetic Protein-2 for Spinal Arthrodesis, JBJS, 95 (2013).

[65] J.T. Potts, Parathyroid hormone: past and present, Journal of Endocrinology, 187 (2005) 311-325.

[66] B. Chertok, M.J. Webber, M.D. Succi, R. Langer, Drug Delivery Interfaces in the 21st Century: From Science Fiction Ideas to Viable Technologies, Molecular Pharmaceutics, 10 (2013) 3531-3543.

[67] B.P. Timko, K. Whitehead, W. Gao, D.S. Kohane, O. Farokhzad, D. Anderson, R. Langer, Advances in Drug Delivery, Annual Review of Materials Research, 41 (2011) 1-20.

[68] L. Qin, L.J. Raggatt, N.C. Partridge, Parathyroid hormone: a double-edged sword for bone metabolism, Trends in Endocrinology & Metabolism, 15 (2004) 60-65.

[69] R.M. Neer, C.D. Arnaud, J.R. Zanchetta, R. Prince, G.A. Gaich, J.-Y. Reginster, A.B. Hodsman, E.F. Eriksen, S. Ish-Shalom, H.K. Genant, O. Wang, D. Mellström, E.S. Oefjord, E. Marcinowska-Suchowierska, J. Salmi, H. Mulder, J. Halse, A.Z. Sawicki, B.H. Mitlak, Effect of Parathyroid Hormone (1-34) on Fractures and Bone Mineral Density in Postmenopausal Women with Osteoporosis, New England Journal of Medicine, 344 (2001) 1434-1441.

[70] S. Kuroshima, B.L. Kovacic, K.M. Kozloff, L.K. McCauley, J. Yamashita, Intra-oral PTH Administration Promotes Tooth Extraction Socket Healing, Journal of Dental Research, 92 (2013) 553-559.

[71] J.D. Bashutski, R.M. Eber, J.S. Kinney, E. Benavides, S. Maitra, T.M. Braun, W.V. Giannobile, L.K. McCauley, Teriparatide and Osseous Regeneration in the Oral Cavity, New England Journal of Medicine, 363 (2010) 2396-2405.

[72] R.T. Franceschi, Biological Approaches to Bone Regeneration by Gene Therapy, Journal of Dental Research, 84 (2005) 1093-1103.

[73] J. Park, R. Lutz, E. Felszeghy, J. Wiltfang, E. Nkenke, F.W. Neukam, K.A. Schlegel, The effect on bone regeneration of a liposomal vector to deliver BMP-2 gene to bone grafts in peri-implant bone defects, Biomaterials, 28 (2007) 2772-2782.

[74] Q. Kang, M.H. Sun, H. Cheng, Y. Peng, A.G. Montag, A.T. Deyrup, W. Jiang, H.H. Luu, J. Luo, J.P. Szatkowski, P. Vanichakarn, J.Y. Park, Y. Li, R.C. Haydon, T.C. He, Characterization of the distinct orthotopic bone-forming activity of 14 BMPs using recombinant adenovirus-mediated gene delivery, Gene Ther, 11 (2004) 1312-1320.

[75] D. Qu, J. Li, Y. Li, Y. Gao, Y. Zuo, Y. Hsu, J. Hu, Angiogenesis and osteogenesis enhanced by bFGF ex vivo gene therapy for bone tissue engineering in reconstruction of calvarial defects, Journal of Biomedical Materials Research Part A, 96A (2011) 543-551.

[76] R.M. Capito, M. Spector, Collagen scaffolds for nonviral IGF-1 gene delivery in articular cartilage tissue engineering, Gene Ther, 14 (2007) 721-732.

[77] T. Gonzalez-Fernandez, E.G. Tierney, G.M. Cunniffe, F.J. O'Brien, D.J. Kelly, Gene Delivery of TGF-β3 and BMP2 in an MSC-Laden Alginate Hydrogel for Articular Cartilage and Endochondral Bone Tissue Engineering, Tissue Eng Part A, 22 (2016) 776-787.

[78] P.-C. Chang, Y.-J. Seol, J.A. Cirelli, G.R. Pellegrini, Q. Jin, L.M. Franco, S.A. Goldstein, L.A. Chandler, B. Sosnowski, W.V. Giannobile, PDGF-B Gene Therapy Accelerates Bone Engineering and Oral Implant Osseointegration, Gene therapy, 17 (2010) 95-104.

[79] F. Geiger, H. Bertram, I. Berger, H. Lorenz, O. Wall, C. Eckhardt, H.-G. Simank, W. Richter, Vascular Endothelial Growth Factor Gene-Activated Matrix (VEGF165-GAM) Enhances Osteogenesis and Angiogenesis in Large Segmental Bone Defects, Journal of Bone and Mineral Research, 20 (2005) 2028-2035.

[80] S. Ghadakzadeh, M. Mekhail, A. Aoude, R. Hamdy, M. Tabrizian, Small Players Ruling the Hard Game: siRNA in Bone Regeneration, Journal of Bone and Mineral Research, 31 (2016) 475-487.

[81] Y. Zhang, L. Wei, R.J. Miron, B. Shi, Z. Bian, Bone scaffolds loaded with siRNA-Semaphorin4d for the treatment of osteoporosis related bone defects, Scientific Reports, 6 (2016) 26925.

[82] K.S. Nitta, K. Numata, Biopolymer-Based Nanoparticles for Drug/Gene Delivery and Tissue Engineering, International Journal of Molecular Sciences, 14 (2013).

[83] P. Guo, O. Coban, N.M. Snead, J. Trebley, S. Hoeprich, S. Guo, Y. Shu, Engineering RNA for Targeted siRNA Delivery and Medical Application, Advanced Drug Delivery Reviews, 62 (2010) 650-666.

[84] D.W. Pack, A.S. Hoffman, S. Pun, P.S. Stayton, Design and development of polymers for gene delivery, Nat Rev Drug Discov, 4 (2005) 581-593.

[85] X. Zhang, W.T. Godbey, Viral vectors for gene delivery in tissue engineering, Advanced Drug Delivery Reviews, 58 (2006) 515-534.

[86] K. Feng, H. Sun, M.A. Bradley, E.J. Dupler, W.V. Giannobile, P.X. Ma, Novel antibacterial nanofibrous PLLA scaffolds, Journal of Controlled Release, 146 (2010) 363-369.

[87] T. Miyai, A. Ito, G. Tamazawa, T. Matsuno, Y. Sogo, C. Nakamura, A. Yamazaki, T. Satoh, Antibiotic-loaded poly-ε-caprolactone and porous β-tricalcium phosphate composite for treating osteomyelitis, Biomaterials, 29 (2008) 350-358.

[88] G. Wei, P.X. Ma, Structure and properties of nano-hydroxyapatite/polymer composite scaffolds for bone tissue engineering, Biomaterials, 25 (2004) 4749-4757.

[89] K. Rezwan, Q.Z. Chen, J.J. Blaker, A.R. Boccaccini, Biodegradable and bioactive porous polymer/inorganic composite scaffolds for bone tissue engineering, Biomaterials, 27 (2006) 3413-3431.

[90] F. Yang, J.G.C. Wolke, J.A. Jansen, Biomimetic calcium phosphate coating on electrospun poly(ε-caprolactone) scaffolds for bone tissue engineering, Chemical Engineering Journal, 137 (2008) 154-161.

[91] X. Liu, L.A. Smith, J. Hu, P.X. Ma, Biomimetic nanofibrous gelatin/apatite composite scaffolds for bone tissue engineering, Biomaterials, 30 (2009) 2252-2258.

[92] G. Wei, P.X. Ma, Macroporous and nanofibrous polymer scaffolds and polymer/bone-like apatite composite scaffolds generated by sugar spheres, Journal of Biomedical Materials Research Part A, 78A (2006) 306-315.

[93] C. He, G. Xiao, X. Jin, C. Sun, P.X. Ma, Electrodeposition on Nanofibrous Polymer Scaffolds: Rapid Mineralization, Tunable Calcium Phosphate Composition and Topography, Advanced Functional Materials, 20 (2010) 3568-3576.

[94] S.P. Baldwin, W. Mark Saltzman, Materials for protein delivery in tissue engineering, Advanced Drug Delivery Reviews, 33 (1998) 71-86.

[95] X. Wang, E. Wenk, X. Zhang, L. Meinel, G. Vunjak-Novakovic, D.L. Kaplan, Growth factor gradients via microsphere delivery in biopolymer scaffolds for osteochondral tissue engineering, Journal of Controlled Release, 134 (2009) 81-90.

[96] E.H. Groeneveld, E.H. Burger, Bone morphogenetic proteins in human bone regeneration, European Journal of Endocrinology, 142 (2000) 9-21.

[97] A.W. James, G. LaChaud, J. Shen, G. Asatrian, V. Nguyen, X. Zhang, K. Ting, C. Soo, A Review of the Clinical Side Effects of Bone Morphogenetic Protein-2, Tissue Engineering. Part B, Reviews, 22 (2016) 284-297.

[98] E.J. Carragee, E.L. Hurwitz, B.K. Weiner, A critical review of recombinant human bone morphogenetic protein-2 trials in spinal surgery: emerging safety concerns and lessons learned, The Spine Journal, 11 471-491.

[99] L.C. Gerstenfeld, D.M. Cullinane, G.L. Barnes, D.T. Graves, T.A. Einhorn, Fracture healing as a post-natal developmental process: Molecular, spatial, and temporal aspects of its regulation, Journal of Cellular Biochemistry, 88 (2003) 873-884.

[100] Z.S. Patel, S. Young, Y. Tabata, J.A. Jansen, M.E.K. Wong, A.G. Mikos, Dual delivery of an angiogenic and an osteogenic growth factor for bone regeneration in a critical size defect model, Bone, 43 (2008) 931-940.

[101] N.J. Shah, M.N. Hyder, M.A. Quadir, N.-M. Dorval Courchesne, H.J. Seeherman, M. Nevins, M. Spector, P.T. Hammond, Adaptive growth factor delivery from a polyelectrolyte coating promotes synergistic bone tissue repair and reconstruction, Proceedings of the National Academy of Sciences, 111 (2014) 12847-12852.

[102] R. Langer, Biomaterials in Drug Delivery and Tissue Engineering: One Laboratory's Experience, Accounts of Chemical Research, 33 (2000) 94-101.

[103] M. Sokolsky-Papkov, K. Agashi, A. Olaye, K. Shakesheff, A.J. Domb, Polymer carriers for drug delivery in tissue engineering, Advanced Drug Delivery Reviews, 59 (2007) 187-206.

[104] M.L. Hans, A.M. Lowman, Biodegradable nanoparticles for drug delivery and targeting, Current Opinion in Solid State and Materials Science, 6 (2002) 319-327.

[105] H.K. Makadia, S.J. Siegel, Poly Lactic-co-Glycolic Acid (PLGA) as Biodegradable Controlled Drug Delivery Carrier, Polymers, 3 (2011).

[106] P.B. Malafaya, G.A. Silva, R.L. Reis, Natural–origin polymers as carriers and scaffolds for biomolecules and cell delivery in tissue engineering applications, Advanced Drug Delivery Reviews, 59 (2007) 207-233.

[107] I.I. Slowing, J.L. Vivero-Escoto, C.-W. Wu, V.S.Y. Lin, Mesoporous silica nanoparticles as controlled release drug delivery and gene transfection carriers, Advanced Drug Delivery Reviews, 60 (2008) 1278-1288.

[108] I.I. Slowing, B.G. Trewyn, S. Giri, V.S.Y. Lin, Mesoporous Silica Nanoparticles for Drug Delivery and Biosensing Applications, Advanced Functional Materials, 17 (2007) 1225-1236.

[109] Y. Zhu, J. Shi, W. Shen, X. Dong, J. Feng, M. Ruan, Y. Li, Stimuli-Responsive Controlled Drug Release from a Hollow Mesoporous Silica Sphere/Polyelectrolyte Multilayer Core–Shell Structure, Angewandte Chemie, 117 (2005) 5213-5217.

[110] W. Fang, J. Yang, J. Gong, N. Zheng, Photo- and pH-Triggered Release of Anticancer Drugs from Mesoporous Silica-Coated Pd@Ag Nanoparticles, Advanced Functional Materials, 22 (2012) 842-848.

[111] H. Dai, Q. Chen, H. Qin, Y. Guan, D. Shen, Y. Hua, Y. Tang, J. Xu, A Temperature-Responsive Copolymer Hydrogel in Controlled Drug Delivery, Macromolecules, 39 (2006) 6584-6589.

[112] Y.-J. Kim, M. Ebara, T. Aoyagi, A Smart Hyperthermia Nanofiber with Switchable Drug Release for Inducing Cancer Apoptosis, Advanced Functional Materials, 23 (2013) 5753-5761.

[113] M. Nazari, M. Rubio-Martinez, G. Tobias, J.P. Barrio, R. Babarao, F. Nazari, K. Konstas, B.W. Muir, S.F. Collins, A.J. Hill, M.C. Duke, M.R. Hill, Metal-Organic-Framework-Coated Optical Fibers as Light-Triggered Drug Delivery Vehicles, Advanced Functional Materials, 26 (2016) 3244-3249.

[114] B.P. Timko, M. Arruebo, S.A. Shankarappa, J.B. McAlvin, O.S. Okonkwo, B. Mizrahi, C.F. Stefanescu, L. Gomez, J. Zhu, A. Zhu, J. Santamaria, R. Langer, D.S. Kohane, Near-infrared–actuated devices for remotely controlled drug delivery, Proceedings of the National Academy of Sciences, 111 (2014) 1349-1354.

[115] A. Schroeder, J. Kost, Y. Barenholz, Ultrasound, liposomes, and drug delivery: principles for using ultrasound to control the release of drugs from liposomes, Chemistry and Physics of Lipids, 162 (2009) 1-16.

[116] A.L. Klibanov, T.I. Shevchenko, B.I. Raju, R. Seip, C.T. Chin, Ultrasound-triggered release of materials entrapped in microbubble–liposome constructs: A tool for targeted drug delivery, Journal of Controlled Release, 148 (2010) 13-17.

[117] G. Jeon, S.Y. Yang, J. Byun, J.K. Kim, Electrically Actuatable Smart Nanoporous Membrane for Pulsatile Drug Release, Nano Letters, 11 (2011) 1284-1288.

[118] T. Hoare, J. Santamaria, G.F. Goya, S. Irusta, D. Lin, S. Lau, R. Padera, R. Langer, D.S. Kohane, A Magnetically Triggered Composite Membrane for On-Demand Drug Delivery, Nano Letters, 9 (2009) 3651-3657.

[119] Z. Zhang, J. Hu, P.X. Ma, Nanofiber-based delivery of bioactive agents and stem cells to bone sites, Advanced Drug Delivery Reviews, 64 (2012) 1129-1141.

[120] H.S. Yoo, T.G. Kim, T.G. Park, Surface-functionalized electrospun nanofibers for tissue engineering and drug delivery, Advanced Drug Delivery Reviews, 61 (2009) 1033-1042.

[121] X. Liu, Y. Won, P.X. Ma, Surface modification of interconnected porous scaffolds, Journal of Biomedical Materials Research Part A, 74A (2005) 84-91.

[122] J.M. Goddard, J.H. Hotchkiss, Polymer surface modification for the attachment of bioactive compounds, Progress in Polymer Science, 32 (2007) 698-725.

[123] S.E. Sakiyama-Elbert, J.A. Hubbell, Development of fibrin derivatives for controlled release of heparin-binding growth factors, Journal of Controlled Release, 65 (2000) 389-402.

[124] M.M. Martino, P.S. Briquez, A. Ranga, M.P. Lutolf, J.A. Hubbell, Heparin-binding domain of fibrin(ogen) binds growth factors and promotes tissue repair when incorporated within a synthetic matrix, Proceedings of the National Academy of Sciences, 110 (2013) 4563-4568.

[125] S.E. Kim, S.-H. Song, Y.P. Yun, B.-J. Choi, I.K. Kwon, M.S. Bae, H.-J. Moon, Y.-D. Kwon, The effect of immobilization of heparin and bone morphogenic protein-2 (BMP-2) to titanium surfaces on inflammation and osteoblast function, Biomaterials, 32 (2011) 366-373.

[126] S. Singh, B.M. Wu, J.C.Y. Dunn, The enhancement of VEGF-mediated angiogenesis by polycaprolactone scaffolds with surface cross-linked heparin, Biomaterials, 32 (2011) 2059-2069.

[127] A.S. Fu, T.R. Thatiparti, G.M. Saidel, H.A. von Recum, Experimental Studies and Modeling of Drug Release from a Tunable Affinity-Based Drug Delivery Platform, Ann Biomed Eng, 39 (2011) 2466-2475.

[128] M. Goldberg, R. Langer, X. Jia, Nanostructured materials for applications in drug delivery and tissue engineering, Journal of Biomaterials Science, Polymer Edition, 18 (2007) 241-268.

[129] J. Gao, L. Niklason, R. Langer, Surface hydrolysis of poly(glycolic acid) meshes increases the seeding density of vascular smooth muscle cells, Journal of Biomedical Materials Research, 42 (1998) 417-424.

[130] G.E. Park, M.A. Pattison, K. Park, T.J. Webster, Accelerated chondrocyte functions on NaOH-treated PLGA scaffolds, Biomaterials, 26 (2005) 3075-3082.

[131] F.M. Veronese, G. Pasut, PEGylation, successful approach to drug delivery, Drug Discovery Today, 10 (2005) 1451-1458.

[132] R.B. Greenwald, Y.H. Choe, J. McGuire, C.D. Conover, Effective drug delivery by PEGylated drug conjugates, Advanced Drug Delivery Reviews, 55 (2003) 217-250.

[133] Z. Zhang, M.J. Gupte, X. Jin, P.X. Ma, Injectable Peptide Decorated Functional Nanofibrous Hollow Microspheres to Direct Stem Cell Differentiation and Tissue Regeneration, Advanced functional materials, 25 (2015) 350-360.

[134] V. Biju, Chemical modifications and bioconjugate reactions of nanomaterials for sensing, imaging, drug delivery and therapy, Chemical Society Reviews, 43 (2014) 744-764.

[135] T.A. Karlsen, J.E. Brinchmann, Liposome Delivery of MicroRNA-145 to Mesenchymal Stem Cells Leads to Immunological Off-target Effects Mediated by RIG-I, Molecular Therapy, 21 (2013) 1169-1181.

[136] J.M. Anderson, M.S. Shive, Biodegradation and biocompatibility of PLA and PLGA microspheres, Advanced Drug Delivery Reviews, 64 (2012) 72-82.

[137] Qi, P. Hu, J. Xu, Wang, Encapsulation of Drug Reservoirs in Fibers by Emulsion Electrospinning: Morphology Characterization and Preliminary Release Assessment, Biomacromolecules, 7 (2006) 2327-2330.

[138] G. Wei, G.J. Pettway, L.K. McCauley, P.X. Ma, The release profiles and bioactivity of parathyroid hormone from poly(lactic-co-glycolic acid) microspheres, Biomaterials, 25 (2004) 345-352.

[139] T.M. Allen, P.R. Cullis, Liposomal drug delivery systems: From concept to clinical applications, Advanced Drug Delivery Reviews, 65 (2013) 36-48.

[140] T.J. Sill, H.A. von Recum, Electrospinning: Applications in drug delivery and tissue engineering, Biomaterials, 29 (2008) 1989-2006.

[141] O.R. Davies, A.L. Lewis, M.J. Whitaker, H. Tai, K.M. Shakesheff, S.M. Howdle, Applications of supercritical CO2 in the fabrication of polymer systems for drug delivery and tissue engineering, Advanced Drug Delivery Reviews, 60 (2008) 373-387.

[142] J.J. Blaker, J.C. Knowles, R.M. Day, Novel fabrication techniques to produce microspheres by thermally induced phase separation for tissue engineering and drug delivery, Acta Biomaterialia, 4 (2008) 264-272.

[143] Q. Jin, G. Wei, Z. Lin, J.V. Sugai, S.E. Lynch, P.X. Ma, W.V. Giannobile, Nanofibrous Scaffolds Incorporating PDGF-BB Microspheres Induce Chemokine Expression and Tissue Neogenesis In Vivo, PLoS ONE, 3 (2008) e1729.

[144] W. Wang, M. Dang, Z. Zhang, J. Hu, T.W. Eyster, L. Ni, P.X. Ma, Dentin regeneration by stem cells of apical papilla on injectable nanofibrous microspheres and stimulated by controlled BMP-2 release, Acta Biomaterialia, 36 (2016) 63-72.

[145] N. Monteiro, A. Martins, R.L. Reis, N.M. Neves, Liposomes in tissue engineering and regenerative medicine, Journal of the Royal Society Interface, 11 (2014) 20140459.

[146] L. Sercombe, T. Veerati, F. Moheimani, S.Y. Wu, A.K. Sood, S. Hua, Advances and Challenges of Liposome Assisted Drug Delivery, Frontiers in Pharmacology, 6 (2015) 286.

[147] F. Tang, L. Li, D. Chen, Mesoporous Silica Nanoparticles: Synthesis, Biocompatibility and Drug Delivery, Advanced Materials, 24 (2012) 1504-1534.

[148] I. Freeman, S. Cohen, The influence of the sequential delivery of angiogenic factors from affinity-binding alginate scaffolds on vascularization, Biomaterials, 30 (2009) 2122-2131.

[149] T.A. Holland, E.W.H. Bodde, V.M.J.I. Cuijpers, L.S. Baggett, Y. Tabata, A.G. Mikos, J.A. Jansen, Degradable hydrogel scaffolds for in vivo delivery of single and dual growth factors in cartilage repair, Osteoarthritis and Cartilage, 15 (2007) 187-197.

[150] D.H.R. Kempen, L. Lu, A. Heijink, T.E. Hefferan, L.B. Creemers, A. Maran, M.J. Yaszemski, W.J.A. Dhert, Effect of local sequential VEGF and BMP-2 delivery on ectopic and orthotopic bone regeneration, Biomaterials, 30 (2009) 2816-2825.

[151] R. Farra, N.F. Sheppard, L. McCabe, R.M. Neer, J.M. Anderson, J.T. Santini, M.J. Cima, R. Langer, First-in-Human Testing of a Wirelessly Controlled Drug Delivery Microchip, Science Translational Medicine, (2012).

[152] S. Kim, Y. Kang, C.A. Krueger, M. Sen, J.B. Holcomb, D. Chen, J.C. Wenke, Y. Yang, Sequential delivery of BMP-2 and IGF-1 using a chitosan gel with gelatin microspheres enhances early osteoblastic differentiation, Acta Biomaterialia, 8 (2012) 1768-1777.

[153] H.J. Lee, W.-G. Koh, Hydrogel Micropattern-Incorporated Fibrous Scaffolds Capable of Sequential Growth Factor Delivery for Enhanced Osteogenesis of hMSCs, ACS Applied Materials & Interfaces, 6 (2014) 9338-9348.

[154] X. Liu, G.J. Pettway, L.K. McCauley, P.X. Ma, Pulsatile release of parathyroid hormone from an implantable delivery system, Biomaterials, 28 (2007) 4124-4131.

[155] S. Mura, J. Nicolas, P. Couvreur, Stimuli-responsive nanocarriers for drug delivery, Nat Mater, 12 (2013) 991-1003.

[156] S. Ganta, H. Devalapally, A. Shahiwala, M. Amiji, A review of stimuli-responsive nanocarriers for drug and gene delivery, Journal of Controlled Release, 126 (2008) 187-204.

[157] N. Rapoport, Physical stimuli-responsive polymeric micelles for anti-cancer drug delivery, Progress in Polymer Science, 32 (2007) 962-990.

[158] T.R. Hoare, D.S. Kohane, Hydrogels in drug delivery: Progress and challenges, Polymer, 49 (2008) 1993-2007.

[159] T. Miyata, T. Uragami, K. Nakamae, Biomolecule-sensitive hydrogels, Advanced Drug Delivery Reviews, 54 (2002) 79-98.

[160] M.P. Lutolf, J.L. Lauer-Fields, H.G. Schmoekel, A.T. Metters, F.E. Weber, G.B. Fields, J.A. Hubbell, Synthetic matrix metalloproteinase-sensitive hydrogels for the conduction of tissue regeneration: Engineering cell-invasion characteristics, Proceedings of the National Academy of Sciences, 100 (2003) 5413-5418.

[161] D. Seliktar, A.H. Zisch, M.P. Lutolf, J.L. Wrana, J.A. Hubbell, MMP-2 sensitive, VEGF-bearing bioactive hydrogels for promotion of vascular healing, Journal of Biomedical Materials Research Part A, 68A (2004) 704-716.

[162] D. Putnam, Polymers for gene delivery across length scales, Nat Mater, 5 (2006) 439-451.

[163] T.G. Park, J.H. Jeong, S.W. Kim, Current status of polymeric gene delivery systems, Advanced Drug Delivery Reviews, 58 (2006) 467-486.

[164] C.M. Wiethoff, C.R. Middaugh, Barriers to nonviral gene delivery, Journal of Pharmaceutical Sciences, 92 (2003) 203-217.

[165] W.T. Godbey, K.K. Wu, A.G. Mikos, Poly(ethylenimine) and its role in gene delivery, Journal of Controlled Release, 60 (1999) 149-160.

[166] S.C. De Smedt, J. Demeester, W.E. Hennink, Cationic Polymer Based Gene Delivery Systems, Pharmaceutical Research, 17 (2000) 113-126.

[167] D.A. Balazs, W. Godbey, Liposomes for Use in Gene Delivery, Journal of Drug Delivery, 2011 (2011).

[168] Z.-G. Gao, H.D. Fain, N. Rapoport, Controlled and targeted tumor chemotherapy by micellar-encapsulated drug and ultrasound, Journal of Controlled Release, 102 (2005) 203-222.

[169] P. Anilkumar, E. Gravel, I. Theodorou, K. Gombert, B. Thézé, F. Ducongé, E. Doris, Nanometric Micelles with Photo-Triggered Cytotoxicity, Advanced Functional Materials, 24 (2014) 5246-5252.

[170] G. Wu, A. Mikhailovsky, H.A. Khant, C. Fu, W. Chiu, J.A. Zasadzinski, Remotely Triggered Liposome Release by Near-Infrared Light Absorption via Hollow Gold Nanoshells, Journal of the American Chemical Society, 130 (2008) 8175-8177.

[171] S.J. Leung, X.M. Kachur, M.C. Bobnick, M. Romanowski, Wavelength-Selective Light-Induced Release from Plasmon Resonant Liposomes, Advanced Functional Materials, 21 (2011) 1113-1121.

[172] J. Ge, E. Neofytou, T.J. Cahill, R.E. Beygui, R.N. Zare, Drug Release from Electric-Field-Responsive Nanoparticles, ACS Nano, 6 (2012) 227-233.

[173] Y. Wang, M.S. Shim, N.S. Levinson, H.-W. Sung, Y. Xia, Stimuli-Responsive Materials for Controlled Release of Theranostic Agents, Advanced Functional Materials, 24 (2014) 4206-4220.

[174] S.-H. Hu, T.-Y. Liu, D.-M. Liu, S.-Y. Chen, Controlled Pulsatile Drug Release from a Ferrogel by a High-Frequency Magnetic Field, Macromolecules, 40 (2007) 6786-6788.

[175] Y. Li, G. Huang, X. Zhang, B. Li, Y. Chen, T. Lu, T.J. Lu, F. Xu, Magnetic Hydrogels and Their Potential Biomedical Applications, Advanced Functional Materials, 23 (2013) 660-672.

[176] A.C. Grayson, Richards Choi, Insung S. Tyler, Betty M. Wang, Paul P. Brem, Henry Cima, Michael J., Langer, Robert, Multi-pulse drug delivery from a resorbable polymeric microchip device, Nat Mater, 2 (2003) 767-772.

[177] A.G. Skirtach, P. Karageorgiev, M.F. Bédard, G.B. Sukhorukov, H. Möhwald, Reversibly Permeable Nanomembranes of Polymeric Microcapsules, Journal of the American Chemical Society, 130 (2008) 11572-11573.

[178] J. Borges, L.C. Rodrigues, R.L. Reis, J.F. Mano, Layer-by-Layer Assembly of Light-Responsive Polymeric Multilayer Systems, Advanced Functional Materials, 24 (2014) 5624-5648.

[179] K. Patel, S. Angelos, W.R. Dichtel, A. Coskun, Y.-W. Yang, J.I. Zink, J.F. Stoddart, Enzyme-Responsive Snap-Top Covered Silica Nanocontainers, Journal of the American Chemical Society, 130 (2008) 2382-2383.

[180] H. Zhang, J. Fei, X. Yan, A. Wang, J. Li, Enzyme-Responsive Release of Doxorubicin from Monodisperse Dipeptide-Based Nanocarriers for Highly Efficient Cancer Treatment In Vitro, Advanced Functional Materials, 25 (2015) 1193-1204.

[181] H.J. Kim, H. Matsuda, H. Zhou, I. Honma, Ultrasound-Triggered Smart Drug Release from a Poly(dimethylsiloxane)– Mesoporous Silica Composite, Advanced Materials, 18 (2006) 3083-3088.

[182] J. Di, J. Price, X. Gu, X. Jiang, Y. Jing, Z. Gu, Ultrasound-Triggered Regulation of Blood Glucose Levels Using Injectable Nano-Network, Advanced Healthcare Materials, 3 (2014) 811-816.

[183] K. Sato, M. Takahashi, M. Ito, E. Abe, J.-I. Anzai, Glucose-induced decomposition of layer-by-layer films composed of phenylboronic acid-bearing poly(allylamine) and poly(vinyl alcohol) under physiological conditions, Journal of Materials Chemistry B, 3 (2015) 7796-7802.

[184] R. Farra, N.F. Sheppard, L. McCabe, R.M. Neer, J.M. Anderson, J.T. Santini, M.J. Cima, R. Langer, First-in-Human Testing of a Wirelessly Controlled Drug Delivery Microchip, Science Translational Medicine, 4 (2012) 122ra121-122ra121.

[185] G.J. Pettway, J.A. Meganck, A.J. Koh, E.T. Keller, S.A. Goldstein, L.K. McCauley, Parathyroid hormone mediates bone growth through the regulation of osteoblast proliferation and differentiation, Bone, 42 (2008) 806-818.

[186] N.S. Datta, G.J. Pettway, C. Chen, A.J. Koh, L.K. McCauley, Cyclin D1 as a Target for the Proliferative Effects of PTH and PTHrP in Early Osteoblastic Cells, Journal of Bone and Mineral Research, 22 (2007) 951-964.

[187] G.J. Pettway, A. Schneider, A.J. Koh, E. Widjaja, M.D. Morris, J.A. Meganck, S.A. Goldstein, L.K. McCauley, Anabolic actions of PTH (1-34): Use of a novel tissue engineering model to investigate temporal effects on bone, Bone, 36 (2005) 959-970.

[188] S. Hou, L.K. McCauley, P.X. Ma, Synthesis and Erosion Properties of PEG-Containing Polyanhydrides, Macromolecular Bioscience, 7 (2007) 620-628.

[189] D. Verma, M.S. Desai, N. Kulkarni, N. Langrana, Characterization of surface charge and mechanical properties of chitosan/alginate based biomaterials, Materials Science and Engineering: C, 31 (2011) 1741-1747.

[190] W. Melitz, J. Shen, A.C. Kummel, S. Lee, Kelvin probe force microscopy and its application, Surface Science Reports, 66 (2011) 1-27.

[191] H. Sun, L. Mei, C. Song, X. Cui, P. Wang, The in vivo degradation, absorption and excretion of PCL-based implant, Biomaterials, 27 (2006) 1735-1740.

[192] K.E. Uhrich, S.M. Cannizzaro, R.S. Langer, K.M. Shakesheff, Polymeric Systems for Controlled Drug Release, Chemical Reviews, 99 (1999) 3181-3198.

[193] H.-L. Chen, B. Demiralp, A. Schneider, A.J. Koh, C. Silve, C.-Y. Wang, L.K. McCauley, Parathyroid Hormone and Parathyroid Hormone-related Protein Exert Both Pro- and Anti-apoptotic Effects in Mesenchymal Cells, Journal of Biological Chemistry, 277 (2002) 19374-19381.

[194] J. Panyam, V. Labhasetwar, Biodegradable nanoparticles for drug and gene delivery to cells and tissue, Advanced Drug Delivery Reviews, 55 (2003) 329-347.

[195] J.M. Anderson, M.S. Shive, Biodegradation and biocompatibility of PLA and PLGA microspheres, Advanced Drug Delivery Reviews, 64, Supplement (2012) 72-82.

[196] L.K. McCauley, A.J. Koh, C.A. Beecher, Y. Cui, T.J. Rosol, R.T. Franceschi, PTH/PTHrP receptor is temporally regulated during osteoblast differentiation and is associated with collagen synthesis, Journal of Cellular Biochemistry, 61 (1996) 638-647.

[197] R. Gopalakrishnan, H. Ouyang, M.J. Somerman, L.K. McCauley, R.T. Franceschi, Matrix γ-Carboxyglutamic Acid Protein Is a Key Regulator of PTH-Mediated Inhibition of Mineralization in MC3T3-E1 Osteoblast-Like Cells, Endocrinology, 142 (2001) 4379-4388.

[198] S.W. Cho, F.Q. Pirih, A.J. Koh, M. Michalski, M.R. Eber, K. Ritchie, B. Sinder, S. Oh, S.A. Al-Dujaili, J. Lee, K. Kozloff, T. Danciu, T.J. Wronski, L.K. McCauley, The Soluble Interleukin-6 Receptor Is a Mediator of Hematopoietic and Skeletal Actions of Parathyroid Hormone, The Journal of Biological Chemistry, 288 (2013) 6814-6825.

[199] J.M. Holzwarth, P.X. Ma, Biomimetic nanofibrous scaffolds for bone tissue engineering, Biomaterials, 32 (2011) 9622-9629.

[200] A.J. Koh, C.M. Novince, X. Li, T. Wang, R.S. Taichman, L.K. McCauley, An Irradiation-Altered Bone Marrow Microenvironment Impacts Anabolic Actions of PTH, Endocrinology, 152 (2011) 4525-4536.

[201] K.E.S. Poole, J. Reeve, Parathyroid hormone — a bone anabolic and catabolic agent, Current Opinion in Pharmacology, 5 (2005) 612-617.

[202] A. Nardi, L. Ventura, L. Cozzi, G. Tonini, R. Zennaro, M. Celi, E. Ramazzina, The bone anabolic therapy, Aging Clinical and Experimental Research, 25 (2013) 121-124.

[203] R.S. Dhillon, E.M. Schwarz, Teriparatide Therapy as an Adjuvant for Tissue Engineering and Integration of Biomaterials, Journal of materials research, 4 (2011) 1117-1131.

[204] S. Zhang, J. Ermann, M.D. Succi, A. Zhou, M.J. Hamilton, B. Cao, J.R. Korzenik, J.N. Glickman, P.K. Vemula, L.H. Glimcher, G. Traverso, R. Langer, J.M. Karp, An inflammation-targeting hydrogel for local drug delivery in inflammatory bowel disease, Science Translational Medicine, 7 (2015) 300ra128-300ra128.

[205] K.M. Woo, V.J. Chen, P.X. Ma, Nano-fibrous scaffolding architecture selectively enhances protein adsorption contributing to cell attachment, Journal of Biomedical Materials Research Part A, 67A (2003) 531-537.

[206] L.A. Smith, X. Liu, J. Hu, P.X. Ma, The influence of three-dimensional nanofibrous scaffolds on the osteogenic differentiation of embryonic stem cells, Biomaterials, 30 (2009) 2516-2522.

[207] J. Hu, X. Liu, P.X. Ma, Induction of osteoblast differentiation phenotype on poly(l-lactic acid) nanofibrous matrix, Biomaterials, 29 (2008) 3815-3821.

[208] P.G. Calò, G. Pisano, G. Loi, F. Medas, L. Barca, M. Atzeni, A. Nicolosi, Intraoperative parathyroid hormone assay during focused parathyroidectomy: the importance of 20 minutes measurement, BMC Surgery, 13 (2013) 1-5.

[209] L.S. Nair, C.T. Laurencin, Biodegradable polymers as biomaterials, Progress in Polymer Science, 32 (2007) 762-798.

[210] T.A. Wynn, A. Chawla, J.W. Pollard, Macrophage biology in development, homeostasis and disease, Nature, 496 (2013) 445-455.

[211] Thomas A. Wynn, Kevin M. Vannella, Macrophages in Tissue Repair, Regeneration, and Fibrosis, Immunity, 44 450-462.

[212] C. Schlundt, H. Schell, S.B. Goodman, G. Vunjak-Novakovic, G.N. Duda, K. Schmidt-Bleek, Immune modulation as a therapeutic strategy in bone regeneration, Journal of Experimental Orthopaedics, 2 (2015) 1.

[213] B. Chazaud, Macrophages: Supportive cells for tissue repair and regeneration, Immunobiology, 219 (2014) 172-178.

[214] B.P. Sinder, A.R. Pettit, L.K. McCauley, Macrophages: Their Emerging Roles in Bone, Journal of bone and mineral research : the official journal of the American Society for Bone and Mineral Research, 30 (2015) 2140-2149.

[215] L.J. Raggatt, M.E. Wullschleger, K.A. Alexander, A.C. Wu, S.M. Millard, S. Kaur, M.L. Maugham, L.S. Gregory, R. Steck, A.R. Pettit, Fracture healing via periosteal callus formation requires macrophages for both initiation and progression of early endochondral ossification, The American journal of pathology, 184 (2014) 3192-3204.

[216] M.K. Chang, L.J. Raggatt, K.A. Alexander, J.S. Kuliwaba, N.L. Fazzalari, K. Schroder, E.R. Maylin, V.M. Ripoll, D.A. Hume, A.R. Pettit, Osteal tissue macrophages are intercalated throughout human and mouse bone lining tissues and regulate osteoblast function in vitro and in vivo, J Immunol, 181 (2008) 1232-1244.

[217] S.W. Cho, F.N. Soki, A.J. Koh, M.R. Eber, P. Entezami, S.I. Park, N. van Rooijen, L.K. McCauley, Osteal macrophages support physiologic skeletal remodeling and anabolic actions of parathyroid hormone in bone, Proceedings of the National Academy of Sciences, 111 (2014) 1545-1550.

[218] A.C. Wu, L.J. Raggatt, K.A. Alexander, A.R. Pettit, Unraveling macrophage contributions to bone repair, BoneKEy Rep, 2 (2013).

[219] M.N. Michalski, A.J. Koh, S. Weidner, H. Roca, L.K. McCauley, Modulation of Osteoblastic Cell Efferocytosis by Bone Marrow Macrophages, J Cell Biochem, (2016).

[220] F. Zhang, S. Tsai, K. Kato, D. Yamanouchi, C. Wang, S. Rafii, B. Liu, K.C. Kent, Transforming growth factor-beta promotes recruitment of bone marrow cells and bone marrow-derived mesenchymal stem cells through stimulation of MCP-1 production in vascular smooth muscle cells, J Biol Chem, 284 (2009) 17564-17574.

[221] M. Ishikawa, H. Ito, T. Kitaori, K. Murata, H. Shibuya, M. Furu, H. Yoshitomi, T. Fujii, K. Yamamoto, S. Matsuda, MCP/CCR2 signaling is essential for recruitment of mesenchymal progenitor cells during the early phase of fracture healing, PLoS One, 9 (2014) e104954.

[222] I.K.H. Poon, C.D. Lucas, A.G. Rossi, K.S. Ravichandran, Apoptotic cell clearance: basic biology and therapeutic potential, Nat Rev Immunol, 14 (2014) 166-180.

[223] C.J. Martin, K.N. Peters, S.M. Behar, Macrophages clean up: efferocytosis and microbial control, Current Opinion in Microbiology, 17 (2014) 17-23.

[224] A. Hochreiter-Hufford, K.S. Ravichandran, Clearing the Dead: Apoptotic Cell Sensing, Recognition, Engulfment, and Digestion, Cold Spring Harbor Perspectives in Biology, 5 (2013) a008748.

[225] K.S. Ravichandran, Find-me and eat-me signals in apoptotic cell clearance: progress and conundrums, The Journal of Experimental Medicine, 207 (2010) 1807-1817.

[226] K. Segawa, S. Nagata, An Apoptotic ‘Eat Me’ Signal: Phosphatidylserine Exposure, Trends in Cell Biology, 25 639-650.

[227] V. Bagalkot, J.A. Deiuliis, S. Rajagopalan, A. Maiseyeu, “Eat me” imaging and therapy, Advanced Drug Delivery Reviews, 99, Part A (2016) 2-11.

[228] E.P. Diamandis, T.K. Christopoulos, The biotin-(strept) avidin system: principles and applications in biotechnology, Clinical chemistry, 37 (1991) 625-636.

[229] J.F. Tait, D. Gibson, Phospholipid binding of annexin V: Effects of calcium and membrane phosphatidylserine content, Archives of Biochemistry and Biophysics, 298 (1992) 187-191.

[230] A. Holmberg, A. Blomstergren, O. Nord, M. Lukacs, J. Lundeberg, M. Uhlén, The biotin-streptavidin interaction can be reversibly broken using water at elevated temperatures, ELECTROPHORESIS, 26 (2005) 501-510.

[231] K.M. Woo, V.J. Chen, H.M. Jung, T.I. Kim, H.I. Shin, J.H. Baek, H.M. Ryoo, P.X. Ma, Comparative evaluation of nanofibrous scaffolding for bone regeneration in critical-size calvarial defects, Tissue Eng Part A, 15 (2009) 2155-2162.

[232] C. Granéli, A. Thorfve, U. Ruetschi, H. Brisby, P. Thomsen, A. Lindahl, C. Karlsson, Novel markers of osteogenic and adipogenic differentiation of human bone marrow stromal cells identified using a quantitative proteomics approach, Stem Cell Research, 12 (2014) 153-165.

[233] W. Huang, S. Yang, J. Shao, Y.-P. Li, Signaling and transcriptional regulation in osteoblast commitment and differentiation, Frontiers in bioscience : a journal and virtual library, 12 (2007) 3068-3092.

[234] Subhra K. Biswas, A. Mantovani, Orchestration of Metabolism by Macrophages, Cell Metabolism, 15 432-437.

[235] D.A. Hume, J.F. Loutit, S. Gordon, The mononuclear phagocyte system of the mouse defined by immunohistochemical localization of antigen F4/80: macrophages of bone and associated connective tissue, Journal of Cell Science, 66 (1984) 189.

[236] R.L. Jilka, R.S. Weinstein, T. Bellido, A.M. Parfitt, S.C. Manolagas, Osteoblast Programmed Cell Death (Apoptosis): Modulation by Growth Factors and Cytokines, Journal of Bone and Mineral Research, 13 (1998) 793-802.

[237] Y.Q. Xiao, C.G. Freire-de-Lima, W.P. Schiemann, D.L. Bratton, R.W. Vandivier, P.M. Henson, Transcriptional and Translational Regulation of Transforming Growth Factor-β Production in Response to Apoptotic Cells, Journal of immunology (Baltimore, Md. : 1950), 181 (2008) 3575-3585.

[238] K.A. Alexander, M.K. Chang, E.R. Maylin, T. Kohler, R. Müller, A.C. Wu, N. Van Rooijen, M.J. Sweet, D.A. Hume, L.J. Raggatt, A.R. Pettit, Osteal macrophages promote in vivo intramembranous bone healing in a mouse tibial injury model, Journal of Bone and Mineral Research, 26 (2011) 1517-1532.

[239] S. Kaur, L.J. Raggatt, L. Batoon, D.A. Hume, J.P. Levesque, A.R. Pettit, Role of bone marrow macrophages in controlling homeostasis and repair in bone and bone marrow niches, Seminars in cell & developmental biology, (2016).

[240] D.P. Vasconcelos, M. Costa, I.F. Amaral, M.A. Barbosa, A.P. Águas, J.N. Barbosa, Development of an immunomodulatory biomaterial: Using resolvin D1 to modulate inflammation, Biomaterials, 53 (2015) 566-573.

[241] Y.-H. Kim, H. Furuya, Y. Tabata, Enhancement of bone regeneration by dual release of a macrophage recruitment agent and platelet-rich plasma from gelatin hydrogels, Biomaterials, 35 (2014) 214-224.

[242] P.A. Pereira, S. Bitencourt Cda, D.F. dos Santos, R. Nicolete, G.M. Gelfuso, L.H. Faccioli, Prostaglandin D2-loaded microspheres effectively activate macrophage effector functions, European journal of pharmaceutical sciences : official journal of the European Federation for Pharmaceutical Sciences, 78 (2015) 132-139.

[243] R. Diab, J. Brillault, A. Bardy, A.V. Gontijo, J.C. Olivier, Formulation and in vitro characterization of inhalable polyvinyl alcohol-free rifampicin-loaded PLGA microspheres prepared with sucrose palmitate as stabilizer: efficiency for ex vivo alveolar macrophage targeting, International journal of pharmaceutics, 436 (2012) 833-839.

[244] T. Harel-Adar, T.B. Mordechai, Y. Amsalem, M.S. Feinberg, J. Leor, S. Cohen, Modulation of cardiac macrophages by phosphatidylserine-presenting liposomes improves infarct repair, Proceedings of the National Academy of Sciences, 108 (2011) 1827-1832.

[245] S. Ait-Oudhia, D.E. Mager, R.M. Straubinger, Application of Pharmacokinetic and Pharmacodynamic Analysis to the Development of Liposomal Formulations for Oncology, Pharmaceutics, 6 (2014) 137-174.

[246] P.P. Deshpande, S. Biswas, V.P. Torchilin, Current trends in the use of liposomes for tumor targeting, Nanomedicine (London, England), 8 (2013) 10.2217/nnm.2213.2118.

[247] K.M. Woo, J.-H. Jun, V.J. Chen, J. Seo, J.-H. Baek, H.-M. Ryoo, G.-S. Kim, M.J. Somerman, P.X. Ma, Nano-fibrous scaffolding promotes osteoblast differentiation and biomineralization, Biomaterials, 28 (2007) 335-343.

[248] X. Zhang, Y. Li, Y.E. Chen, J. Chen, P.X. Ma, Cell-free 3D scaffold with two-stage delivery of miRNA-26a to regenerate critical-sized bone defects, Nature Communications, 7 (2016) 10376.

[249] J. Chang, A.J. Koh, H. Roca, L.K. McCauley, Juxtacrine interaction of macrophages and bone marrow stromal cells induce interleukin-6 signals and promote cell migration, Bone research, 3 (2015) 15014.